THE DESIGN OF A NEW ELBOW PROSTHESIS

Richard Boddington

"Submitted to the University of Cape Town in partial fulfillment of the requirements for the degree of Master of Science in Medicine, in Biomedical Engineering."

February 1994

I, Richard Boddington hereby declare that the work on which this thesis is based is my original work (except where acknowledgements indicate otherwise) and that neither the whole work nor any part of it has been, is being or is to be submitted for another degree in this or any other University.

I empower the university to reproduce for the purpose of research either the whole or any portion of the contents in any manner whatsoever.

Signed

.....

SIGNATURE

25-02-1994

.....

DATE

ABSTRACT

Total elbow replacement arthroplasty is often used as a surgical procedure in patients who suffer from severe arthritis. Existing prostheses are either resurfacing models which are unsuitable for elbows which exhibit even moderate bone stock loss, or they have intramedullary stems or stirrup-like projections requiring excessive removal of bone. Relatively poor clinical results associated with elbow joint arthroplasty are an added indication for the need for further investigation into the design aspects of elbow joint prostheses. The objectives of this study were to develop a total elbow prosthesis using criteria such as: minimal invasion of surrounding bone, good fixation, ease of insertion, and the ability to reproduce the natural joint articulation and kinematics.

The articular surfaces and the extra-articular geometry of the distal humerus and proximal ulna were studied using a biostereometric three-dimensional technique. Following accurate observations of the articular surfaces, various mathematical approximations were made. An attempt was made to fit mathematical functions ("hyperbolic paraboloid", "helix", "circle" in the sagittal plane) to the data obtained for the articular surfaces. The fit of the hyperbolic paraboloid to the data was not acceptable, with errors in the order of 1 mm in certain traces.

A poor fit was also achieved testing the helical hypothesis, indicating that the trochlea is not a circular helix in form. However, the trochlear groove was inclined at an angle in the anterior-posterior aspect. The results of the circularity study revealed that the curved surface of the trochlea is circular in the sagittal plane and that the centres of these circles lie virtually on a straight line. The ulna surface was found to have two distinct articular facets with noncoincident centres of curvature.

The exact description of the curvature, extra-articular geometry, and cartilage thickness aided in establishing the design specifications of the prosthesis after undertaking an extensive geometrical analysis and using a computer-aided design package.

Prototypes of the designed components were manufactured. The components were inserted into bone models and the "minimal bone resection" concept observed. A rig was then built, simulating some muscular and ligamentous activity, for initial basic functional testing of these components. The aims of these tests were to: examine the range of motion, investigate the possibility of component impingement and/or dislocation, and test the alignment of the prosthesis and articular stability. The results obtained revealed that the prototype of the prosthesis functioned satisfactorily. Problem areas like component impingement with the bone were identified and design changes were indicated. The prospects for future developments include: additional functional testing following the insertion of the prototype into cadavers,

strength and contact area tests, accurate assessment of the instrument requirements, salvage procedures, and surgical approach.

ACKNOWLEDGEMENTS

- Mr. A. Spirakis, Head of the Biomechanics Group, Department of Biomedical Engineering, for his supervision, professional advice, and continuous support.
- Prof. I.D. Learmonth of the Department of Orthopaedic Surgery, for his co-supervision.
- Prof. L. Adams, Ms. A. Tredidga, and Ms. B. van Geems of the Biostereometrics Unit of the Department of Biomedical Engineering, for permission to use their hardware and software, and for their generous assistance and professional advice.
- Mr. John Ireland, Mr. Horst Kronenburg, and Mr. Mike Price of the Department of Biomedical Engineering mechanical workshop, for their assistance in the manufacturing of the prototypes and various rigs.
- Dr. Charles Breckon for the removal of elbow joints.
- Mr. Hall and his staff from the Department of Anatomy, for provision of elbow joints and for their assistance in the preparation of the fresh specimens.
- The Department of Forensic Medicine for permission to remove elbow joints, and especially Dr. Siroca for her assistance.
- Dr. Ruth Smart of the Department of Applied Mathematics, for her professional advice.
- Mr. Hugh Till of Polynates (PTY) LTD for supplying material for prototype manufacture.

CONTENTS

LIST OF FIGURES

LIST OF TABLES

CHAPTER 1: INTRODUCTION

Total Elbow Arthroplasty is commonly used as a surgical procedure in patients who suffer from severe arthritis. Whilst there are many patients whose elbow joints have been significantly damaged by arthritis, they may not be suitable or merit joint replacement with current prostheses. One major concern being that many current prostheses require the resection of too much bone. Poor clinical results associated with elbow joint replacement arthroplasty have also resulted in the procedure being infrequently performed. The incidence of elbow disease in rheumatoid arthritic patients can be as high as 72 percent (Table 1.1). The patient with bilateral involvement may have considerable pain and be significantly disabled - unable to dress or feed oneself.

	INCIDENCE (%)	NO. OF PATIENTS	AVE. DISEASE DURATION (yrs)
Laine & Vainio, 1969	21	191	-
Freyberg, 1968	38	-	5 - 25
Porter et al, 1974	72	225	-

TABLE 1-1. Incidence of elbow involvement in rheumatoid arthritis.

It is therefore very important that some form of surgical

intervention be considered, and elbow joint replacement arthroplasty could be the preferential choice because it offers the possibility of restoring mobility and eliminating the pain.

The development of the Total Elbow Arthroplasty (TEA) can be divided into four eras (Table 1.2).

ERA	TIME PERIOD	CHARACTERISTICS
First	1885 - 1947	resection, interposition, and anatomic arthroplasty
Second	1947 - 1970	partial and occasional total (hinge) joint arthroplasty
Third	1970 - 1975	constrained metal-to-metal hinge-joint replacement with methacrylate fixation
Fourth	to present	semi-constrained metal-to-polyethylene hinge of snap-fitting prostheses and unlinked resurfacing arthroplasty

TABLE 1.2. Four eras of Total Elbow Arthroplasty. (Morrey, 1985c).

As can be seen in the second era, there had been reports of hinged arthroplasty of the elbow as early as 1937, but this technique only became established in the third era with the development of methylmethacrylate for component fixation. Short-term results were good, but loosening of the components soon became a major problem requiring revision surgery. The current, fourth, era has brought about the development of two basic types of elbow prostheses: the linked (constrained) and the unlinked

(unconstrained resurfacing arthroplasty) prostheses. Short-term follow up studies have indicated that the complication and failure rate is very high for all types of total elbow arthroplasty (Table 1.3).

AUTHORS	COMPLICATIONS (%)	AVE. FOLLOW-UP (yrs)
Inglis & Pellicci 1980	51.0	3.7
Ewald et al 1980	42.0	3.5
Morrey et al 1981	55.0	4.1
Soni & Cavendish 1984	57.5	3.5
Rosenburg & Turner 1984	50.0	2.9
Roper et al 1986	23.0 minor 27.0 major 50.0	5.1
Gschwend et al 1988	5.6 permanent 21.1 transient 26.7	4.0
Brumfield et al 1990	50.0	8.0
Ruth & Wilde 1992	52.5	6.5

TABLE 1.3. Reported complication rates of total elbow arthroplasty.

These major clinical complications encountered are to a certain extent due to design faults (Goldberg et al, 1988). Thus,

to reduce these high complication rates, a critical part of the design process must be the analysis of the biomechanics of the elbow joint. Complex kinematics, anatomical features, and load distribution at the elbow joint are parameters which influence the long-term survival of a total elbow prosthetic component.

Furthermore, the use of some of even the most current designs will require the resection of an excessive amount of bone to allow for the insertion and placement of components. This is an important factor, since should the implant fail there is insufficient bone stock for a revision arthroplasty. The added concern is that the diseased elbow already has a bone stock deficiency, thus conservation of maximum bone stock is essential.

The foremost problem with current designs is that the insertion of the prosthesis is a difficult surgical procedure. Correct alignment of the elbow prosthesis is critical to its success and this can be a complex task for the surgeon.

The main objective of this study was to design a total elbow prosthesis using the following criteria:

a) minimal invasion of the surrounding bone
b) ease of insertion
c) appropriate articulation - normal alignment and kinematics reproduced
d) use of natural load bearing sites to support the complex loading pattern
e) and good fixation.

It was felt that this could be accomplished by:

a) undertaking a critical evaluation of design features of existing prostheses

b) using a biostereometric technique to undertake an extensive geometrical analysis of the elbow joint
c) making a theoretical design
d) production of a prototype
d) and basic functional testing of the prototype.

With regards to the articular geometry, the "helix", "circularity", and "hyperbolic paraboloid" hypotheses were tested. With the excellent accuracy and precision obtained with the reflex microscope, the joint profiles can be accurately measured and the assumption that the trochlea, coronoid sulcus, and olecranon sulcus are circular in the sagittal plane (Shiba et al 1988, London 1981) can be validated. This will ensure that kinematically the elbow joint has a single axis of rotation during flexion and extension. The "helix" hypothesis was tested because the central groove of the trochlea has been described as being helical in form. Another reason for this type of test was that the Helfet prosthesis as developed by an implant manufacturer (DePuy, U.S.A) was a circular helix. Regarding the "hyperbolic paraboloid" test, this was undertaken because the trochlea, when divided in half, appears to resemble the shape of this known mathematical function.

The mathematical description of the articular surface geometry is of paramount importance in the design process because this will directly influence the kinematics, contact areas, and loading patterns of a replaced elbow joint.

CHAPTER 2: LITERATURE REVIEW

2.1 ANATOMY OF THE ELBOW JOINT

Three bones comprise the elbow joint: the distal humerus, the proximal ulna, and the proximal radius (Figure 2.1).

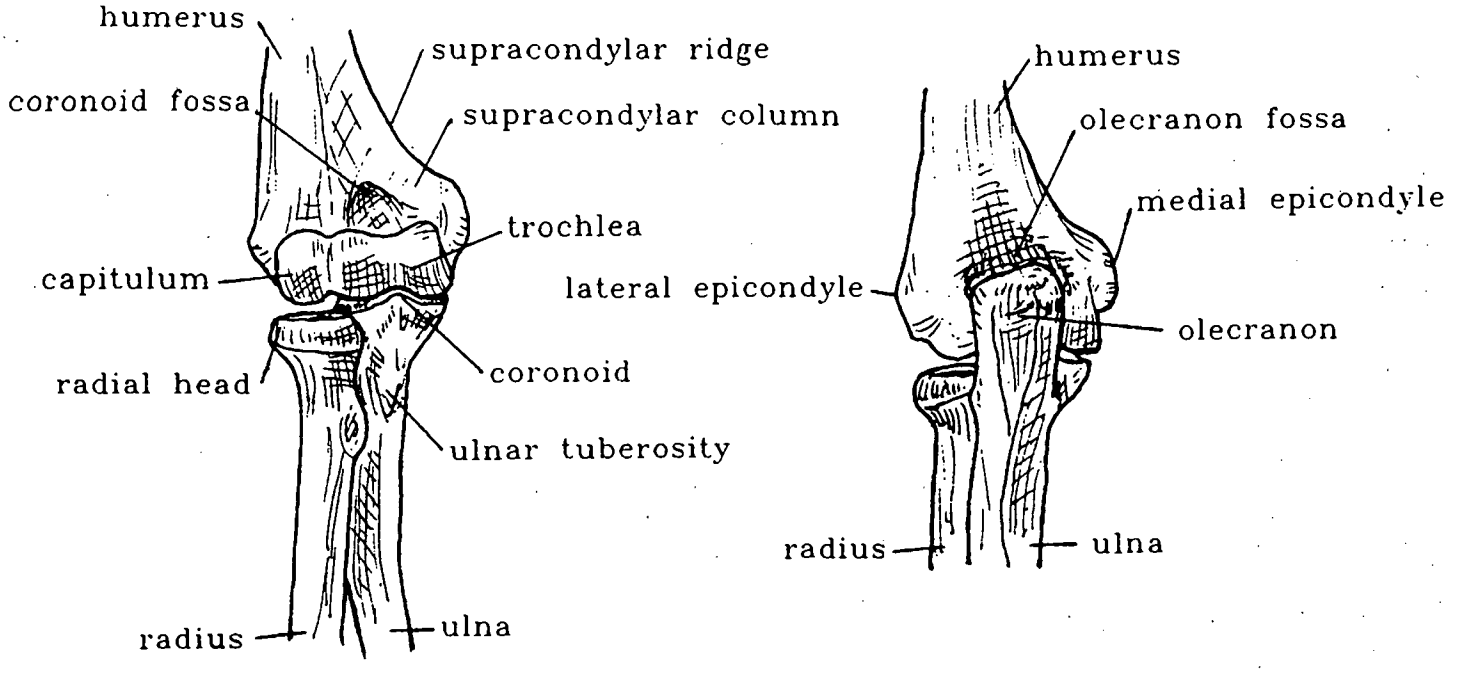

FIGURE 2.1. Osteology of the right elbow joint. (Adapted from Kapandji, 1970).

The humerus consists of two articulating surfaces, the trochlea and capitulum. The ulna also has two articulating

surfaces, the trochlear notch and the radial notch. The proximal part of the radius is the radial head which comprises two articulating surfaces. Thus, the capitulum articulates with the radial head, the trochlea with the trochlear notch, and the radial notch with the radial head. Special emphasis will be placed on the humero-ulnar articulation, i.e. the trochlea and trochlear notch, since most of the prosthesis designs require the resection of the radial head.

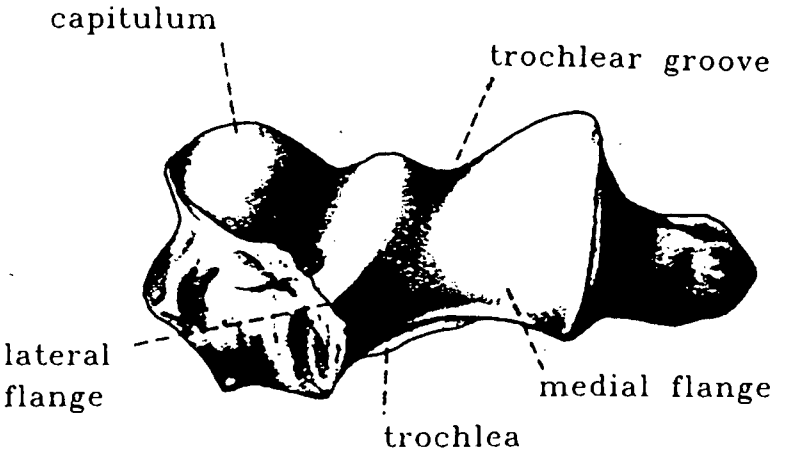

FIGURE 2.2. The trochlea articulating surface (distal humerus). (Adapted from Morrey, 1985a).

The trochlea (Figure 2.2) is the bobbin-shaped surface that articulates with the notch of the ulna. An arch is formed of about 300 to 330 degrees, and the surface is covered by a continuous cartilage layer that covers the anterior, distal, and posterior aspects. The trochlea is not symmetrical because the medial flange is larger and projects more distally than does the lateral part. The two flanges are separated by a groove, the

trochlear groove.

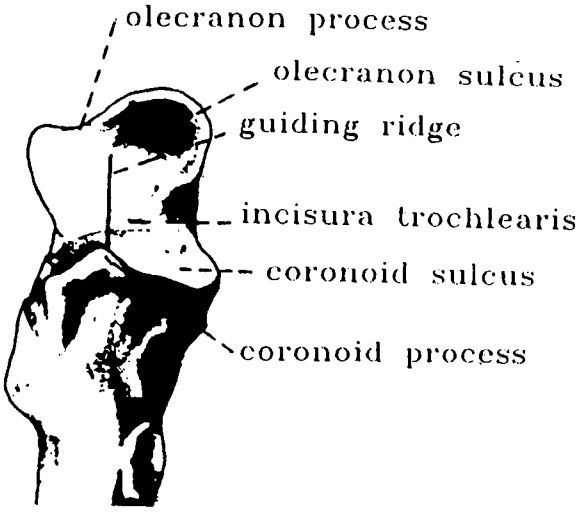

FIGURE 2.3. The trochlear notch articulating surface (proximal ulna). (Adapted from Morrey, 1985a).

The semilunar trochlear notch articulating surface (Figure 2.3) is not covered entirely by hyaline cartilage. A transverse fatty tissue section divides the notch into two distinct articulating surfaces, the olecranon sulcus which lies posteriorly and the coronoid sulcus situated anteriorly. The notch is also divided into medial and lateral sections by the guiding ridge, which extends from the olecranon process to the coronoid process.

The relevant ligaments essential for maintaining joint

stability are the collateral ligaments. The most important is the medial collateral ligament (MCL) which consists of three parts; anterior, posterior, and transverse segments. The anterior bundle is the primary stabilizer, the posterior bundle a secondary stabilizer, and the transverse bundle contributes relatively little to elbow stability (Morrey, 1985a). The other ligament is the lateral ulnar collateral ligament (LCL) which originates from the lateral epicondyle of the humerus and inserts into the annular ligament. The orientations of these ligaments are shown in Figure 2.4.

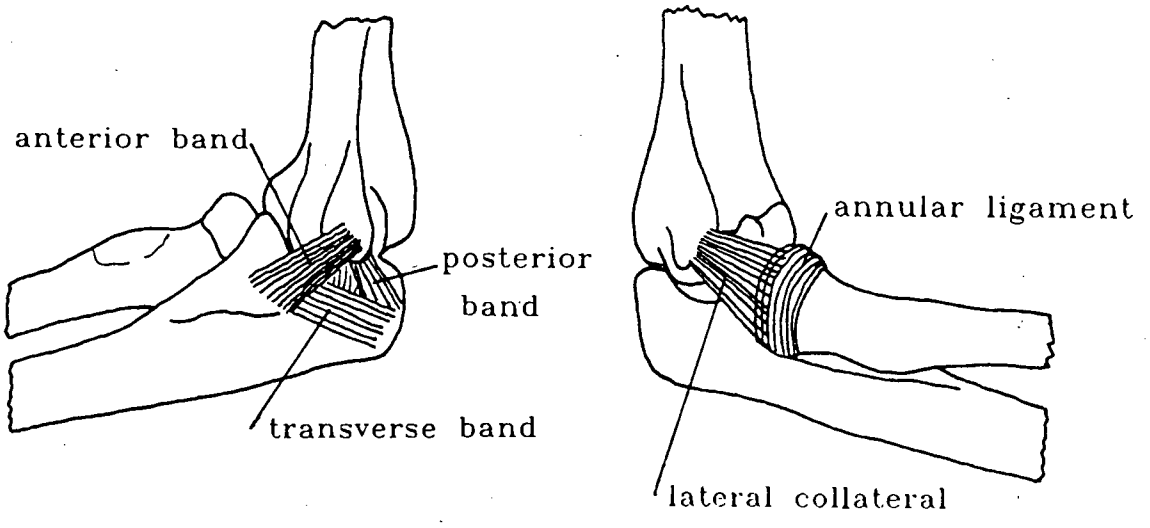

FIGURE 2.4. The relevant ligaments of the elbow joint. (Adapted from Tobias et al, 1988).

The muscles that cross the elbow joint are shown in Figure 2.5. The origin and insertion sites of several muscles at the

joint are clearly indicated in the figure.

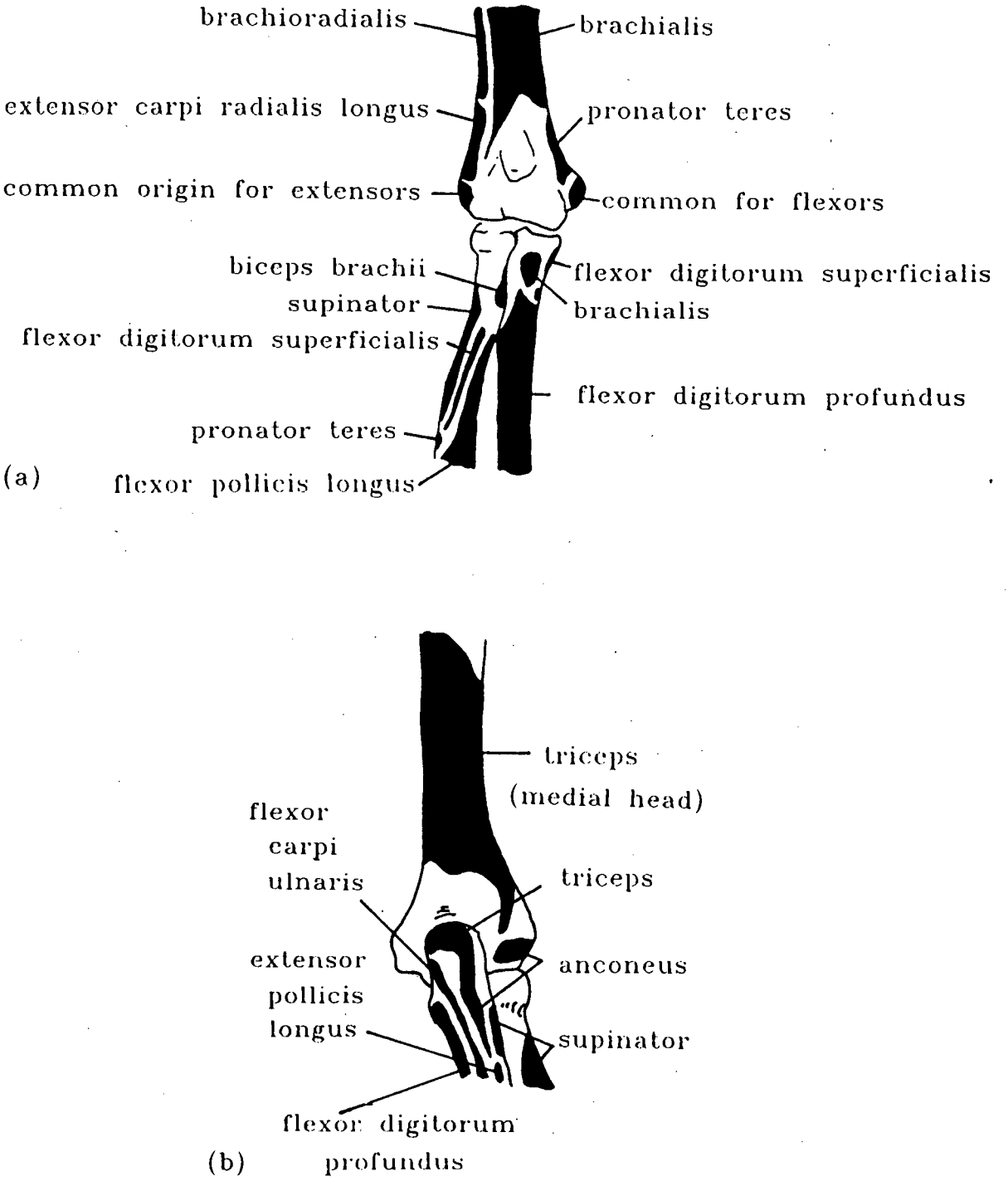

FIGURE 2.5. The muscles that cross the elbow joint: a) anterior view, b) posterior view. (Adapted from Basmajian, 1982).

It is important to be aware of the neuro-vascular structures around the elbow joint when designing a prosthesis because of the importance of these structures and the surgical limitations that they can present to the designer and surgeon. This is notably evident in Total Elbow Arthroplasty where studies have revealed a high occurrence of ulnar nerve neuropraxia (Ruth and Wilde 1992, Brumfield et al 1990). Thus, the location of the ulnar nerve, for example, at the elbow joint is something that the designer must be aware of when determining the geometry of the components, surgical instrumentation, and the surgical technique.

The blood supply is derived from the arterial anastomosis around the joint (Figure 2.6).

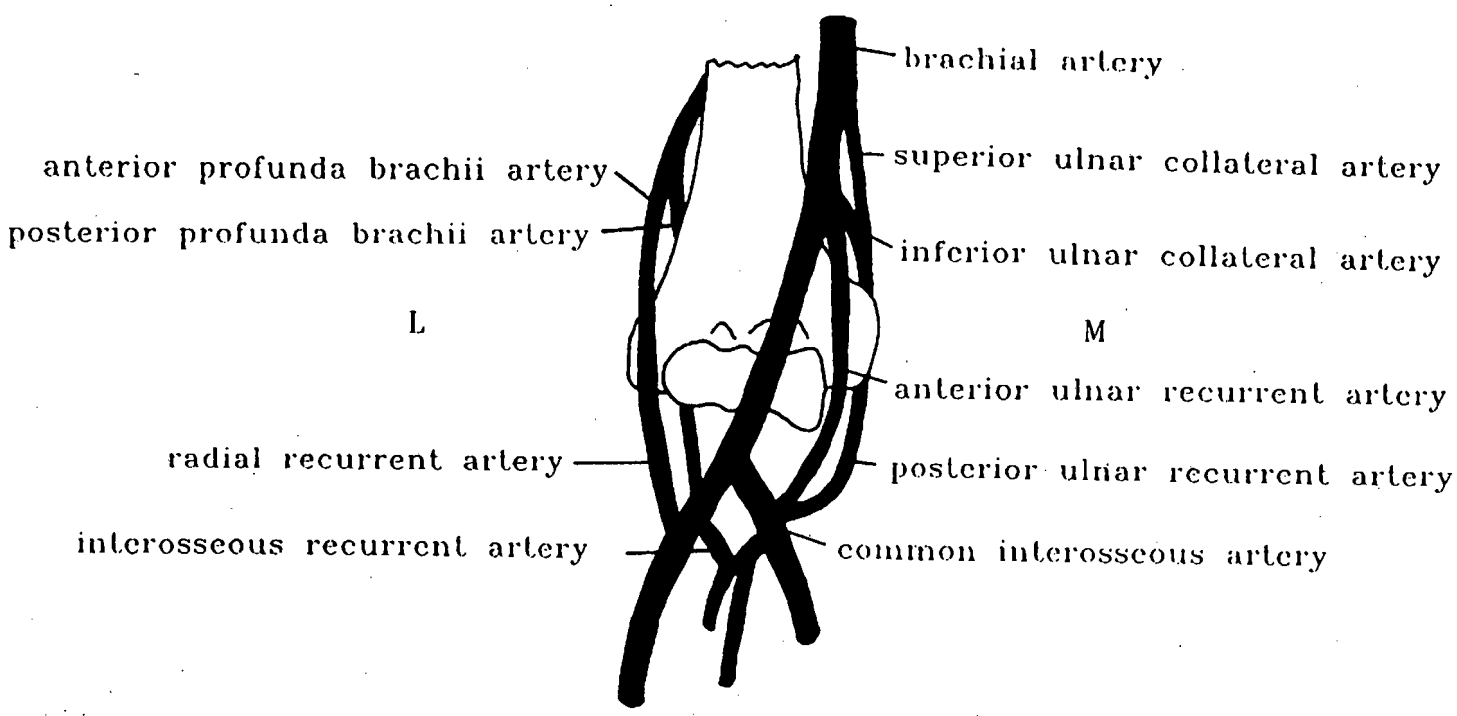

FIGURE 2.6. Arterial anastomosis around the elbow. (Adapted from Tortora, 1989).

The nerves in the region of the elbow joint all give twigs to it, and the common pattern of the ulnar, radial, median, and musculocutaneous nerves is indicated in Figure 2.7.

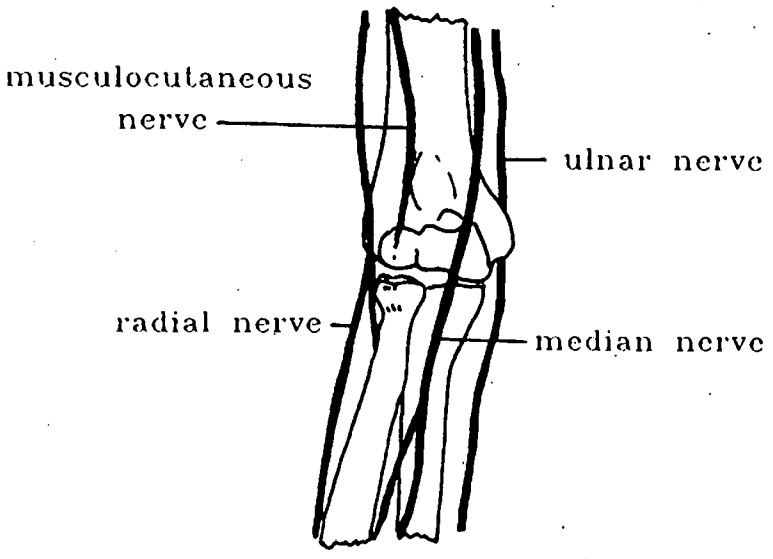

FIGURE 2.7. The nerves of the elbow region. (Adapted from Tortora, 1989).

2.2 BIOMECHANICS OF THE ELBOW JOINT

2.2.1 Contact areas of the elbow joint

Research work has been done by Goodfellow and Bullough (1967) using a dye technique, and Goel et al (1982) using a wax casting technique in order to determine the contact areas of the elbow joint. There is some agreement as to the regions of contact, with the most notable differences appearing to be during full extension (Figure 2.8).

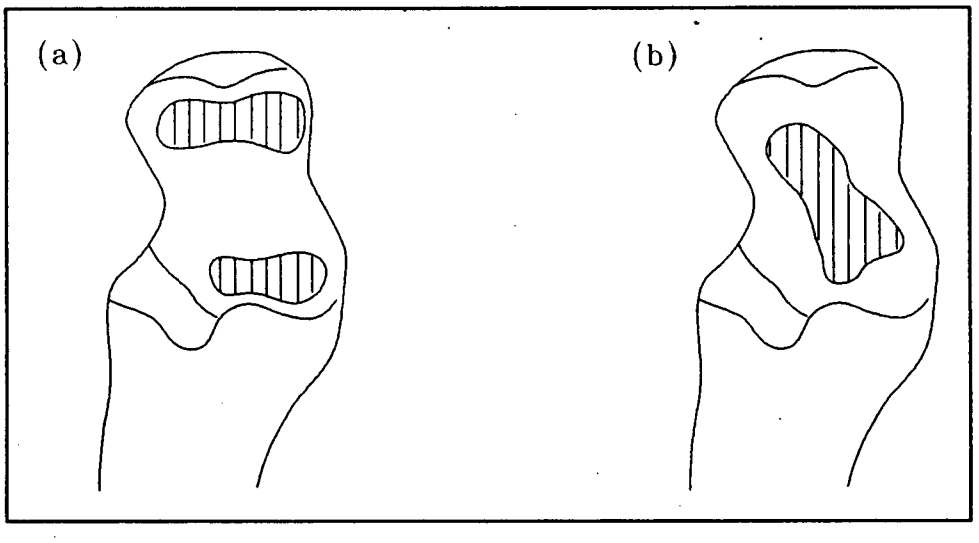

FIGURE 2.8. Contact areas during full extension; (a) Goodfellow and Bullough, 1967, (b) Goel et al, 1982.

During flexion, a similar contact area on the ulna is noted (Figure 2.9).

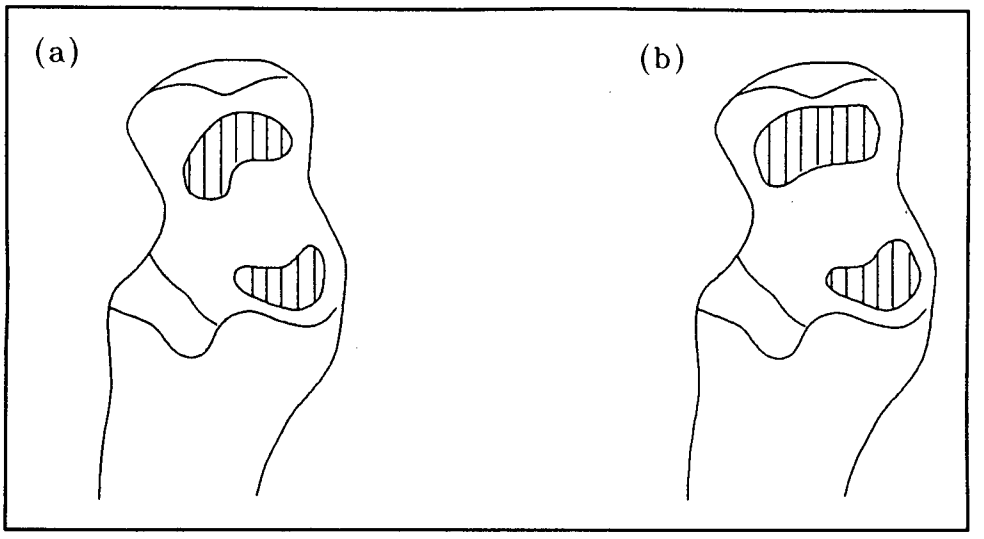

FIGURE 2.9. Contact areas at full flexion; (a) Goodfellow and Bullough, 1967, (b) Goel et al, 1982.

The shape and size of the contact areas were found to change in different elbow positions. These areas of contact were observed under no, or a light, external load. No literature was found showing contact areas during extreme loading conditions which could possibly change these results. Considering contact studies of the lower limb, an increased load increased the contact region (Goel et al, 1982). In a contact study of the elbow joint by Stormont et al (1985), one specimen was mounted upon an MTS machine with no muscular or soft tissue constraints, and the load increased from 50 N to 350 N. It was observed that the increase in load not only increased the size of the contact area but the location was also shifted. This study compared

different experimental contact techniques and it was not the primary object of the study to determine elbow joint contact areas, however, it is still useful in furthering the understanding of how the elbow reaches a stable articulating configuration. These studies yield valuable information at least for the general location of centroids of the area of contact.

2.2.2 Kinematics of the elbow joint

Elbow kinematics has been a controversial subject in the literature. Conflicting results have been reported and these appear to be due to the different measuring techniques that have been used (London, 1981) and possibly also to experimental error.

From a practical point of view, Amis and Miller (1982) and Morrey et al (1985b) have accepted London's (1981) results for flexion-extension. There is agreement that the forearm moves as a uniaxial articulation, except at the extremes (last 5-10 degrees) of flexion and extension, with the axis of rotation passing through the centre of the arcs formed by the trochlear sulcus and the capitulum. In the normal elbow, the range of motion is from 0 degrees in extension to about 150 degrees in flexion.

The carrying angle, which is the angle formed by the long axis of the humerus and the long axis of the ulna during extension, measures 10-15 degrees in men and about 5 degrees more in women (Beals, 1976). During flexion of the elbow, the carrying

angle is defined as the acute angle formed by the long axis of the humerus and the long axis of the ulna measured in the plane of the axis of flexion (London, 1981). Using this definition, London observed that the carrying angle changes less than 1 degree during the full elbow flexion.

Forearm rotation, or pronation-supination, is achieved by the radius rotating around the ulna. Generally, the longitudinal axis of the forearm runs from the centre of the radial head to the distal end of the ulna. Axial rotational movements of the ulna have also been observed and it is also suggested that varus-valgus movement of the ulna occurs depending on the forearm's rotational axis (Youm et al, 1979). In the normal elbow, the range of motion is from about 80 degrees in pronation to 85 degrees in supination.

Elbow motion ranges are thought to be limited by the geometry of the joint surfaces, surrounding bone, capsules, ligaments, and muscles (Morrey, 1985b). However, the extent to which these structures limit motion is arguable (Morrey 1985b, Kapandji 1970). The factors limiting extension are the anterior ligament and capsule, flexor muscles, and the impact of the olecranon process on the olecranon fossa. Parameters that limit flexion at the joint are the impacts of the radial head against the radial fossa, the coronoid process against the coronoid fossa, and tension from the triceps and capsule (Kapandji, 1970).

Table 2.1 presents a summary of the studies undertaken to describe the elbow kinematics using different experimental methods. These studies provide essential information required for the design of an elbow prosthesis.

AUTHOR	TECHNIQUE	MEASURED PARAMETERS
London 1981	Refinement of Reuleaux's tech: 2-d roentgeno-graphic method	Axis of rotation, carrying angle, type of motion, axial rotation suggestions
Morrey & Chao 1976	Taylor & Blashke technique: 3-d roentgeno-graphic method	Rotational motion of forearm, carrying angle, axis of rotation
Youm et al 1979	Photographic tech. applying LED methodology	Carrying angle, centre of rotation, axial rotation, proximal ulnar motion.
Amis et al 1977	Goniometer	Carrying angle changes.
Chao et al 1980	Electrogoniometer	Elbow joint rotation, elbow range of motion in daily activities
Morrey et al 1991	Magnetic tracking device	Valgus stability of normal elbow with radial head resected.

TABLE 2.1. A summary of elbow kinematic studies.

2.2.3 Forces at the elbow joint

An et al (1981) and Amis et al (1980) examined the relative forces of muscles crossing the elbow joint and determined the major muscles which have to be considered in joint force calculations. There are three main elbow flexors; brachialis, biceps brachii, and brachioradialis. The two main extensor muscles are the triceps and anconeus. The main muscles of pronation are the pronator quadratus and pronator teres. The main

muscles of supination are the supinator and biceps brachii.

A detailed, three dimensional analysis of these muscle forces crossing the elbow joint leads to an indeterminate problem and several methods have been used for solution. Firstly, an electromyographic (EMG) analysis, which becomes unworkably complex, and secondly, the optimization method. But these procedures have little practical confirmation. An alternative method - the equal-stress concept - was considered by An et al (1981) and Amis et al (1980).

The basis of this method is that during maximal activity, the muscle fibres will be stressed in a group of co-operating muscles. Individual muscle forces will be proportional to the number of muscle fibres present and during maximum tension proportional to the physiological cross-sectional area of the muscle.

Muscle actions normally cause the major part of joint force, so it is essential in a joint force analysis for prosthesis design that the relative contributions of various muscles for strenuous activities be known. The maximal elbow joint forces can then be estimated with the availability of the following information:

- The muscles active for specific activities, following results of EMG investigations (Cnockaert et al, 1975).

- Biomechanical parameters controlling the joint (Amis et al 1980, and Morrey et al 1981): the centroid lines representing the muscle action lines, moment arms, component of moment and force generated by each muscle for a given external force action.

Using this method, Morrey et al (1985b) have determined the elbow joint reaction forces for various flexion angles with external loads applied at the wrist. Amis et al (1980) determined elbow joint forces during strenuous isometric flexion and extension actions. Morrey et al (1985b) and Amis et al (1980) agreed that maximum joint reaction forces occur at about 30 degrees flexion, and then under static loading conditions these forces can exceed three times body weight. Amis et al (1980), predicted contact forces up to 5.4 kN on the ulna following radial head resection. It is therefore apparent that the elbow should be considered a weight-bearing joint for the purposes of implant design.

2.3 ELBOW JOINT ARTHROPLASTY

2.3.1 Background

There are two quite separate generations of total elbow arthroplasty (TEA).

1) The first generation of TEA designs were the totally constrained type (Figure 2.10). It incorporates a fixed hinge, and the design may or may not permit some degree of rotation above or below the hinge. The two components articulate about a single axis.

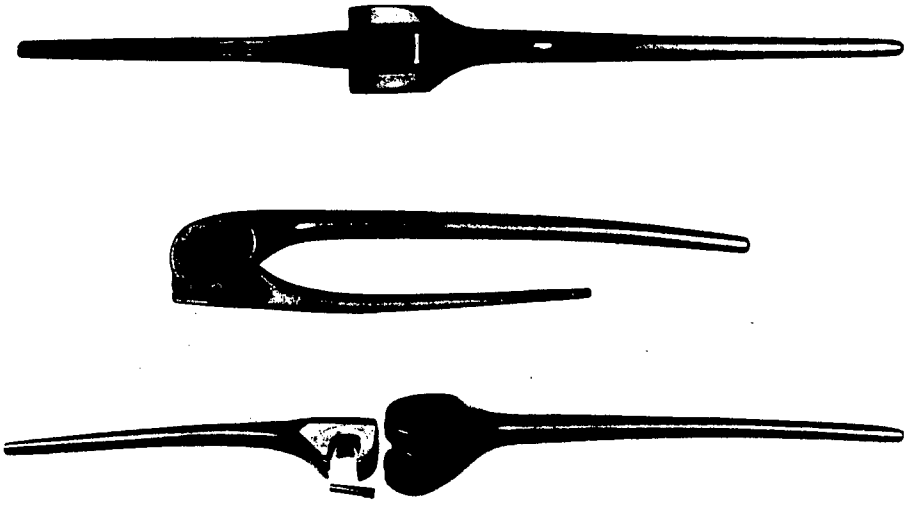

FIGURE 2.10. Example of the St. Georg constrained elbow prosthesis. (Adapted from Engelbrecht et al, 1977).

The principal problems associated with these replacements were loosening and loss of bone stock (Souter, 1981). The failure of these replacements was due to the fact that a simple hinge was inserted into a joint which is not fundamentally a hinge since its centre of rotation moves throughout the joints motion (Morrey and Chao, 1976), thereby causing excessive loosening. These design types require excessive removal of bone stock for their insertion. Thus, in the event of the failure of the prosthesis there is no bone remaining to form any type of stable articulation and gross instability is likely to result (Souter, 1977).

2) Most of the second generation elbow prostheses can be described as non-constrained models (Figure 2.11). The other prosthesis types available are semi-constrained articulated devices with intramedullary stems (Figure 2.12).

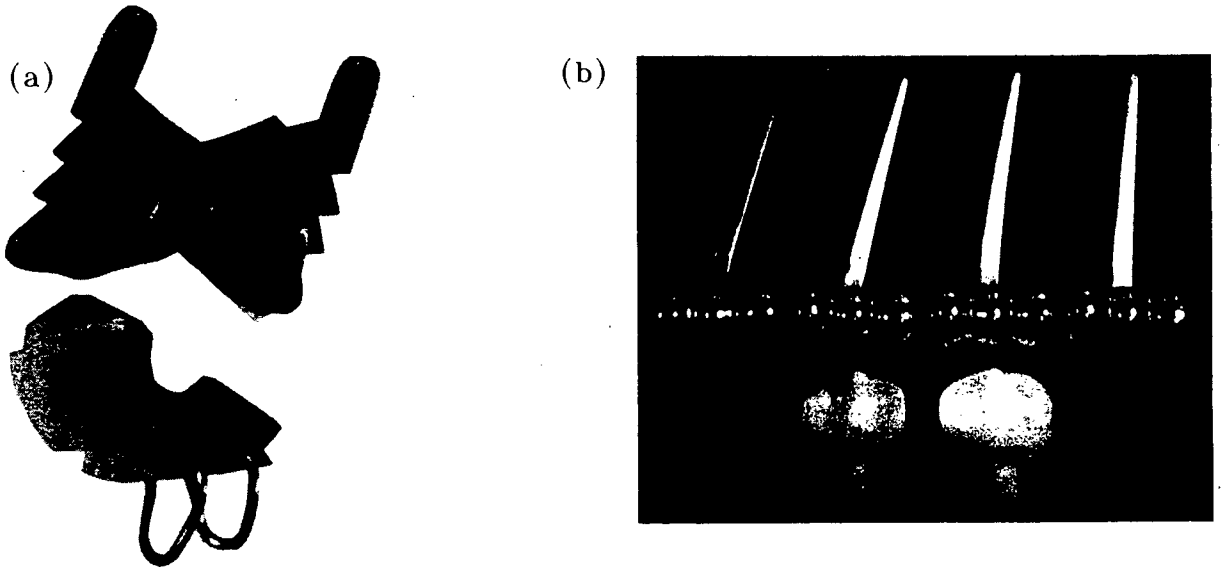

FIGURE 2.11. Examples of non-constrained (unlinked) elbow prostheses; (a) Liverpool (From Cavendish and Elloy, 1977), (b) Capitello-Condylar, (From Ewald et al, 1977).

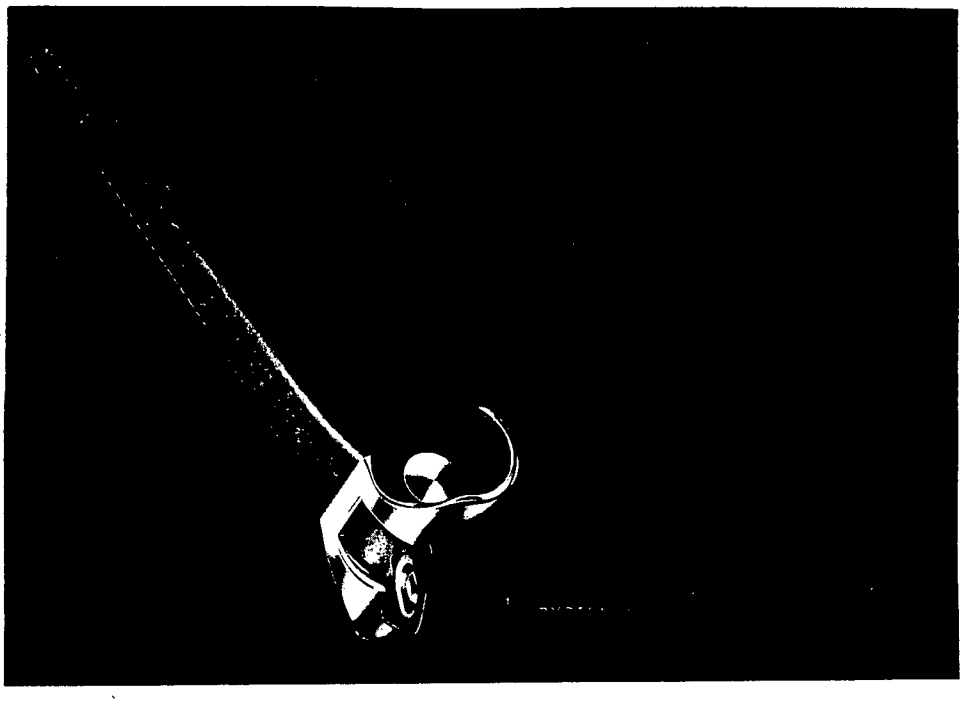

FIGURE 2.12. Example of the GSB semi-constrained elbow prosthesis. (From Gschwend et al, 1988).

The current status of total elbow arthroplasty can be traced back to the early 1970's with the introduction of minimally constrained cemented implants. Semi-constrained implants developed at that time included the Schlein, Pritchard-Walker, Coonrad, AMC, GSB, and triaxial prostheses. A comparison of mechanical design parameters indicated that implants with the fewest constraints and kinematics, nearly approaching those of the anatomical elbow, were the most successful (Goldberg et al, 1988). This brought about the development of non-constrained (unlinked) implants such as the Kudo, Liverpool, London, Souter/Strathclyde, and Capitello-Condylar prosthesis (Goldberg

et al, 1988).

Thus, currently available elbow implants have evolved into two basic types; unlinked and linked devices.

With the use of unlinked implants, a resurfacing procedure is followed which simply resurfaces the ulna and humerus and relies on its own inherent stability. These implants offer a satisfactory reconstruction of the natural centre of rotation. They require the elbow joint to have intact collateral ligaments and metaphyseal bone (Sourmelis et al, 1986).

Linked implants incorporate some degree of inherent stability within the prosthetic design. The two components are linked by a hinge which provides varying degrees of laxity. These implants consist of stemmed humeral and ulnar components. They tolerate more soft tissue insufficiency and loss of bone stock than do the resurfacing implants. However, aseptic loosening is a long-term problem caused by the substitution of mechanical constraints for normal articulation constraints and soft tissue support (Goldberg et al, 1988).

Several designs of the unlinked type have resurfaced the radial head (eg. Pritchard, Capitello-Condylar) in an attempt to gain load transmission stability. These prostheses have had mixed results due to difficulties in balancing the radio-capitellar, radio-ulnar, and the trochleo-ulnar joints during the operation. Most prostheses have been reported to have unsatisfactory rates of loosening and dislocation (Goldberg et al, 1988) as it will be described in the following section.

Tables 2.2 and 2.3 list the important advantages and disadvantages of the two implant categories.

ADVANTAGES	DISADVANTAGES
Satisfactory reconstruction of the natural centre of rotation	Not suitable for patients with deficient bone stock
The soft tissue is permitted to absorb some of the force during use, instead of direct force transmission to the bone-cement interface	It requires the collateral ligaments to be fully functional

TABLE 2.2. Unlinked prostheses.

ADVANTAGES	DISADVANTAGES
Tolerate some loss of bone stock	Substitute mechanical constraints for soft tissue support: - high local stresses - compromise of implant fixation
Used successfully in careful selection of patients who do not have ligamentous or soft tissue competence and in revision surgery	

TABLE 2.3. Linked prostheses.

2.3.2 Complications

The type and frequency of complications after implantation of different types of prostheses vary. Loosening and dislocation appear to be the two complications most frequently reported for the linked and unlinked type respectively. Common complications (usually requiring further surgery) and the relative frequencies of each complication are listed in Tables 2.4 and 2.5. The prosthesis type and follow up period are also included in these tables.

COMPLICATION	FREQ. (%)	PROSTHESIS (FOLLOW-UP (YRS))	
-Infection	3	Souter/Strath.(4)	Poll 1991
	7.8	Capitello(6.5)	Ruth 1992
-Loosening	3	Souter/Strath.(4)	Poll 1991
	23	Guildford	Karanjia 1990
	15	ICLH(5.1)	Roper 1986
	5	Wadsworth(2.5)	Rydholm 1984
	14	Kudo(9.5)	Kudo 1990
-Instability:			
Persistent subluxation	3	Kudo(9.5)	Kudo 1990
	13	Capitello(3.5)	Davis 1982
Dislocation	12	Souter/Strath(4)	Poll 1991
	4	Capitello(3)	Rosenburg 1983
	6	Capitello(6.5)	Ruth 1992
	9.2	Capitello(3.5)	Ewald 1980

TABLE 2.4. Unlinked prostheses.

COMPLICATION	FREQ. (%)	PROSTHESIS (FOLLOW-UP (YRS))	
-Infection	4	Pritchard Mark 2 (3)	Madsen 1989
	6	Stanmore(7)	Johnson 1984
-Loosening	12	Mayo(5)	Morrey 1981
	7	Stanmore(7)	Johnson 1984
	4	Pritchard Mark 2 (3)	Madsen 1989
	6	Pritchard-Walker (3.7)	Inglis 1980

TABLE 2.5. Linked prostheses.

These relatively short-term clinical results achieved with the different elbow prostheses are not very encouraging. Nonetheless, the major types of complications have been indicated from these studies, and an understanding of what causes these problems will improve the long-term success of TEA's.

The possible factors accounting for aseptic loosening are:

- prosthesis design,
- normal force transmission (cyclical loading),
- surgical technique (inadequate cementing technique, inaccurate positioning of components).

The possible factors accounting for instability (dislocation) are:

- prosthesis design,
- surgical technique,
- ligamentous and soft tissue "incompetence".

2.4 DESIGN CONSIDERATIONS

2.4.1 Current prosthetic designs

Design features and possible drawbacks for current, unlinked type, prostheses are presented in the following table (Table 2.6).

DESIGN TYPE	FEATURES	DRAWBACKS
Amis-Miller	- Fixation concepts determined by a detailed study of forces - Minimal resection of bone - no humeral stem, no PMMA	- Correct alignment and positioning uncertain - especially with added complexity of a radial component - Problematic radial component - The ulnar component assumed to have a single axis of rotation; no data available - Anatomical articular shape, but diameters measured using radiographs - accuracy questionable
Capitello-Condylar	- Anatomical humeral articular surface - from wax impression	- Ulnar component conformed to trochlea - Radiographic measurements provided attitude and angles - accuracy questionable - Excessive bone stock invasion
Guildford	- No information regarding design and testing located.	- Probable excessive removal of posterior cortex of bone(humerus) - Inadequate fixation of the articular part of the humeral component within the condyles (Karanjia and Stiles 1990)

DESIGN TYPE	FEATURES	DRAWBACKS
ICLH - Roper-Tuke	- Minimal bone resection - Limited information regarding design and testing located.	- Components have congruent, cylindrical articulating surfaces which can slide freely medio-laterally, thus valgus-varus stability is questionable, and there is the possibility of the collateral ligaments being excessively tensioned - Correct alignment and positioning of a non-anatomical prosthesis regarding the natural axis of rotation is questionable
Kudo	- The articulating surfaces are not congruent - Limited information regarding design and testing located	
Liverpool	- Fixation was tested in vitro - Solid trochlea with ribs provides adequate fixation - Minimal bone resection	- The asymmetric shaped normal trochlea is replaced by a symmetric shaped bobbin - Correct alignment with regards to natural axis of rotation questionable
Lowe	- Limited information regarding design and testing located.	- The humeral component is made of UHMWPE and the ulnar component of a metal alloy which might lead to unacceptable long-term wear - Anatomical complexity of the humero-ulnar articulation was disregarded

DESIGN TYPE	FEATURES	DRAWBACKS
Pritchard	- Snap-on spacers and stems - No further information regarding design and testing located.	- The insertion of the radial component is complex - Alignment of components questionable
Sorbie	- Extensive articulation analysis - Minimal resection of bone - Limited design information located (especially ulnar and radial component).	- Radial head component requiring a relatively complex alignment and insertion technique
Souter/ Strath-clyde	- Biomechanical analysis - Anatomical design	- Removal of excessive amount of bone
No information regarding the design features was located for the following prostheses: AMC, London, R-C, Ishizuki, Imura, Norwegian, Wadsworth.		

TABLE 2.6. Design features and possible drawbacks for unlinked type elbow prostheses.

2.4.2 Established concepts influencing prosthesis design

A detailed study of the forces imposed on the elbow joint was undertaken by Amis et al, in 1979 and 1980. This force analysis provided essential data for the design of a joint replacement, and the following results will be considered in the design of the components:

1) Tensile forces at the elbow joint can be disregarded.

2) Forces on the humerus act in an arc on the anterior aspect, thus, the fixation of the humeral component should resist axial compression when the elbow is extended and anterior-posterior forces when the elbow is flexed.

3) Very little net medial-lateral stress is encountered on the humeral component fixation; it must resist predominantly sagittal plane forces.

4) The problem of loosening of the humeral component's stem has been linked to the components fixation design being unable to resist torsion. Ligament tension and articular compression prevent this in the normal elbow, and a prosthesis should retain the ligaments and support the forearm on a wide base.

5) The ulnar fixation must resist the likelihood of shearing off the olecranon because the humero-ulnar articulation can absorb varus-valgus moments.

Adequate fixation has been achieved with cementless humeral component type designs (Kudo, Sorbie, Amis-Miller), and these types of prostheses allow for minimal resection of bone.

The majority of components are not highly constrained, and are so designed so as to dislocate during excessive loading; instead of applying excessive stresses at the interface. This will prevent the loosening of the components.

The replacement of the radial head is a controversial issue in the literature. Amis et al (1979a) examined the joint forces at the elbow joint and concluded that a radial head replacement be considered vital for a total elbow arthroplasty, especially for an active person. In a later paper, Amis et el (1979b) analyzed the elbow joint forces in patients with rheumatoid arthritis and found isometric elbow flexion strengths (using a tensiometer) to be about 45 percent to that of a normal person. However, these researchers were still concerned about the prevention of valgus deformity and proximal migration of the radius.

Morrey et al, in 1979, studied the biomechanics of the elbow following excision of the radial head and determined that the extent of proximal migration of the radius did not correlate with the functional results. Therefore, it is doubtful whether prosthetic replacement of the radial head offers a significant functional improvement. In a later study, Morrey et al (1991) found that absence of the radial head does not significantly alter the 3-dimensional characteristics of motion in the elbow joint.

Clinical results with a current unlinked elbow prosthesis (Capitello-Condylar) indicate that prosthesis incorporating a radial head replacement have a higher complication rate than those without a radial head component (Ewald et al, 1984). Prostheses that replace the radial head have been reported to have unsatisfactory rates of loosening and dislocation and they are no longer recommended for use (Goldberg et al, 1988).

The surgical technique also becomes more complex with a radial head component because it becomes more difficult for the surgeon to obtain the correct alignment of the three components (as compared to two) during surgery, and this is critical to the success of the prosthesis.

2.4.3 Materials used in TEA

Listed below is a list of the requirements that a material must comply with in order to be considered as an implant material (Jobbins, 1981).

1) Adequate mechanical strength for both static and fatigue loading, in tension, compression, and shear.
2) Sufficient stiffness and ductility.
3) Resistance to corrosion in the presence of body fluids and other materials.
4) Long term stability.
5) Wear resistance (in relation to corresponding parts).
6) Sufficient hardness.
7) The capacity of being sterilized.

Commonly used materials are:

- Metals:

Wrought austenitic stainless steel types 316L; Cobalt-Chromium-molybdenum cast alloy (known variously as sellite,

vinertia, vitallium etc); and pure titanium and titanium alloy.

- Ultra-high molecular weight polyethylene (UHMWPE).

The metal and UHMWPE articulation is now standard with most elbow implant designs. This combination is chosen because of the low friction and reduced wear rates if compared to other polymers. However, even minimal wear of UHMWPE can result in the debris particles producing an adverse biological reaction in the surrounding tissue. This reaction can cause resorption of the bone which can cause loosening of the component (King et al, 1993).

Polymethylmethacrylate (PMMA) bone cement is the current method of obtaining fixation of most of the prosthetic components. There is some interest in cementless fixation (use of porous materials) which relies on bony in- or ongrowth into suitable surface features. But, any micro-movement between the component and bone might compromise ingrowth fixation.

2.4.4 Surgical technique

The positioning and alignment of the components is crucial to the function and durability of a prosthesis. The centre of rotation of the prosthesis must coincide as closely as possible to the normal centre of rotation of the natural elbow (Ewald et al, 1980). In a functional analysis by Figgie et al (1986), the neutral range of positioning of a semi-constrained prosthesis was

found to be very narrow, and allowed for a variation in placement of no more than four degrees anteriorly, eight degrees posteriorly, and no increase in the distal offset of the humerus relative to the anatomical centre of rotation. If the ulnar component is positioned excessively anteriorly and proximally, the arm is functionally lengthened creating excessive tension on the triceps and the ulnar nerve.

Thus, it is imperative that the surgical technique is not a complex procedure, thereby allowing the surgeon to accurately insert and position the components.

CHAPTER 3: METHODOLOGY AND RESULTS

This chapter has combined both the methodology and the results of each step of the hypothesis testing, design, and prosthesis evaluation phases. With the several distinct stages of a design process, it was felt that the results of each stage's methodology should follow it directly, and not have all the results combined into one chapter. This allows for a smoother flowing reading preventing the reader from continually having to page back to a specific section in the methodology correlating with something observed in the results chapter.

3.1 INTRODUCTION

Morrey and An, 1983, have shown that the 3-D motion of the elbow joint is primarily influenced by the shape of the articular surfaces. And this shape is essential to maintain the correct balance and tension amongst the muscles, ligaments, and soft tissues to enable the normal kinematics of the elbow joint to be enforced.

Malarticulation can lead to high contact stresses which

leads to excessive wear of the UHMWPE articular surface which might lead to granulomater formations and loosening of the implant. Thus, various researchers, in an attempt to recreate the normal anatomical shape of the articular surfaces, indicate that their designs are resurfacing or replacing the diseased articular surfaces in an "anatomical manner". However, except for the Sorbie design, none of them have replaced the surfaces with a geometrically accurate truly anatomical prosthesis. These designs range from a "bobbin-shaped" type humeral component to "simplified, geometrically matched components". Numerous assumptions and predictions appear to have been made, with very little detailed geometrical analysis of the articular surfaces.

It is with this background and the disappointing clinical results with the use of current "resurfacing" designs that an extensive geometrical analysis was performed.

The objectives were to accurately model the anatomical articular surfaces of the trochlea and proximal ulna and incorporate the information obtained from this modelling procedure into the design of the artificial components. To accomplish these objectives, several techniques were considered: a slicing technique, close-range stereophotogrammetry, and the usage of a biostereometric tool (reflex microscope). The slicing technique (Shiba et al, 1988) was rejected as a method of choice because we had concerns about its precision mainly due to the fact that it is based on "manual" cutting of the bone and subsequent digitisation of the photographed sections. Based on the reported accuracies (Huiskes et al, 1985: 0.14 - 0.27 mm and Ateshian et al 1991: 0.09 - 0.4 mm) using analytical

stereophotogrammetry, it was decided to employ the reflex microscope as the measuring instrument (accuracies of ± 0.02 mm, Scott 1981).

Following accurate 3-dimensional observations of the articular surfaces, mathematical approximations were made. Various mathematical functions were considered: a hyperbolic paraboloid, a circle (in the sagittal plane), and a helix. If the "fit" of these functions to the data obtained for the articular surfaces is not acceptable, the articular surfaces could be reconstructed in three-dimensions using a computer-aided design package (AutoCAD v11). The exact description of the curvature for establishing the design specifications of the articular surfaces of the prosthesis could therefore be obtained.

3.2 MEASURING TECHNIQUE

Three dimensional binocular microscopes have two separate lines of sight, as opposed to conventional microscopes with a single objective and a beam splitter to bring the same view to the two oculars. The principle of the reflex microscope is described below.

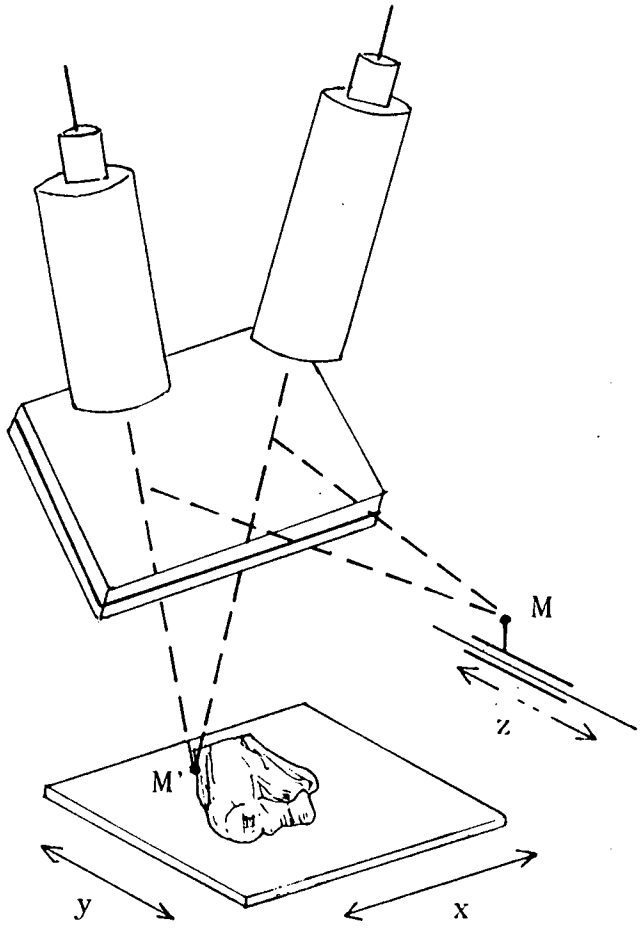

FIGURE 3.1. The principle of the reflex microscope (Adapted from Scott, 1981).

The distal humerus or proximal ulna is placed on an XY translation base in the field of view of the 3-D microscope (Figure 3.1), and a measuring mark M can then be projected onto the distal humerus or proximal ulna by reflecting it in a half-silvered mirror. This mark is evident at M′ and translation of M horizontally causes M′ to move in a direction normal to the XY base. Observations of the humerus and ulna are shared between the XY movement of the bones themselves on the base and the Z movement of M.

The reflex microscope used (Figure 3.2) uses a 2x microscope and three micrometer drums of 100 mm range and 0.01 mm least count. M, the measuring mark, is a single strand of optic fibre illuminated by a low power lamp, and has a diameter of 20 μm. The measuring marks direction of movement is fixed and the mirror can be adjusted by the adjusting screws to make the movement of the reflection M′ normal to the XY plane.

FIGURE 3.2. The reflex microscope.

3.3 SPECIMEN ACQUISITION, PREPARATION, AND MOUNTING

Dry cadaveric bones

Five humeral and four ulnar cadaveric bones were obtained from the Department of Anatomy at the University of Cape Town. The bones were boiled and defatted prior to acquisition. The cadaveric bones were chosen after careful inspection of the articular surfaces in consultation with an anatomist. Bones having noticeable abnormalities (eg. erosion) were not considered.

The distal humerus was resected about 1 cm proximal to the articular surface. The trochlea was marked with a felt-tipped marker to indicate the profiles to be digitised (Figure 3.3). The profiles were marked in the sagittal plane parallel to the trochlear groove. The trochlea was divided into an anterior and posterior view by a mark perpendicular to the groove. The anterior and posterior views were divided up into nine and eleven profiles respectively.

Similarly, the ulna was divided into two views - the coronoid and olecranon facets separated by the incisura trochlearis. The profiles were marked in the sagittal plane parallel to each other. The olecranon facet had eleven profiles and the coronoid facet had nine profiles (Figure 3.4).

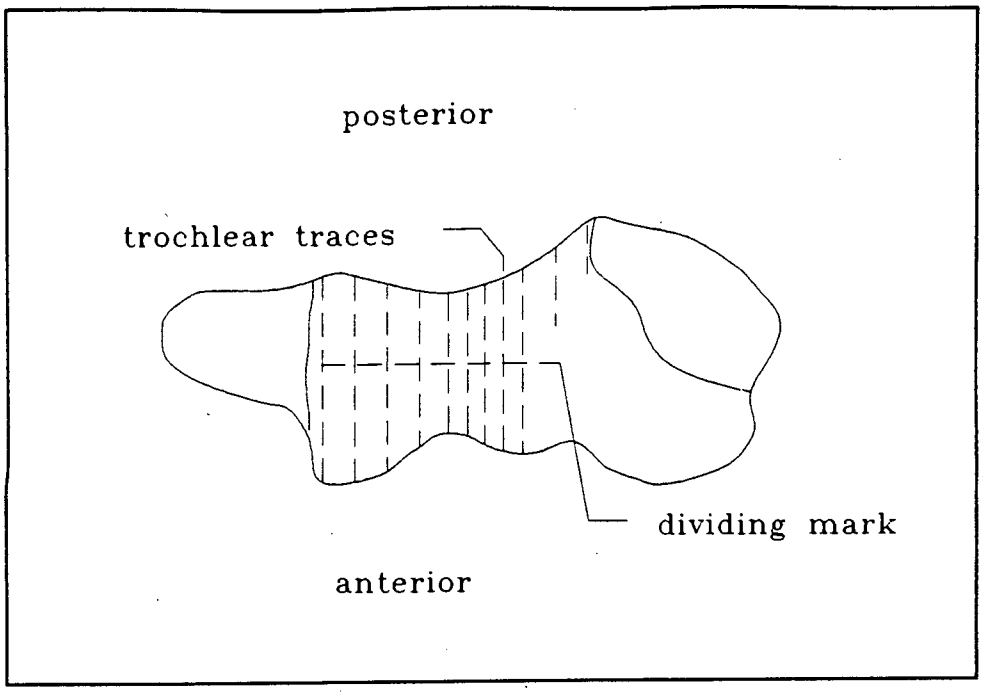

FIGURE 3.3. Trochlea markings for profile digitisation.

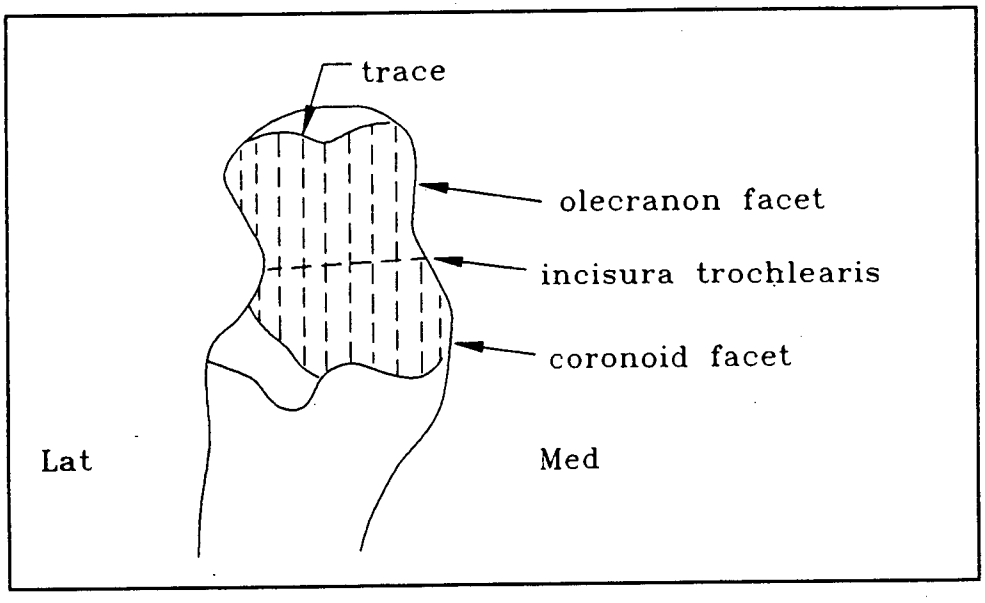

FIGURE 3.4. Coronoid and olecranon facet markings for profile digitisation.

The specimen was mounted on the device shown in Figure 3.5.

FIGURE 3.5. Ball and socket mounting device.

The ball and socket articulation allowed the "stage" to be rotated so that several views of the specimen were possible. The extent of rotation was sufficient to allow an anterior and posterior view of the trochlea, and views of the coronoid and olecranon facets. The specimen was then fixed to the "stage" using an adhesive material (Pratley). This is sufficient to hold the specimen in a fixed position for the short period of time required for digitisation.

The square-shaped "stage" was made of casting resin and had

four steel pins inserted in the resin in the vicinity of the four corners. The pins had sharpened points and these points would be the "transformation", or control points.

Fresh specimens

Four fresh human cadaver elbows were harvested from the South African Police Mortuary in Cape Town after obtaining permission from the Department of Forensic Medicine at the University of Cape Town. The four elbow joints (distal humerus and proximal ulna) were removed from four different cadavers and consisted of two left and two right elbows. All of the elbows were removed from the cadavers less than twenty four hours following death. The cadavers were chosen based upon the following criteria: no traumatic injury to the elbow joint, no degenerative joint disease, and normal appearance upon visual inspection.

Upon removal of the specimens, they were placed in a sealed plastic bag and stored in ice. All specimens were mounted under the reflex microscope prepared for observations within four hours of being removed. Each specimen was prepared for observation individually. The articular cartilage of the trochlea of the distal humerus was marked lightly with a felt-tipped marker to indicate the profiles to be digitised (Figure 3.6). Two pieces of welding rod were joined by another piece in the shape of an "H"; the four ends were cut to form sharp points and these formed

the four control points. This "H arrangement" was then inserted through two holes, drilled into the bone to a slightly smaller diameter so that a press-fit was achieved, and the rods were then bent to the position shown in Figure 3.6.

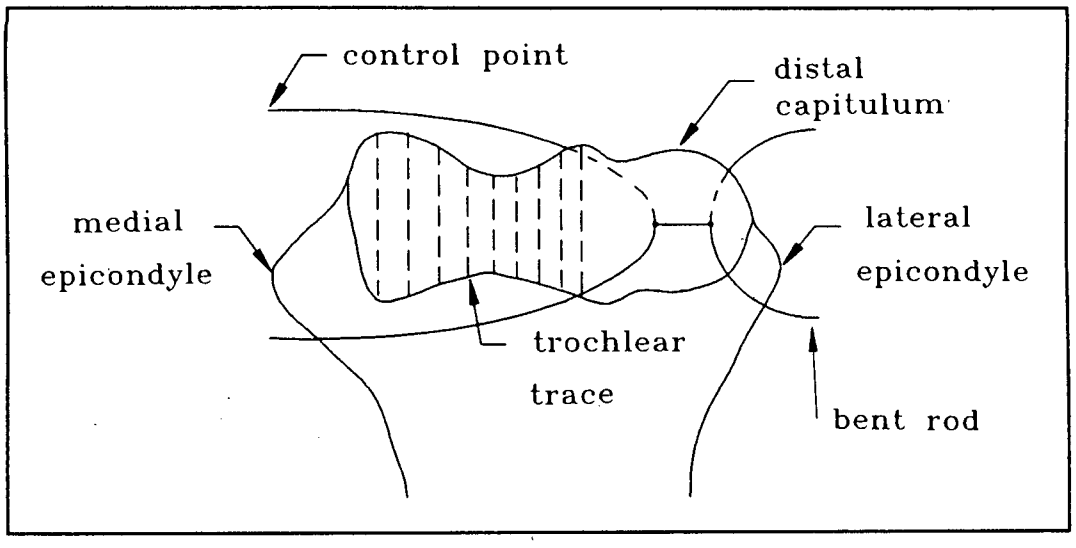

FIGURE 3.6. Humeral specimen prepared for observation (Anterior-posterior (A-P) view).

A similar process was followed for the proximal ulna. The articular surface was divided into two observation views - the coronoid and olecranon facets separated by the incisura trochlearis. The trochlear notch was marked with lines parallel to each other forming profiles in the sagittal plane. Welding rods with sharpened points were press-fitted into holes drilled through the radial notch, and then bent (Figure 3.7).

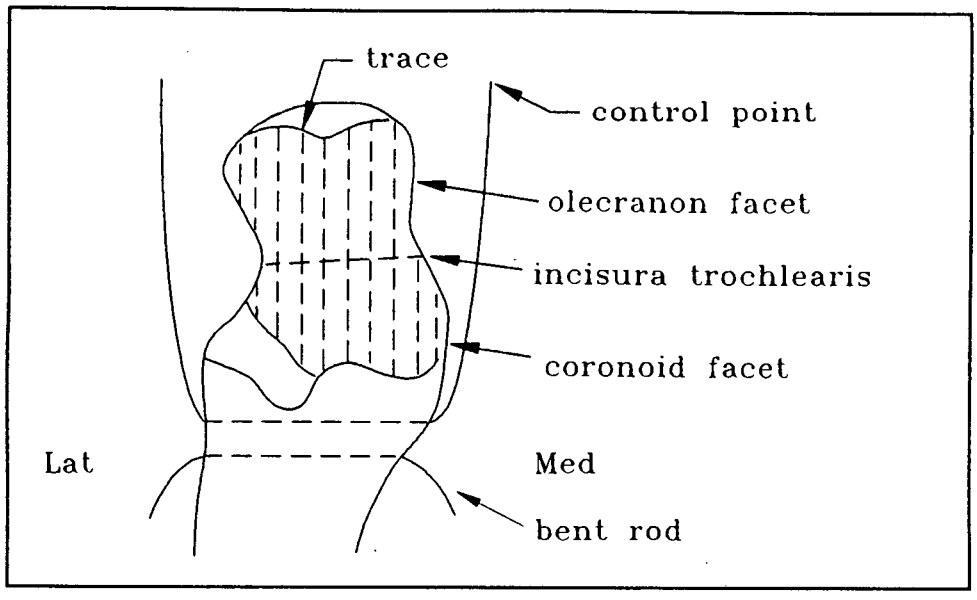

FIGURE 3.7. Ulnar specimen prepared for observation.

Steel pins were also inserted at several locations in the bone to give exact coordinates of extra-articular landmarks and also to act as backup control points should any of the original control points be displaced by accident. These pins were positioned at the medial and lateral epicondyle of the humerus and the most distal point of the capitulum. On the ulna, they were inserted at the olecranon and coronoid processes and the medial and lateral points of the incisura trochlearis.

Once the fresh specimen's articular surface was measured, the specimen was boiled in water until all of the cartilage was removed. The bone articular surface of the trochlea was then marked with a felt-tipped marker in the same way as the cartilage

surface was marked. The same procedure was followed for the ulna surface. During the boiling process, care was taken to avoid any movement of the control points.

After insertion of the rods, the specimens were mounted on the ball and socket articulation device, which was described previously for the dry bone mounting and shown in Figure 3.5.

3.4 DATA ACQUISITION SYSTEM

The microcomputer was an IBM PC 486. True Basic was used in conjunction with shell and communication support libraries. The steps involved in observing the joint, digitising a point, and storing the data are shown in the flow diagram in Appendix A. The distal humerus and the proximal ulna were both observed in two views. The distal humerus was observed firstly in the anterior view - the anterior half of the trochlea divided in half in the coronal plane. The four control points were digitised in a specific order from one to four. The measuring mark (illuminated optic fibre) was then placed on the articular surface by adjusting the X, Y, and Z adjusting screws. To digitise the point, the foot switch was depressed and the cartesian co-ordinates recorded and subsequently transmitted to the computer. When all of the profiles of the anterior articular surface had

been digitised, the data was stored on disk. Similarly, the posterior articular surface was observed and the data stored in a separate file on disk.

The same procedure was followed for the coronoid and olecranon facets of the ulna. The stored data was transferred to the microcomputer. The separate co-ordinate systems were then mathematically transformed into a single homogeneous co-ordinate system (i.e. the anterior and posterior views of the trochlea were combined to form a single complete view of the entire surface), using the transformation method in Appendix B.

3.5 MATHEMATICAL APPROXIMATION OF THE ARTICULAR SURFACES

3.5.1 Hyperbolic paraboloid hypothesis

The trochlea, divided into two equal halves (as the two views measured), appears to resemble the shape of a hyperbolic paraboloid (Figure 3.8). An attempt was thus made to find an equation defining the articular surfaces of the trochlea and proximal ulna that would give a geometrical approximation for the design of an anatomically exact prosthesis surface. The hyperbolic paraboloid was fitted to the data obtained from observations of the trochlea articular surface using the reflex microscope. A mathematical description of the trochlea and

proximal ulna could then satisfy the machining and manufacturing requirements of the articular surfaces of the prosthesis.

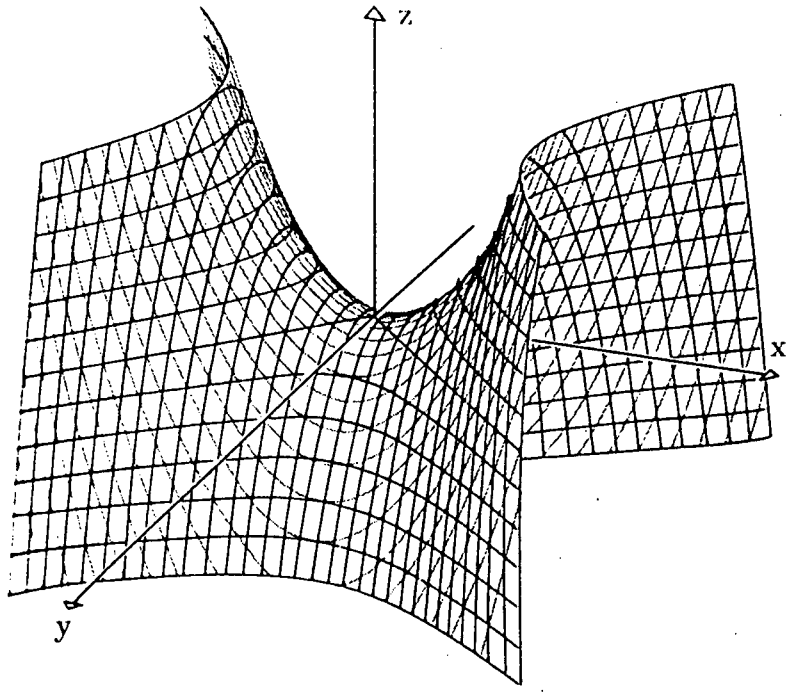

FIGURE 3.8. Hyperbolic paraboloid.

An attempt was also made to fit a hyperbolic paraboloid to the articular surface of the proximal ulna since this surface is the counterpart of the trochlea articular surface and a certain amount of congruency should exist. Shiba et al, 1988, suggests the possibility of two distinct bearing surfaces at the humero-ulnar articulation. This observation led to the fitting of the hyperbolic paraboloid to both the olecranon and coronoid surface.

Three trochlear bone articular surfaces and one trochlear

cartilaginous articular surface were used to test the validity of the hyperbolic paraboloid hypothesis. For the ulna, two surfaces of the following were used; olecranon, coronoid, and entire trochlear notch. A program, written in True Basic, was developed to fit the known equation of a hyperbolic paraboloid to the data obtained using the reflex microscope. The estimated errors for each point in the x, y, and z direction and the resultant error vectors were determined to indicate the quality of the fit.

Mathematical principles

The assumption is made that the co-ordinates of a number of points on the actual articular surface describe a surface in space close to a known quadric surface - the hyperbolic paraboloid. The method used to compare the theoretically designed surface and the observed co-ordinates, is a best fitting process using the methodology of least squares. The designed surface is fitted to the reflex microscope co-ordinates, and the adjusted co-ordinates and their residual errors are then determined. The methodology was adapted from, and employed by, Fotiou et al, 1991, who used this procedure to verify if the design of a constructed dome was close to an elliptic paraboloid.

The geometry and the reference systems of the hyperbolic paraboloid are shown in Figure 3.9. If the system O(X,Y,Z) is considered parallel to the T(x,y,z) system, the equation is

written in the form

$$\left(\frac{x-x_0}{a}\right)^2 - \left(\frac{y-y_0}{b}\right)^2 - \frac{z-z_0}{c} = 0 \ ,$$

where x_0, y_0, z_0 are the real co-ordinates of the origin 'O' with respect to the T(x,y,z) system. The parameters **a**, **b**, and **c** define the shape of the hyperbolic paraboloid while x_0, y_0, z_0 define its position in space.

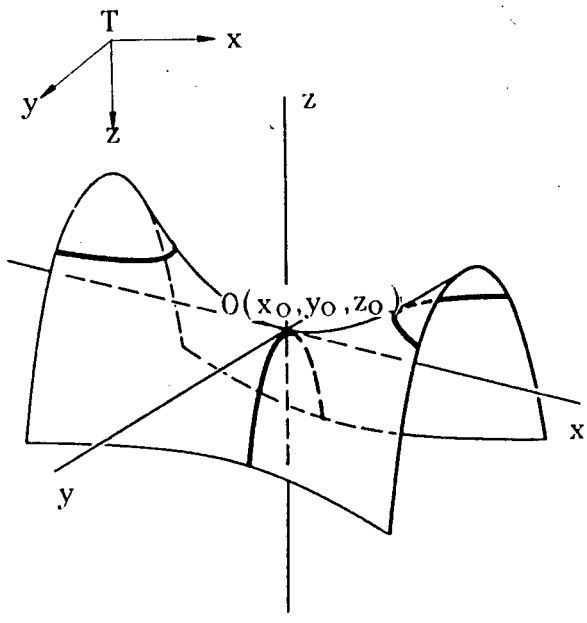

FIGURE 3.9. The geometry and reference systems of the hyperbolic paraboloid. (Adapted from Anton, 1984).

The best fit process, as an optimization problem described by Fotiou et al, 1991, can be found in Appendix C.

Results

The estimated errors indicate that the fit of the hyperbolic paraboloid to the trochlear articular surface is not acceptable. Figure 3.10 shows the locations where the co-ordinates formed profiles in the xz-plane, and Table 3.1 lists the mean resultant errors for the points forming the respective traces.

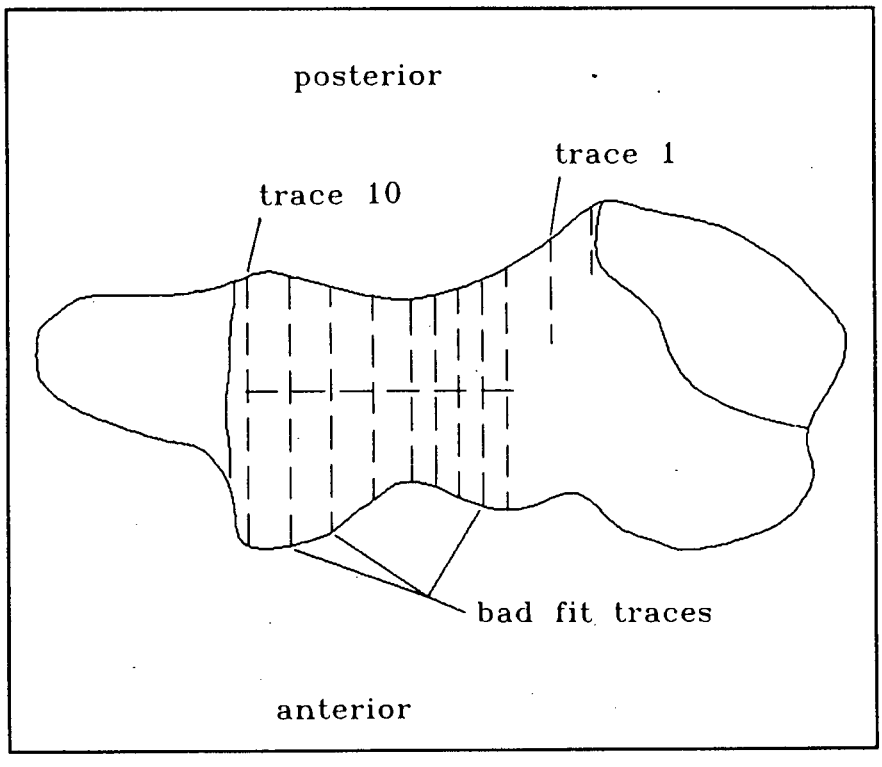

FIGURE 3.10. Profiles of the trochlea with the traces of bad fit. (Errors are presented in Table 3.1).

MEAN RESULTANT ERROR (mm)										
Trace	1	2	3	4	5	6	7	8	9	10
Ant.	.44	.49	.50	.56	.31	.51	.88	.41	1.08	
Post.	.40	.38	.33	.43	.21	.75	.81	.27	.82	.42

TABLE 3.1. The mean resultant errors for the fitting of the hyperbolic paraboloid to the trochlea. Average number of points digitised: 120.

These initial results indicate that a desirable fit would not be achieved and errors in the one millimetre size were found in the regions where the flanges appear to slope away from the curve.

Since the fit to the trochlea surface was not acceptable, a good fit to the ulnar articular surfaces was not expected. This was the case, with the estimated errors for the entire ulnar surface, and the olecranon and coronoid surfaces being similar to those reported for the trochlea (Table 3.2).

	ENTIRE ULNA	OLECRANON	CORONOID
Error (mm)	.53	.57	.62

TABLE 3.2. The mean resultant errors for the fitting of the hyperbolic paraboloid to the proximal ulna.

3.5.2 Circularity hypothesis

Observations (XYZ co-ordinates) of the profiles shown in Figure 3-11 were made using the reflex microscope. Using these co-ordinate values an attempt was made to fit a circle to the sagittal plane profiles of the trochlea, entire ulna, olecranon, and coronoid articular surfaces.

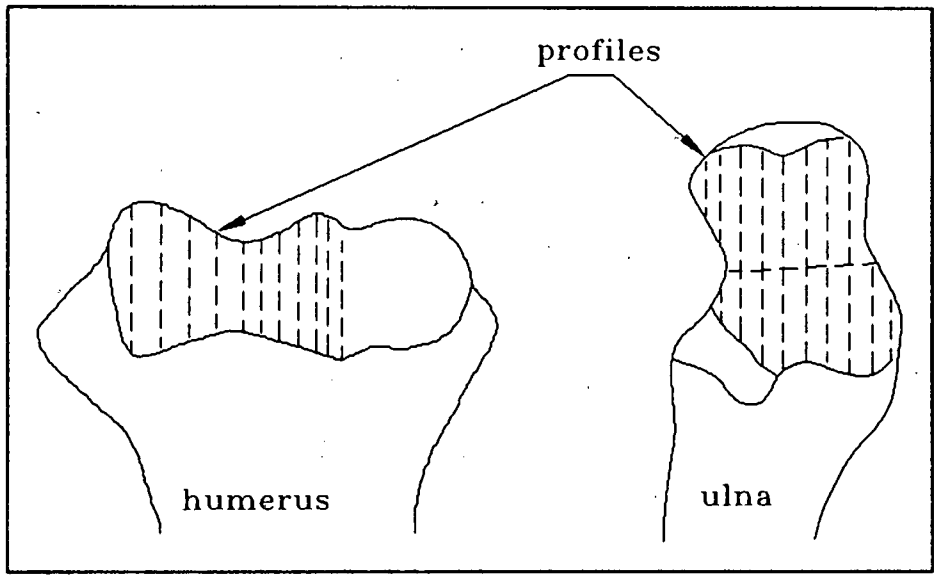

FIGURE 3-11. Trochlea and trochlear notch profiles.

The co-ordinates of the centre of the circle, and the radius of the circle, from the observation of points on the profile were determined using the mathematical method in Appendix D. The

residual differences (i.e the vector distance between the actual measured point and calculated point of the mathematically defined radius) were calculated for each point on the profile to indicate the appropriateness of the fit.

To test the validity of the circle theory, eleven trochlear (seven bone, four fresh (i.e. with cartilage)), seven proximal ulnar (three bone, four fresh), seven olecranon (three bone, four fresh), and seven coronoid (three bone, four fresh) articular surfaces were measured.

Results

The diameter, the centre of the circle, and standard error for each profile, and the residual errors for each point on those profiles, were determined.

Trochlea

The standard errors of a single observation for each profile of the observed specimens have been tabulated (Table 3.3).

STANDARD ERROR OF A SINGLE OBSERVATION (mm)										
Trace	1	2	3	4	5	6	7	8	9	10
Bone Spec.										
1	.2				.2				.2	
2	.1		.1		.0		.0		.0	
3	.25		.09		.06		.14		.26	
4	.14		.19		.24		.35		.54	
F1	.28	.22	.31	.34	.28	.28		.38	.60	.04
F3	.30	.19	.17	.06	.09	.21	.16	.13	.12	.10
F4	.30	.14		.11	.12	.10		.16	.35	.06
Fresh Spec.										
F1	.21	.19	.19	.11	.09	.13		.14	.27	.04
F2	.08	.09	.09	.05	.05	.09	.12	.24	.48	.04
F3	.16	.04	.09	.06	.11	.12	.15	.15	.24	.07
F4	.33	.26	.24	.16	.15	.06	.10	.17	.21	.06

TABLE 3.3. The standard errors for the fitting of a circle to the trochlea.

A study of the magnitude of these deviations indicate a strong support for the circle theory. The observations for the fresh cartilaginous specimens displayed small deviations with 99.4 percent of the individual residual errors being less than 0.50 mm.

The calculated centres for each trochlear profile lay within an area of less than 1 mm diameter for both the bone and

cartilaginous specimens. The X,Y,Z co-ordinates of the calculated circle centres of the specimens were plotted and the three-dimensional plot of a specimen is shown in Figure 3.12. The circle centres lie virtually on a straight line except for the posterior lateral flange section which is seen in the plot as the first two co-ordinates.

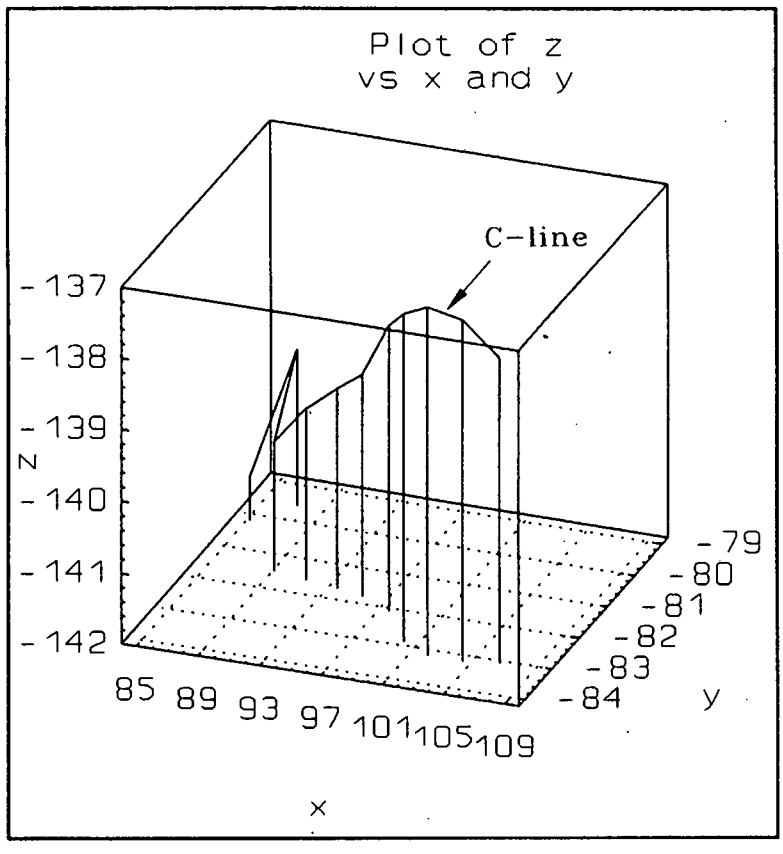

FIGURE 3.12. Calculated circle centres of the trochlea.

The circle centres of each profile were then fitted to a straight line. Figure 3.13 shows the circle centres of the

trochlea without the posterior lateral flange section and indicates the fitted circle centres on a straight line, which will be called the C-line (centre-line).

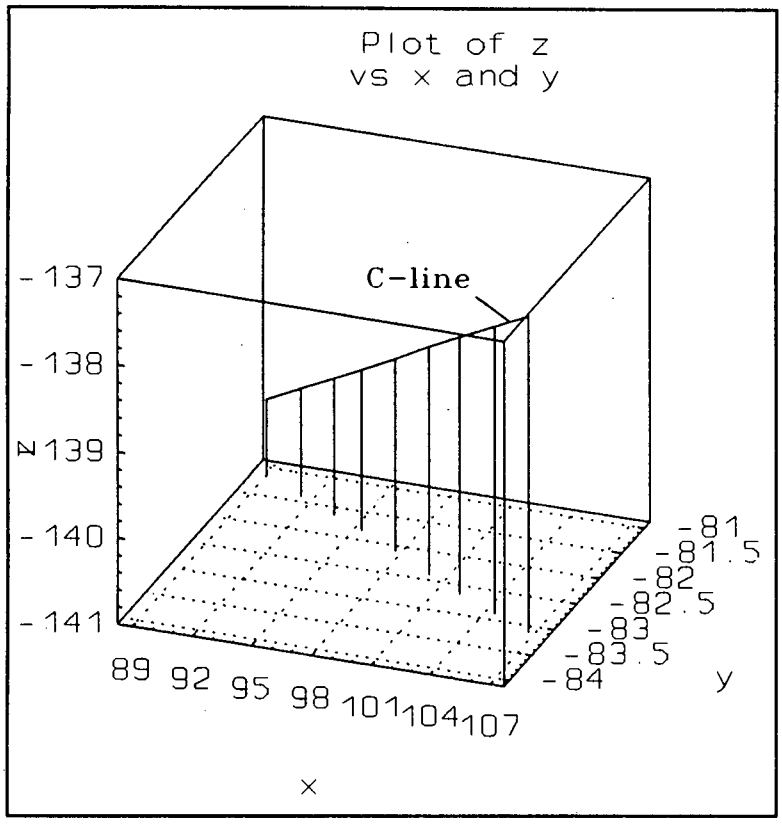

FIGURE 3.13. Fitted circle centres of the trochlea.

From an anterior view (Figure 3.14), the centre-line sloped down toward the medial side at an angle of 2 degrees to the epicondylar line and 3 degrees to the trochlear groove. From a distal view, the centre-line ran parallel to the epicondylar

line.

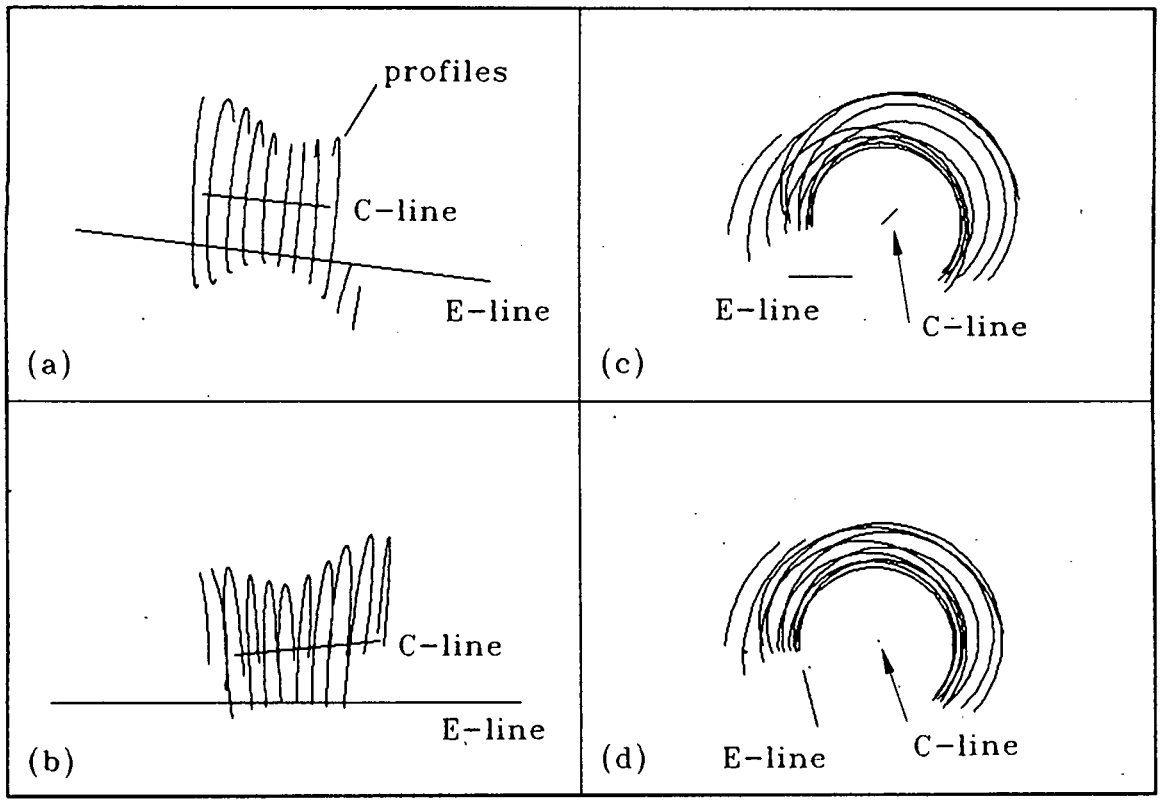

FIGURE 3.14. Views of the trochlear articular surface: (a) distal-proximal, (b) anterior-posterior, (c) medio-lateral, (d) true lateral.

Ulna

The standard errors of a single observation for each profile of the entire ulnar articular surface are tabulated in Table 3.4.

STANDARD ERROR OF A SINGLE OBSERVATION (mm)										
Trace	1	2	3	4	5	6	7	8	9	10
Bone Spec.										
F2	.31	.24	.36	.35	.31	.29	.24	.13		
F3	.09	.06	.37	.37	.46	.56	.41	.36	.22	.12
F4	.08	.14	.13	.37	.35	.38	.37	.20	.33	.19
Fresh Spec.										
F1	.16	.06	.29	.24	.07	.22	.06	.29	.12	
F2	.10	.35	.12	.21	.13	.07	.09			
F3		.11	.33	.22	.17	.13	.13	.23	.21	.10
F4		.05	.33	.25	.14	.12	.21		.14	.10

TABLE 3.4. The standard errors for the fitting of a circle to the entire proximal ulnar articular surface.

The co-ordinates of the calculated circle centres are shown in Figure 3.15.

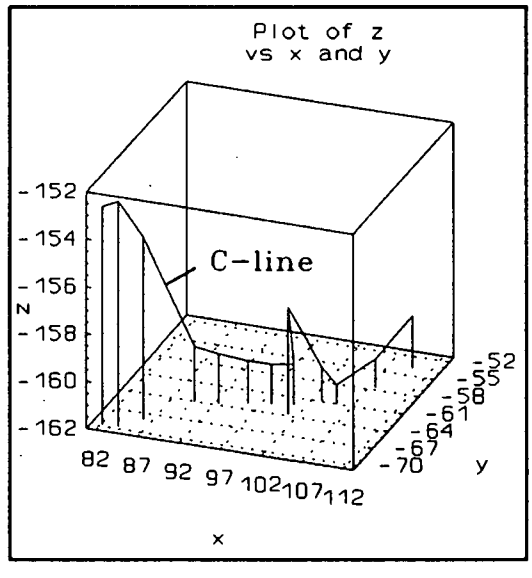

FIGURE 3.15. Calculated circle centres of the trochlear notch.

Although the magnitude of the deviations show support for the profiles of the entire surface being circular, the olecranon sulcus and the coronoid sulcus (Tables 3.5 and 3.6) display a stronger support for the circle theory.

STANDARD ERROR OF A SINGLE OBSERVATION (mm)										
Trace	1	2	3	4	5	6	7	8	9	10
Bone Spec.										
F1	.10	.15	.12	.17	.13	.08	.06			
F2	.03	.12	.08	.08	.11	.05				
F3	.14	.13	.04	.09	.16					
Fresh Spec.										
F1	.03	.06	.04	.04	.08	.09	.12	.06	.04	
F2	.05	.25	.02	.11	.06	.07	.09			
F3	.05	.06	.11	.14	.11	.08	.04	.05	.06	.05
F4	.04	.06	.05	.03	.02	.05	.04	.15	.05	.02

TABLE 3.5. The standard errors for the fitting of a circle to the olecranon articular surface.

The observations of the coronoid sulcus cartilaginous surface had 99.7% of the individual residual errors less than 0.20 mm. The olecranon sulcus revealed a 99% residual error of less than 0.20 mm.

STANDARD ERROR OF A SINGLE OBSERVATION (mm)										
Trace	1	2	3	4	5	6	7	8	9	10
Bone Spec.										
F1	.03	.07	.03	.07	.12	.14	.12			
F2	.16	.09	.08	.23	.14	.04				
F3	.10	.05	.05	.06	.06	.09	.17			
Fresh Spec.										
F1	.06	.11	.14	.07	.05	.06	.04			
F2	.01	.04	.06	.06	.05					
F3	.05	.06	.10	.04	.07	.13	.03	.03	.07	
F4	.05	.06	.05	.05	.10	.06	.03	.04	.02	.01

TABLE 3.6. The standard errors for the fitting of a circle to the coronoid articular surface.

The three-dimensional plots of a typical coronoid sulcus indicating the co-ordinates of the calculated and fitted circle centres of the profiles are shown in Figures 3.16 and 3.17.

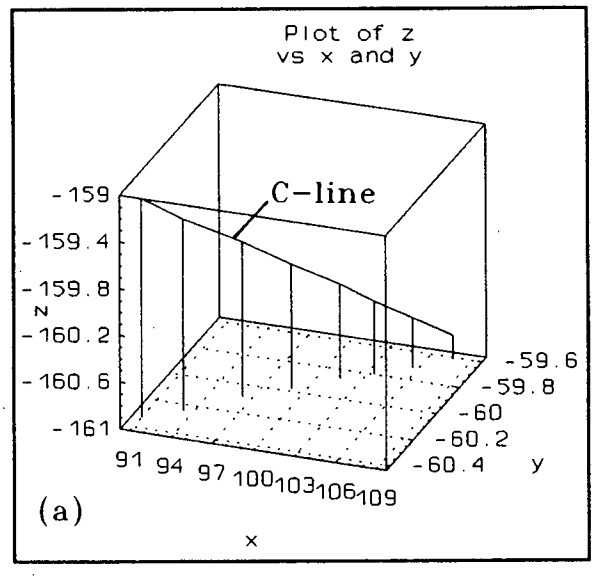

FIGURE 3.16 (a). Fitted circle centres of coronoid sulcus.

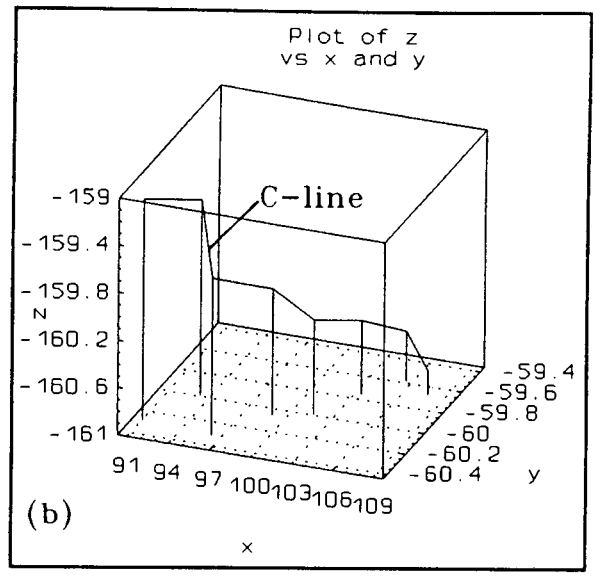

FIGURE 3.16 (b). Calculated circle centres of the coronoid sulcus articular surface.

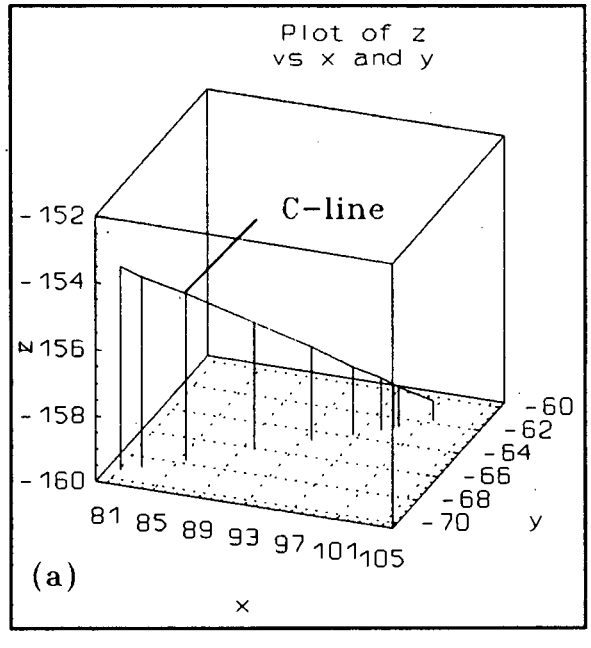

FIGURE 3.17 (a). Fitted circle centres of the olecranon sulcus articular surface.

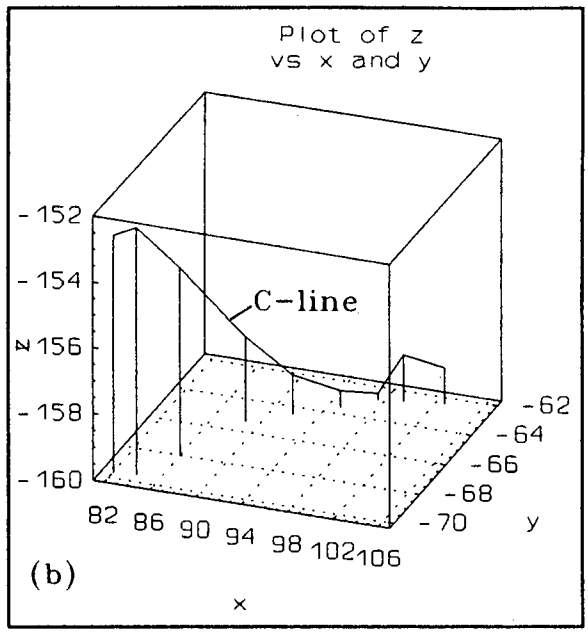

FIGURE 3.17 (b). Calculated circle centres of the olecranon sulcus articular surface.

Figure 3.18 displays the two distinct centre lines of the olecranon sulcus and the coronoid sulcus. When viewed from a proximal distal direction, the curvature of the coronoid and olecranon surfaces faces a slightly lateral direction. From an anterior aspect, the centre lines of both the olecranon and coronoid surfaces sloped down toward the lateral side.

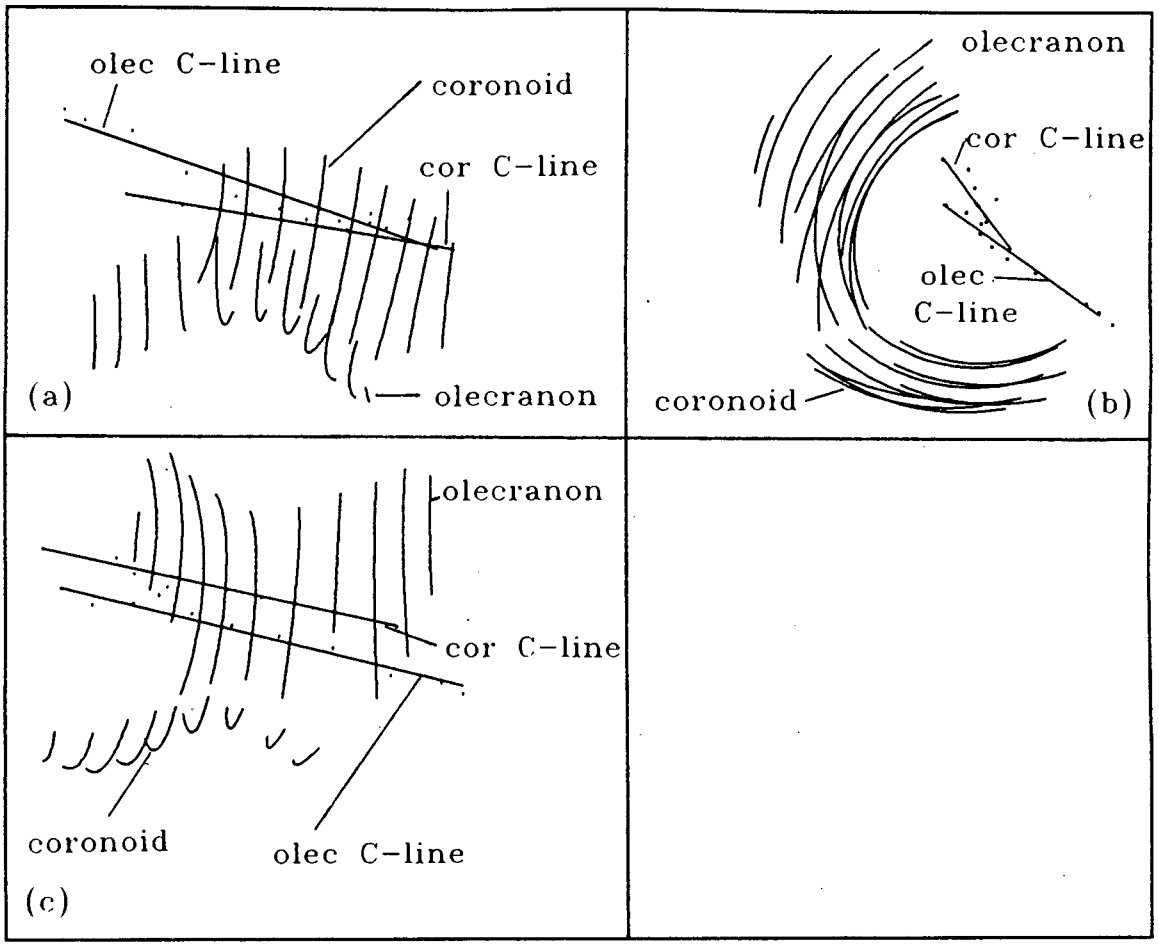

FIGURE 3.18. Views of the olecranon and coronoid articular surfaces; (a) proximal-distal, (b) anterior-posterior, (c) lateral.

These results indicate that in the design of the prosthesis a single axis of rotation should exist in the humeral component and the ulnar component must have two distinct bearing surfaces. The humeral component should also have a posterior lateral flange section with a deviated centre of curvature.

The prosthesis articular surfaces were reconstructed on

computer using AutoCAD (Figures 3.19 and 3.2)) and the radii of curvature determined.

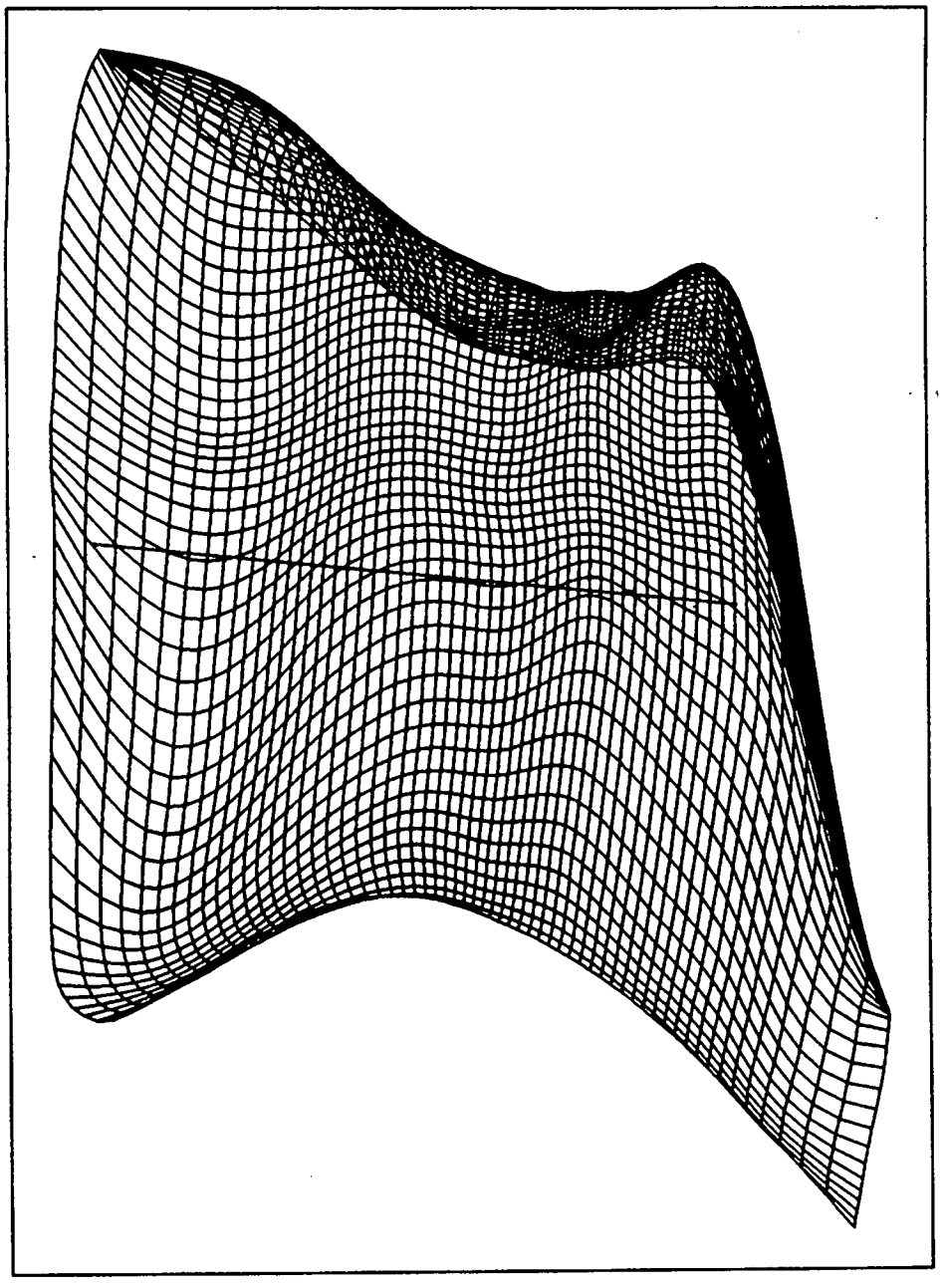

FIGURE 3.19. Computer reconstruction of trochlear articular surface with C-line.

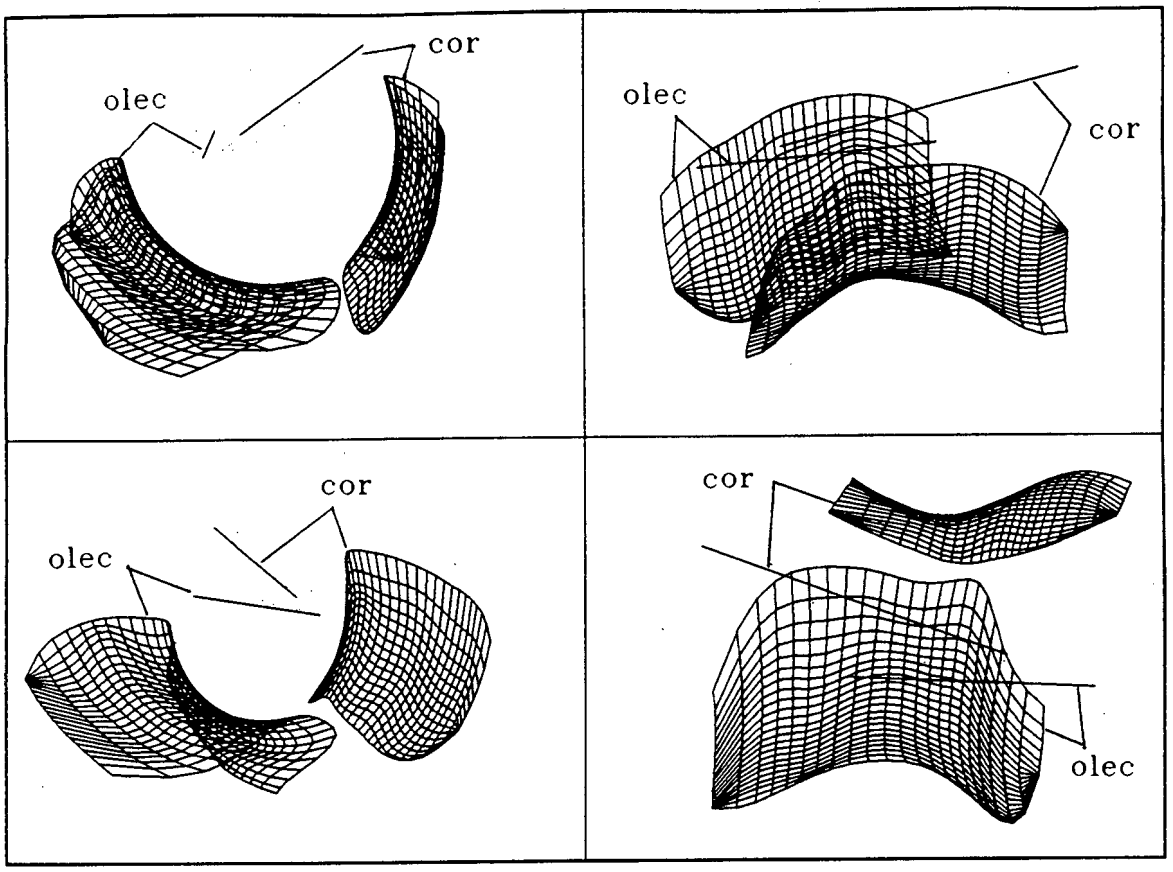

FIGURE 3.20. Computer reconstruction of the olecranon and coronoid articular surfaces with C-lines indicating in different views the noncoincidence of the olecranon and coronoid C-lines.

The centre-line with the radii of curvature for the articular surfaces of the humeral component and ulnar component are shown in Figures 3.21 and 3.22.

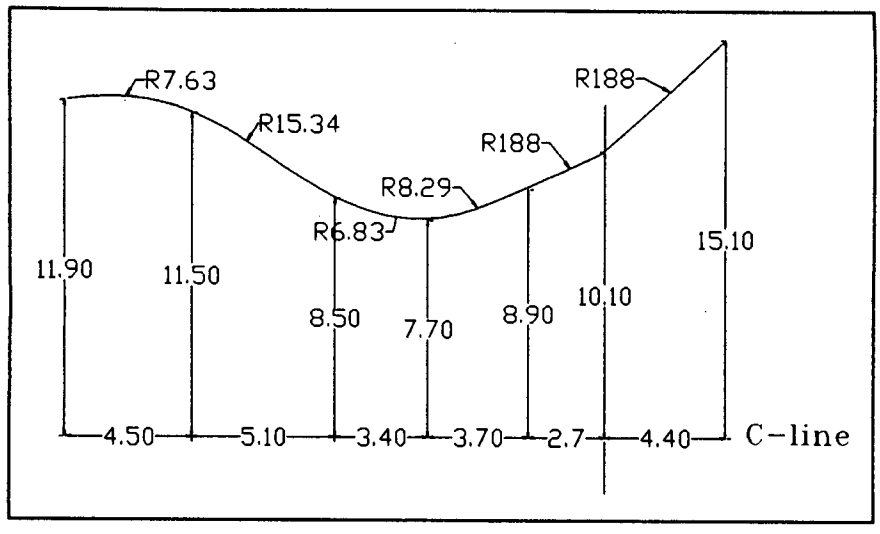

FIGURE 3.21. Radii of curvature of the humeral component articular surface.

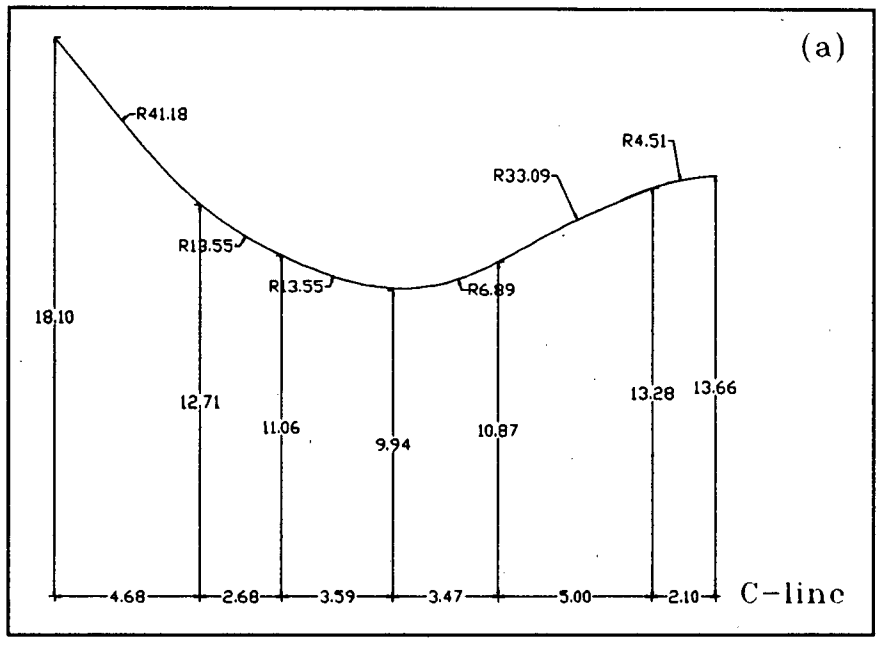

FIGURE 3.22 (a). Radii of curvature of the ulnar component: olecranon articular surface.

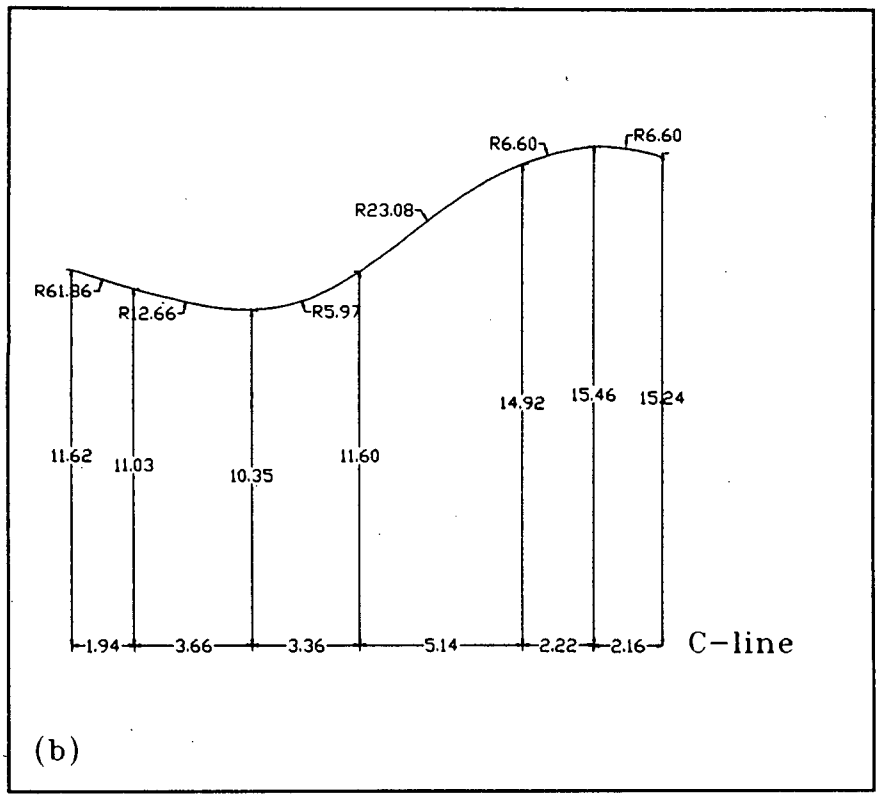

FIGURE 3.22 (b). Radii of curvature of the ulnar component: coronoid articular surface.

3.5.3 Helix hypothesis

A similar method to that used in the preceding section was used to determine if the structure has the form of a circular helix. Two trochlear bone articular surfaces and the humeral component of a commercially available helical prosthesis were used for this analysis.

The specimens were secured above an inclined two-mirror system to allow for a 360 degree view of the trochlea (Figure 3.23). Two steel rods were fixed above the mirrors to support the specimens and four points of cut and sharpened pins were attached to the rods to be control points. The specimen was placed on the two rods with the distal part of the trochlea facing upwards. Two lines equidistant medially and laterally and running parallel to the trochlear groove were marked on the specimens to indicate the position and orientation of the assumed helix.

The top view was measured first, and then the mirror images of the anterior and posterior views. The three-dimensional co-ordinates of the three views were measured and recorded to three separate files with independent orthogonal co-ordinate systems. The separate co-ordinate systems were then transformed into a single "homogeneous" co-ordinate system using the transformation method in Appendix B.

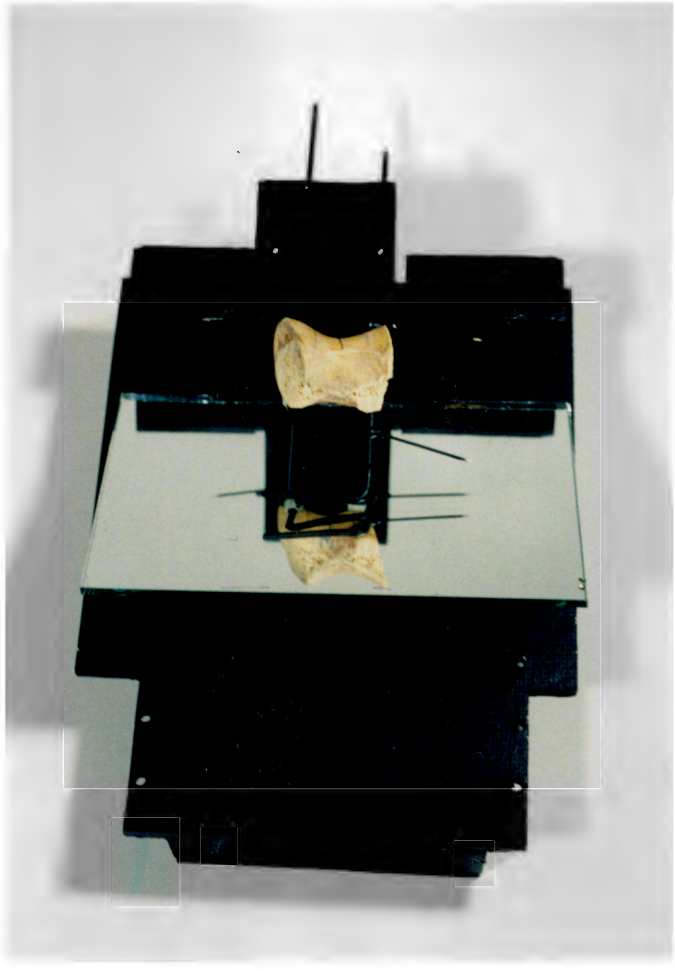

FIGURE 3.23. Mirror system used for observations.

Mathematical principles

The x,y,z co-ordinates of observations which lie on a helix may be defined mathematically, in parametric form by the constants **a** and **b** and the parameter θ in the following:

$$x = a \sin(\theta)$$

$$y = a \cos(\theta)$$

$$z = b(\theta).$$

a is the radius of the cylinder on which the helix lies (Figure 3.24), **b** is a function of the angle with which the helix cuts the cylinder and is a measure of the tightness of coiling, and θ is the angle in radians.

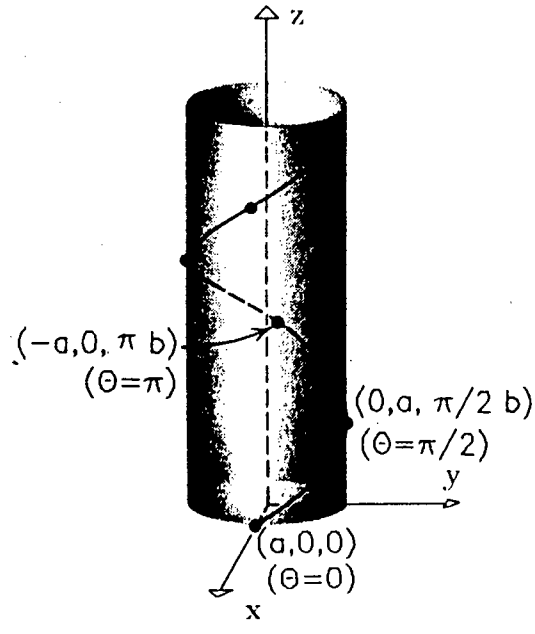

FIGURE 3.24. The geometry of the circular helix. (Adapted from Anton, 1984).

From the three-dimensional measurements, it was then possible to mathematically derive the constants **a** and **b** and the parameter θ for each helix using the theory of least squares.

A method similar to that in Appendix D was used to derive the axis passing through the centre of the trochlea using the least squares method of the measures of the radius **a**. Having

determined **a**, θ could then be calculated for each point using $x = a \sin(\theta)$ and $y = a \cos(\theta)$. **b** could then be calculated according to the definition of the helix: $z = b(\theta)$.

A measure of the validity of the helix hypothesis would be to study the magnitude of the residual differences (i.e. the vector distance between the actual measured point and the calculated point of the "best fit" helix) in each case.

Results

The residual errors of the components (dx, dy, dz) of the individual observations were determined and the mean residual errors for the two specimens and one prosthesis have been tabulated (Table 3.7).

MEAN RESIDUAL ERRORS (mm)			
	Dx	Dy	Dz
Prosthesis	.11	.13	.59
Specimen A	.32	.45	6.69
Specimen B	.30	.28	4.60

TABLE 3.7. The mean residual errors of the fitting of a helix to the trochlear groove.

A study of the magnitude of these deviations indicate that the prosthesis type which includes a helix in its design does indeed have the form of a circular helix. The calculated angle of inclination for the prosthesis was 10.3 degrees.

The magnitude of the Dz component (6.69 mm and 4.60 mm) of the two bone specimens reveal that the trochlea is not helical in form. The large residual errors of the two specimens when compared to the error of the known helical design of 0.59 mm further suggests that the anatomical specimens are not helical in form.

The results indicate that there is no helical motion taking place about the trochlea, but that the trochlear groove is inclined at an angle in the anterior posterior aspect. When viewed from a distal aspect, the trochlear groove plane is perpendicular to the trochlea centre line (Figure 3.25).

Thus, in the design of the humeral component a 3 degree inclination angle will be included in the anterior-posterior aspect, and in the distal-proximal aspect the trochlear groove will lie perpendicular to the C-line.

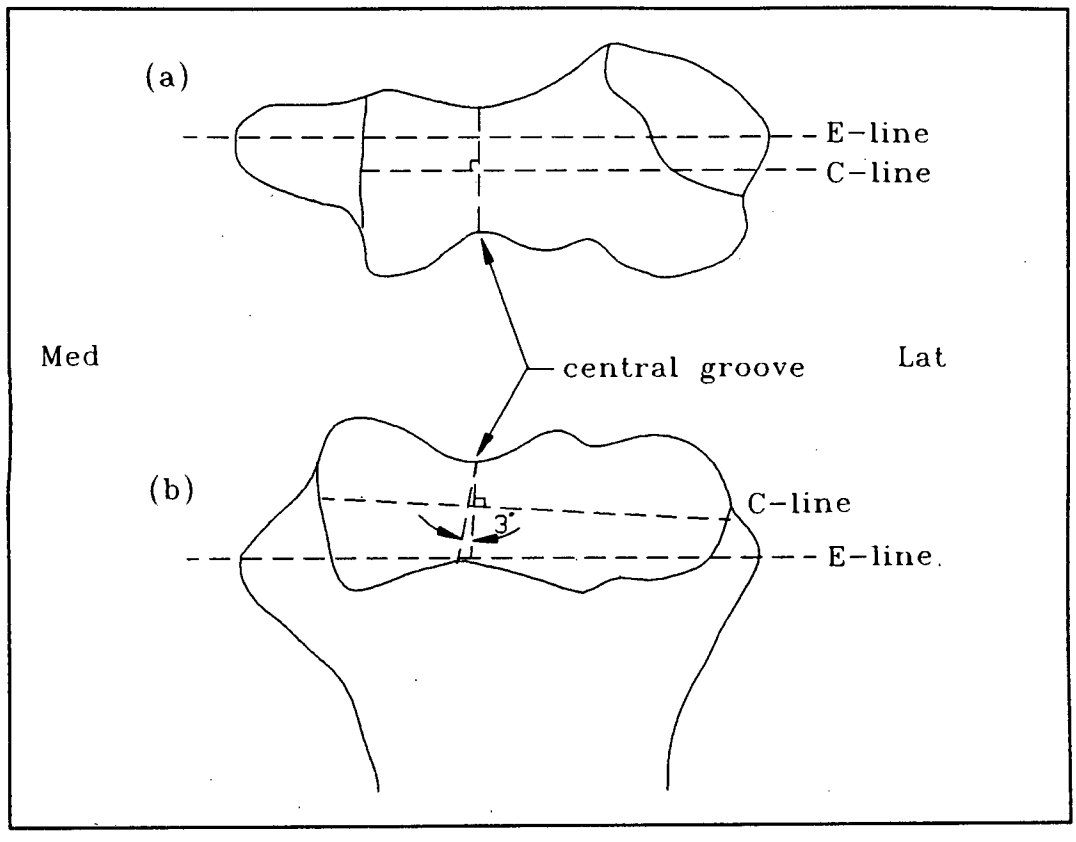

FIGURE 3.25. Inclination angle of the trochlear groove; (a) proximal-distal view, (b) anterior-posterior view.

3.6 CARTILAGE THICKNESS

Using the biostereometric technique, the precise three-dimensional topography of the cartilage and bone articular surfaces of the elbow joint has been obtained. Following this, the cartilage thickness of the trochlea and ulnar facets was determined.

This information will aid in: (1) obtaining an accurate three-dimensional model of the elbow joint, (2) development of an anatomically accurate artificial joint.

In considering the variations of cartilage thickness over the surfaces, it is hypothesized that areas of thicker cartilage correspond to increased weight bearing areas (Stockwell, 1987). This will assist in determining areas of increased or decreased loading for consideration in prosthesis design. The thickness of the cartilage will be included in the design and the thickness data will help provide accurate design specifications with regard to articular surface and subchondral bone geometries.

Methods

Two trochlea, two olecranon facets, and two coronoid facets from the fresh specimens were included in this part of the study. The data obtained from the three-dimensional observation of the cartilage and underlying bone surfaces using the reflex microscope was used to determine the cartilage thickness.

The x,y,z co-ordinates, and the four common control points, of the cartilage and bone surfaces of each specimen were stored in separate files. The bone surfaces of each specimen were then transformed onto the respective cartilage surfaces using the transformation method described in Appendix B.

Each specimen now had two data files (cartilage and bone surfaces) with a single "homogeneous" co-ordinate system. A SACLANT program called GRIDDER was executed to take the arbitrarily spaced data of each file and interpolate it onto a rectangular equidistant grid. A brief description of the interpolation algorithm and the parameters that control it can be seen in Appendix E. Each specimen now had two gridded data files (cartilage and bone surfaces) with identical grid parameters. A total of 3600 grid points (nodes) for each surface now existed with common equidistant X and Y values (example - Figure 3.26).

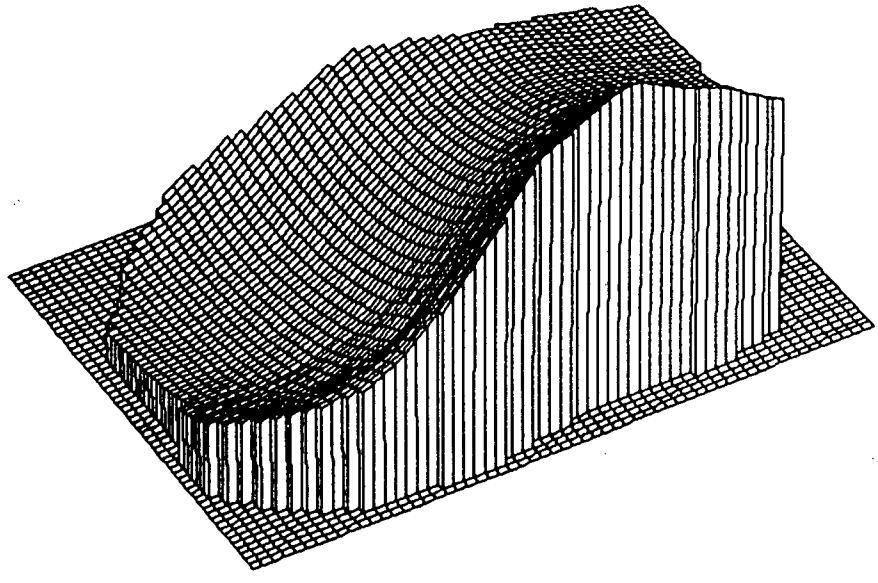

FIGURE 3.26. Three-dimensional plot of gridded cartilage surface (coronoid facet).

A program was written in Fortran to subtract the Z values of the corresponding cartilage and bone nodes and these values represented the cartilage thickness of the surface of this specimen (Figure 3.27).

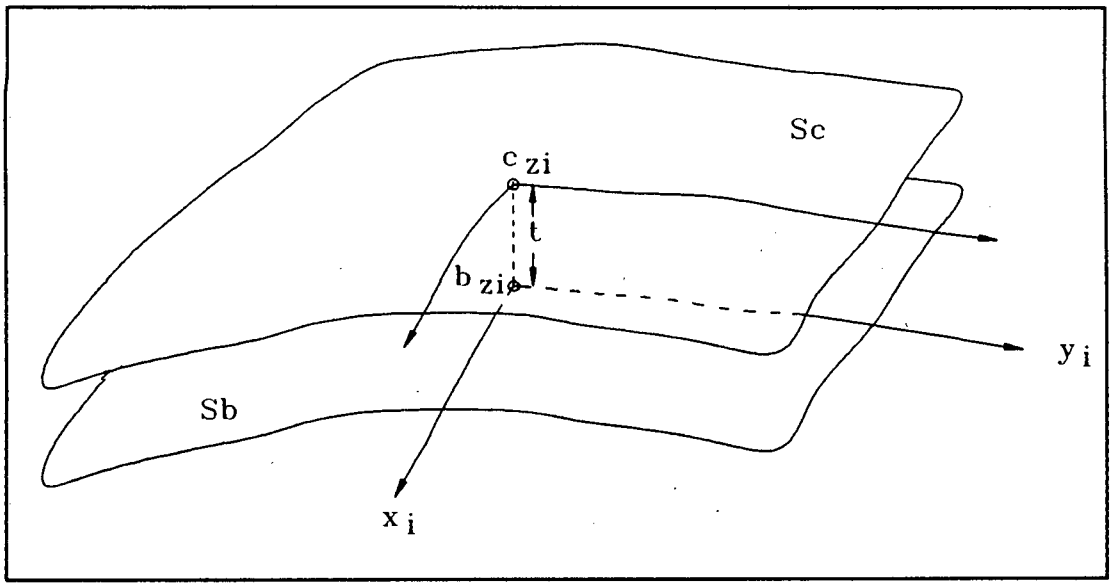

FIGURE 3.27. Cartilage thickness at a corresponding cartilage and bone node ($\mathbf{c}_{zi}$, $\mathbf{b}_{zi}$) on the joint surface: **Sc**, cartilage surface; **Sb**, bone surface; **t**, thickness.

Results

Contour plots of each of the anterior and posterior trochlea, coronoid facets, and olecranon facets of the cartilage thickness were constructed from the data. These plots serve as

maps of the cartilage thickness and will allow exact distance and height (thickness) measurements of different points on the articular surfaces.

Three-dimensional computer images and grey-shaded plots demonstrating the variation of cartilage thickness over the various surfaces have been generated as another method of presenting the data.

The various images and plots of the cartilage thickness of a fresh specimen are presented in the Figures (3.28 - 3.31).

(a)

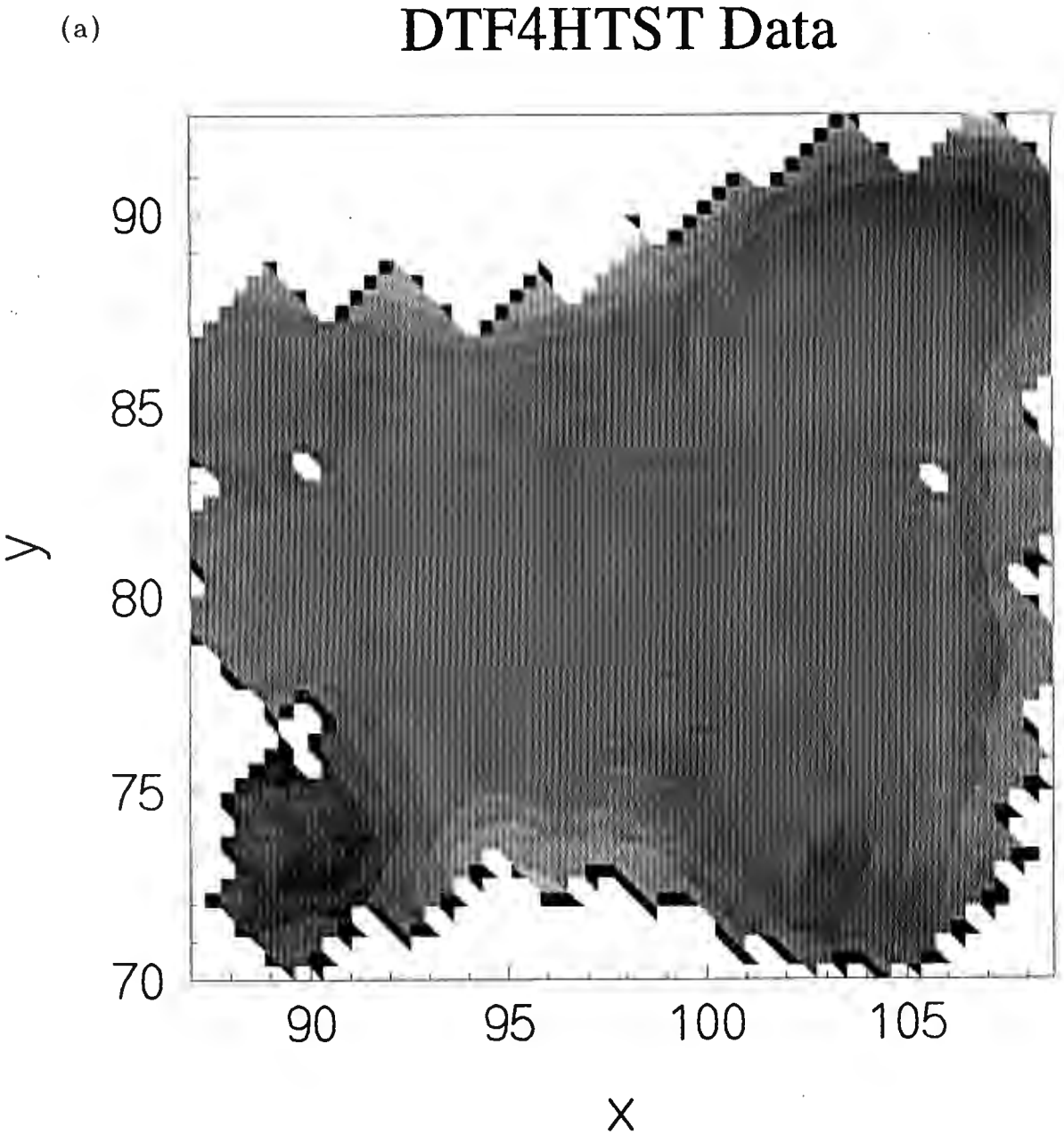

FIGURE 3.28 (a). Grey-shaded plot of anterior trochlea cartilage thickness.

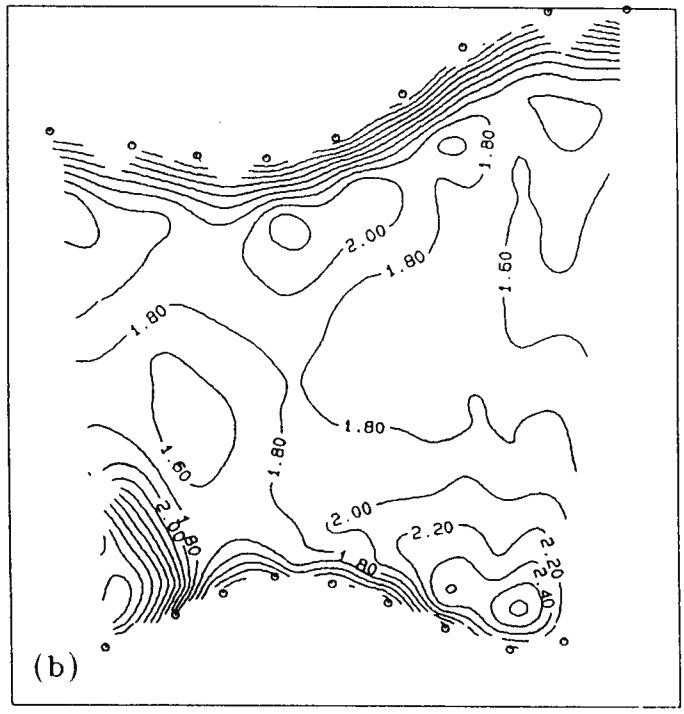

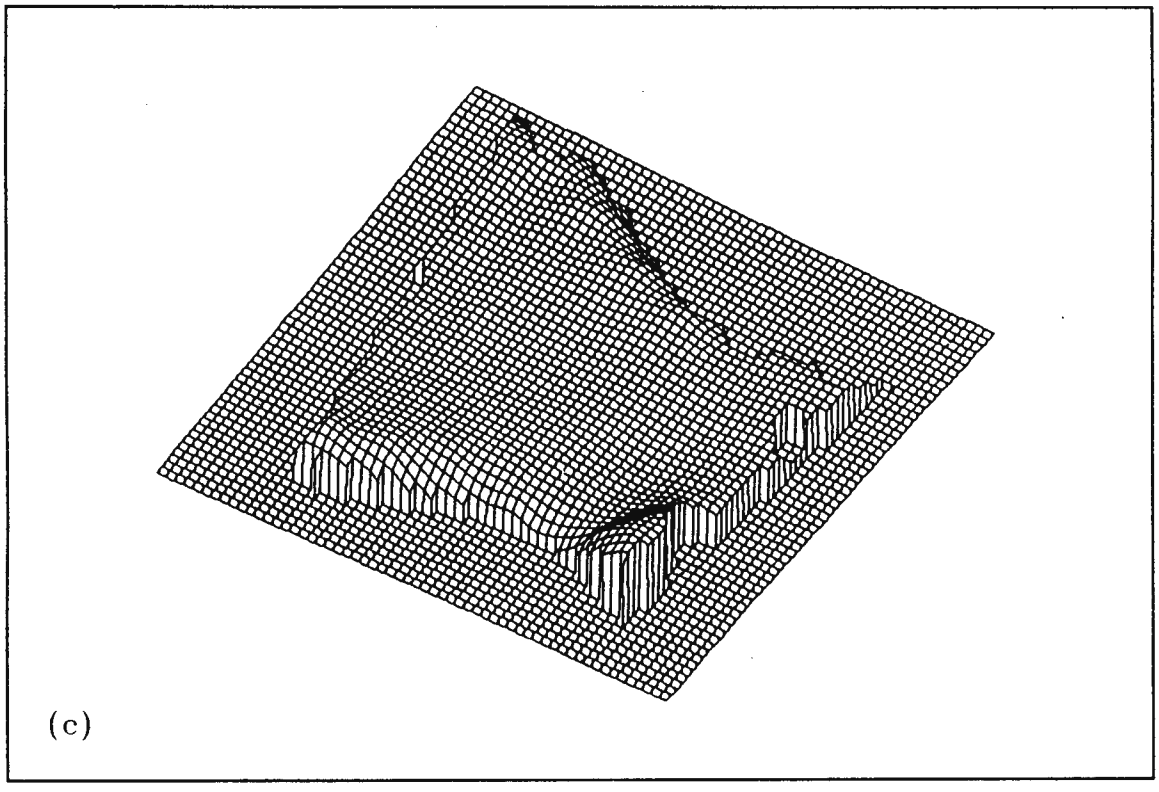

FIGURE 3.28. Anterior trochlea cartilage thickness: (b) contour plot, (c) 3-d representation.

(a)

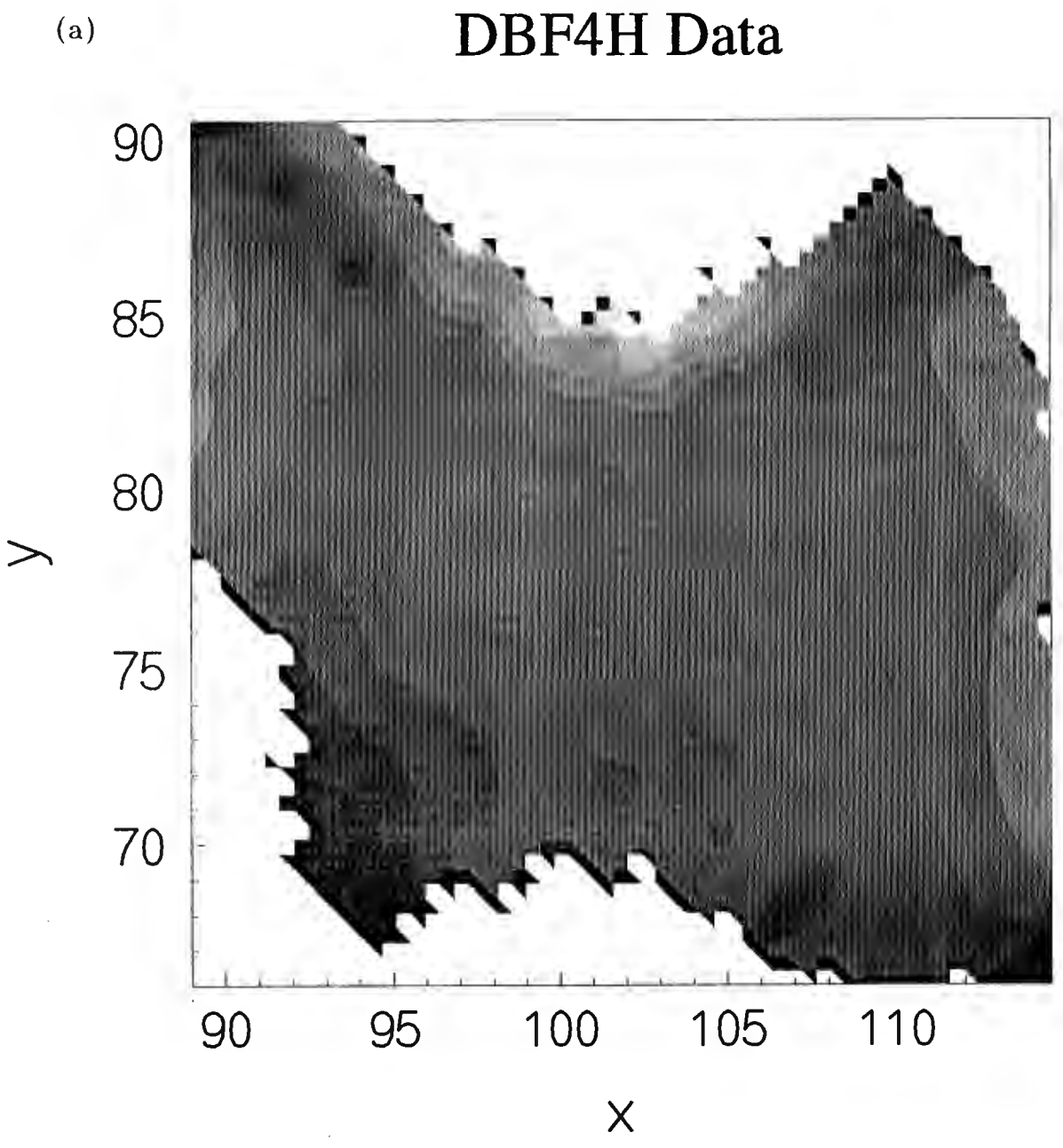

FIGURE 3.29 (a). Grey-shaded plot of posterior trochlea cartilage thickness.

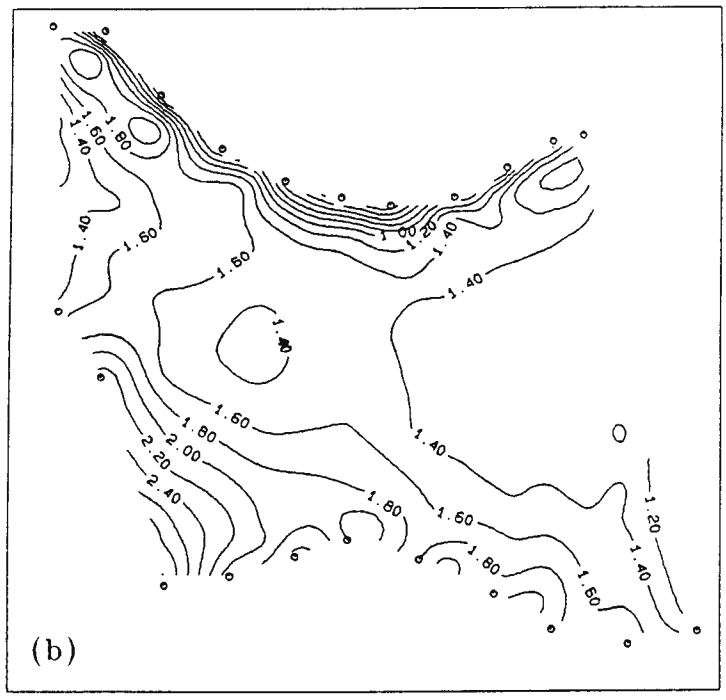

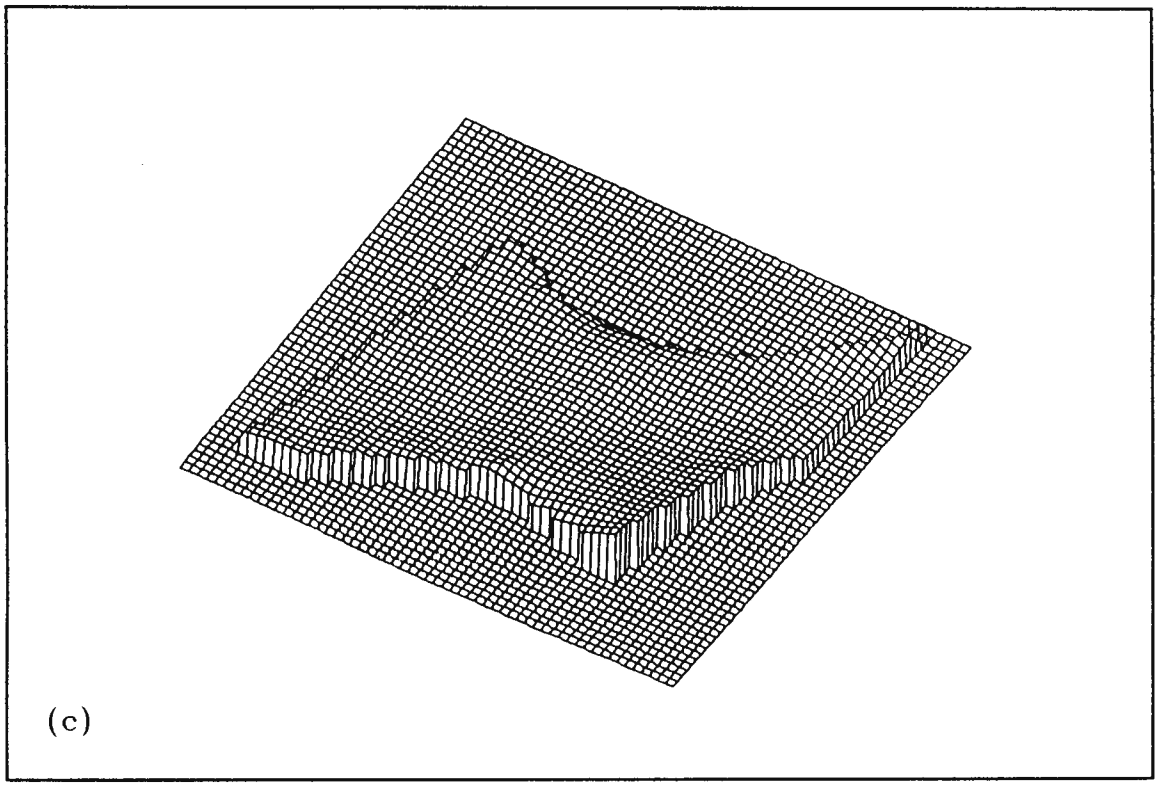

FIGURE 3.29. Posterior trochlea cartilage thickness: (b) contour plot, (c) 3-d representation.

(a)

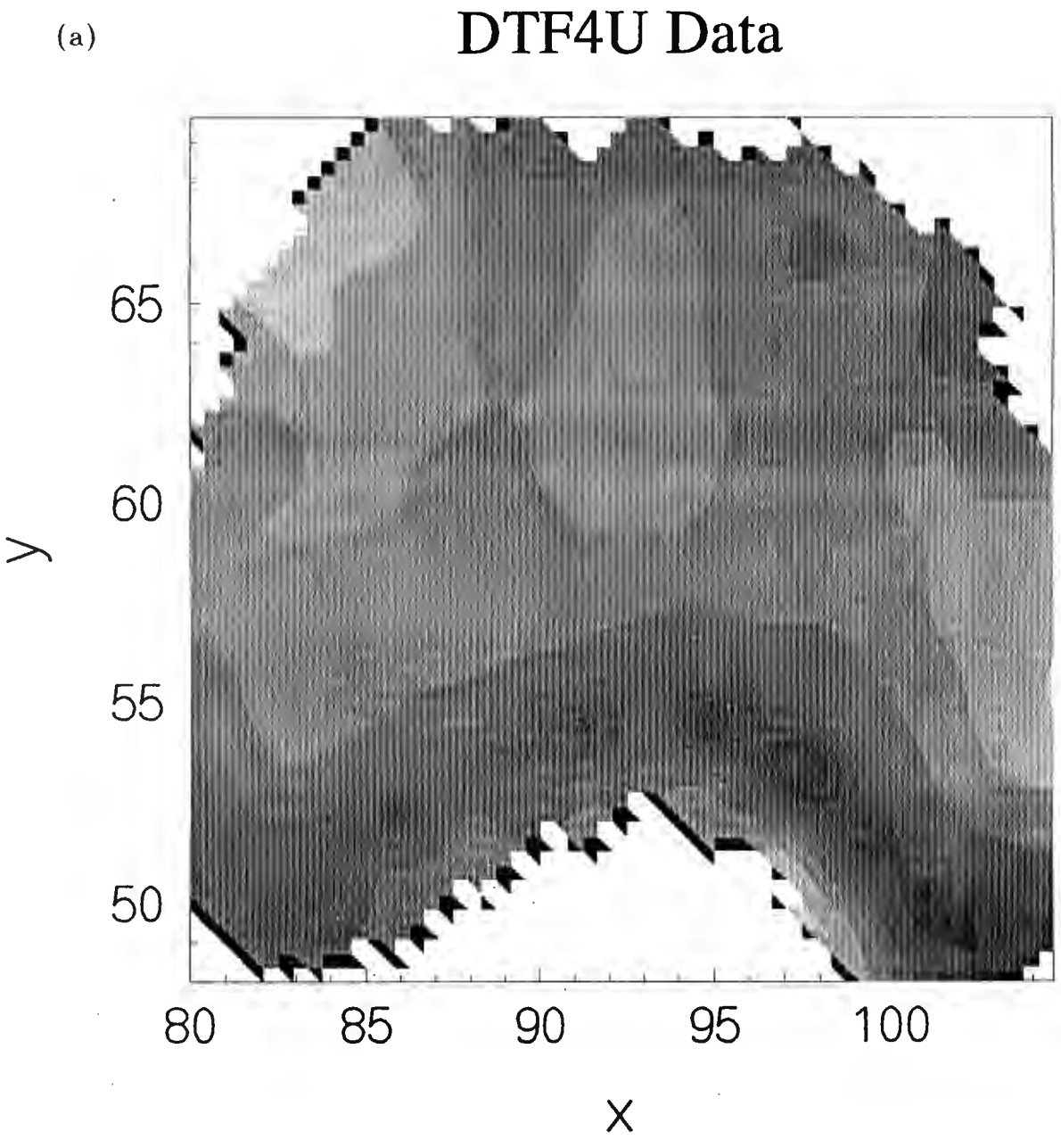

FIGURE 3.30 (a). Grey-shaded plot of olecranon sulcus cartilage thickness.

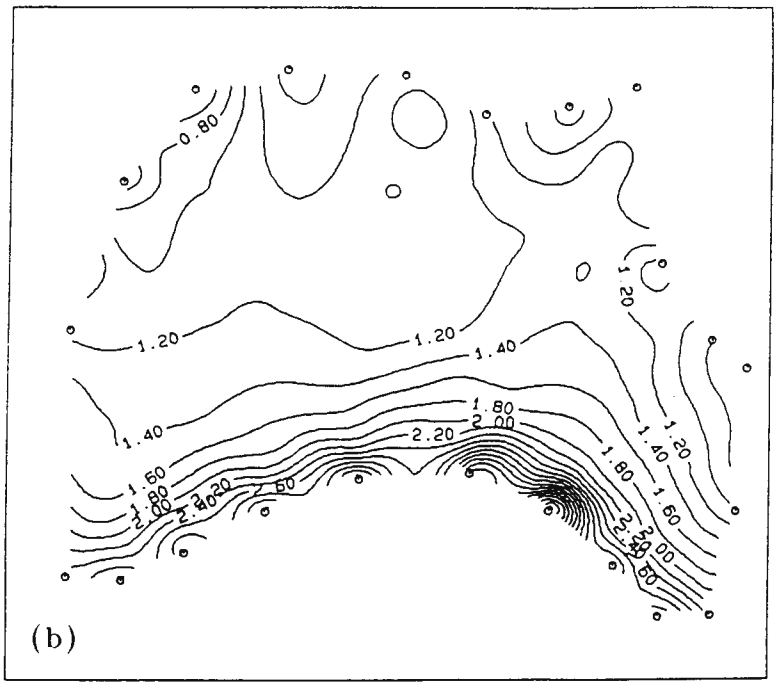

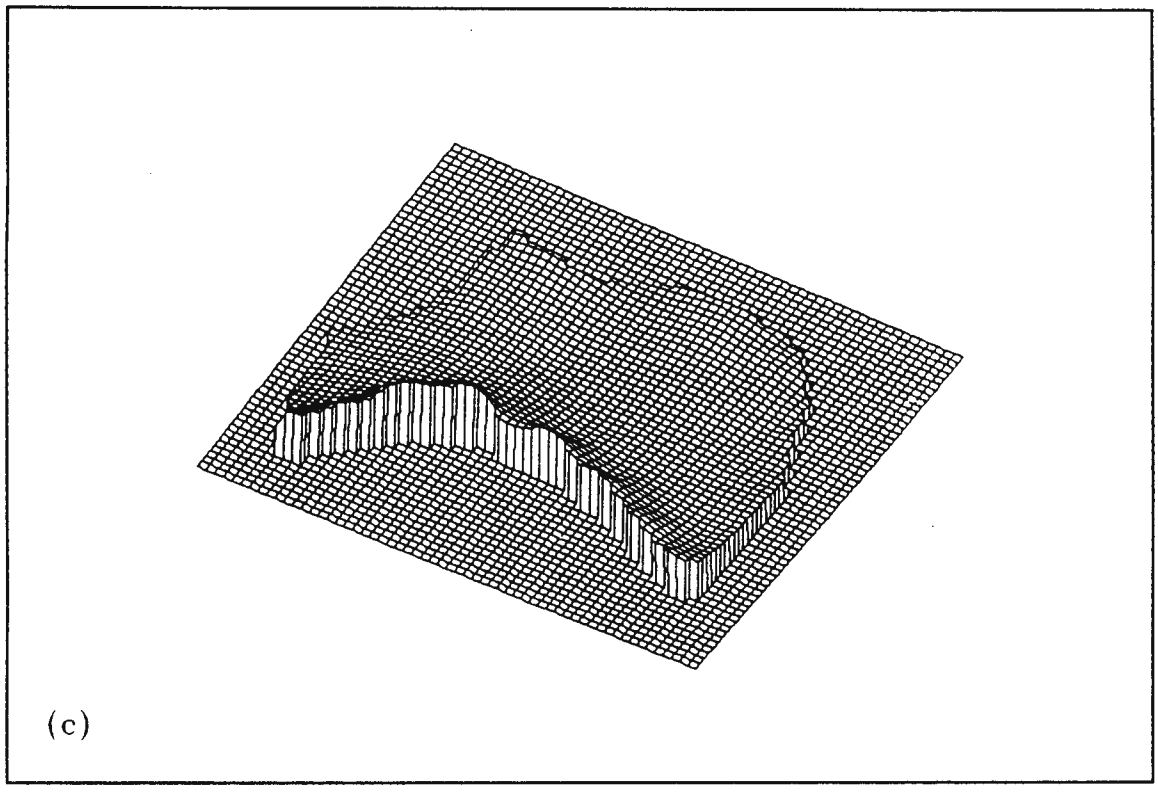

FIGURE 3.30. Olecranon sulcus cartilage thickness: (b) contour plot, (c) 3-d representation.

(a)

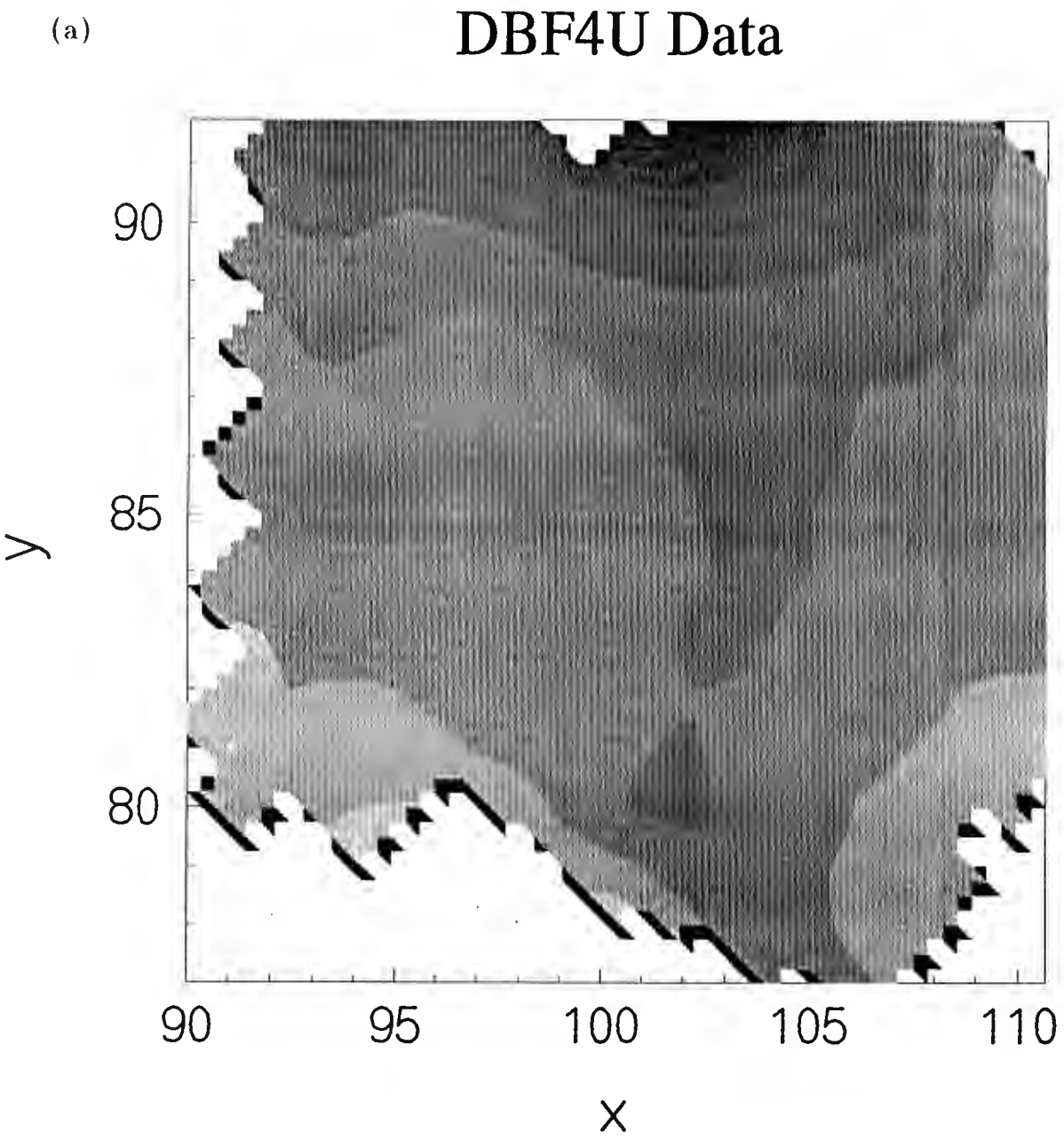

FIGURE 3.31 (a). Grey-shaded plot of coronoid sulcus cartilage thickness.

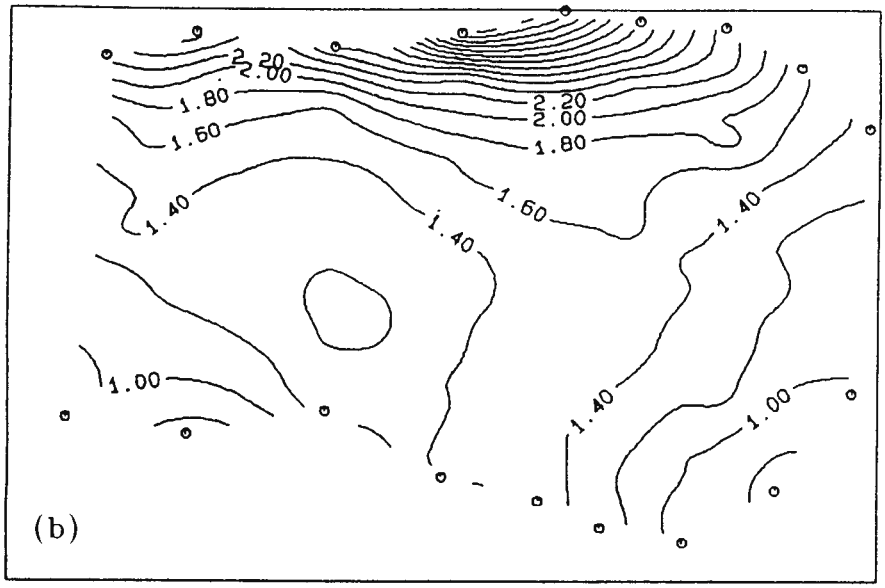

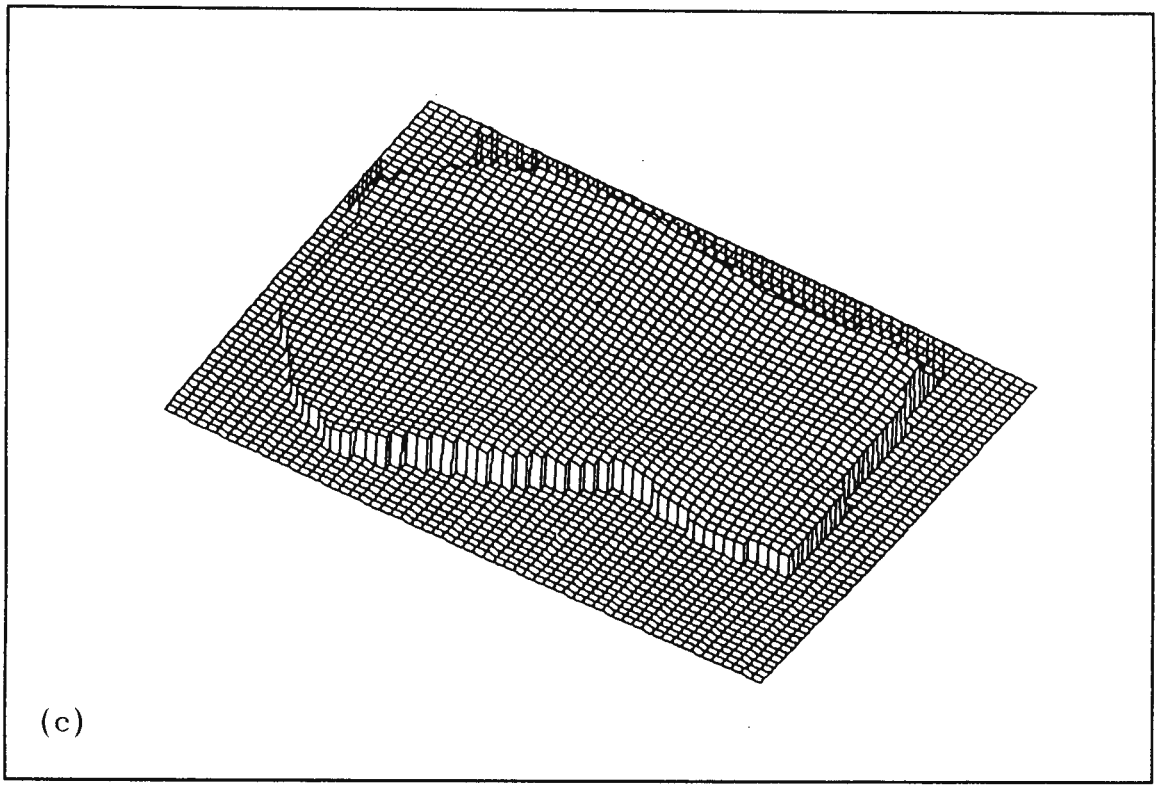

FIGURE 3.31. Coronoid sulcus cartilage thickness: (b) contour plot, (c) 3-d representation.

Accurate three-dimensional geometric data of the cartilage surface and underlying bone surface of the trochlea and proximal ulna has been determined, and for each specimen the cartilage thickness was evaluated at all the nodes of the joint surface. Results show that the cartilage thickness on the anterior trochlea varies randomly over the surface with a general variation of less than 0.4 mm. The posterior trochlea displayed similar results with a general variation of less than 0.5 mm.

The olecranon facet and the coronoid facet displayed a more uniform cartilage thickness variation over the surfaces with a variation of about 1.2 mm. On the olecranon facet, the cartilage increased in thickness from the olecranon process border to the proximal incisura trochlearis border. Similarly, the coronoid facet cartilage increased in thickness from the coronoid process border to the distal incisura trochlearis border.

3.7 EXTRA-ARTICULAR GEOMETRY

The objectives of obtaining accurate three-dimensional data of the entire distal humerus and proximal ulna were: (1) to determine the relationship of axes of rotation to extra-articular geometry to ensure accurate positioning and alignment of the prosthesis (2) to indicate natural load bearing locations for sites of fixation stems and flanges of the prosthesis and (3) to ensure minimal invasion of bone stock.

Specimen acquisition and preparation

The specimen studied for the geometrical analysis of the extra-articular outer and inner cortex was a complementing distal humerus and proximal ulna acquired from the Department of Forensic Medicine.

The shaft of the distal humerus was fixed in a polyester resin. Three screws with sharpened points were inserted into the resin to serve as the new control points. Likewise, the shaft of the proximal ulna was fixed in resin with three screws inserted as in Figure 3.32.

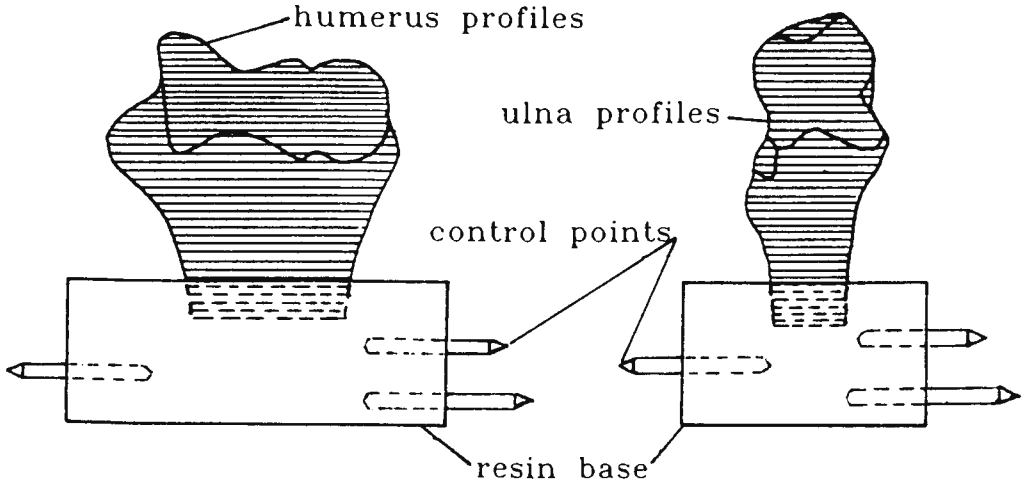

FIGURE 3.32. Prepared distal humerus and proximal ulna specimens indicating profiles of observation.

Observation of the outer and inner cortex.

The specimen was mounted in the reflex microscope and the old and new control points were digitised and the data stored in a single file. The old control points were then removed from the specimen. A one millimetre slice of bone was removed perpendicular to the shaft of the specimen using a Universal milling machine (Bridgeport). The specimen was again mounted in the reflex microscope and the three new control points digitised followed by digitisation of the outer and inner cortex profiles. The profiles were then stored on disk in a single file. This

process was repeated until all of the bone had been cut, removed, and observed.

Transformation process

There were 40 proximal ulnar slices constituting 40 outer cortical profiles and 40 inner cortical profiles with 3525 points digitised. The distal humerus constituted 35 outer and 35 inner cortical profiles with 4690 points digitised.

Each profile was transformed (transformation method Appendix B) onto the first profile and the combined profiles were then divided into two files with one file containing the outer profiles and the other file the inner profiles.

Three-dimensional reconstruction of joint

The data files were converted into AutoCAD drawing files using a computer program written in True Basic. A flow diagram for the conversion into drawing files and subsequent three-dimensional reconstruction of the joint can be found in Appendix F.

Three-dimensional reconstructions of the distal humerus (Figure 3.33 (a) - (d)) and the proximal ulna (Figure 3.34 (a) - (d)) indicate the relationship of the axes of rotation (C-lines), epicondylar line, and articular surface profiles to the extra-articular geometry of the elbow joint.

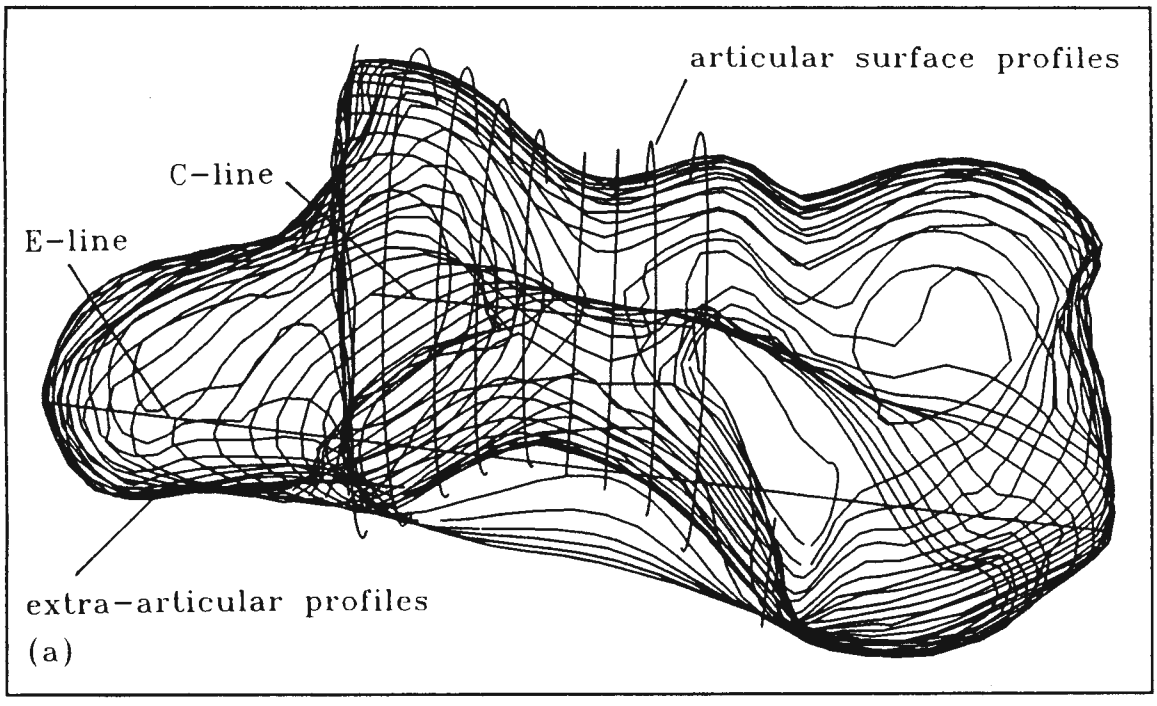

FIGURE 3.33 (a). 3-d reconstruction of the distal humerus: Distal view.

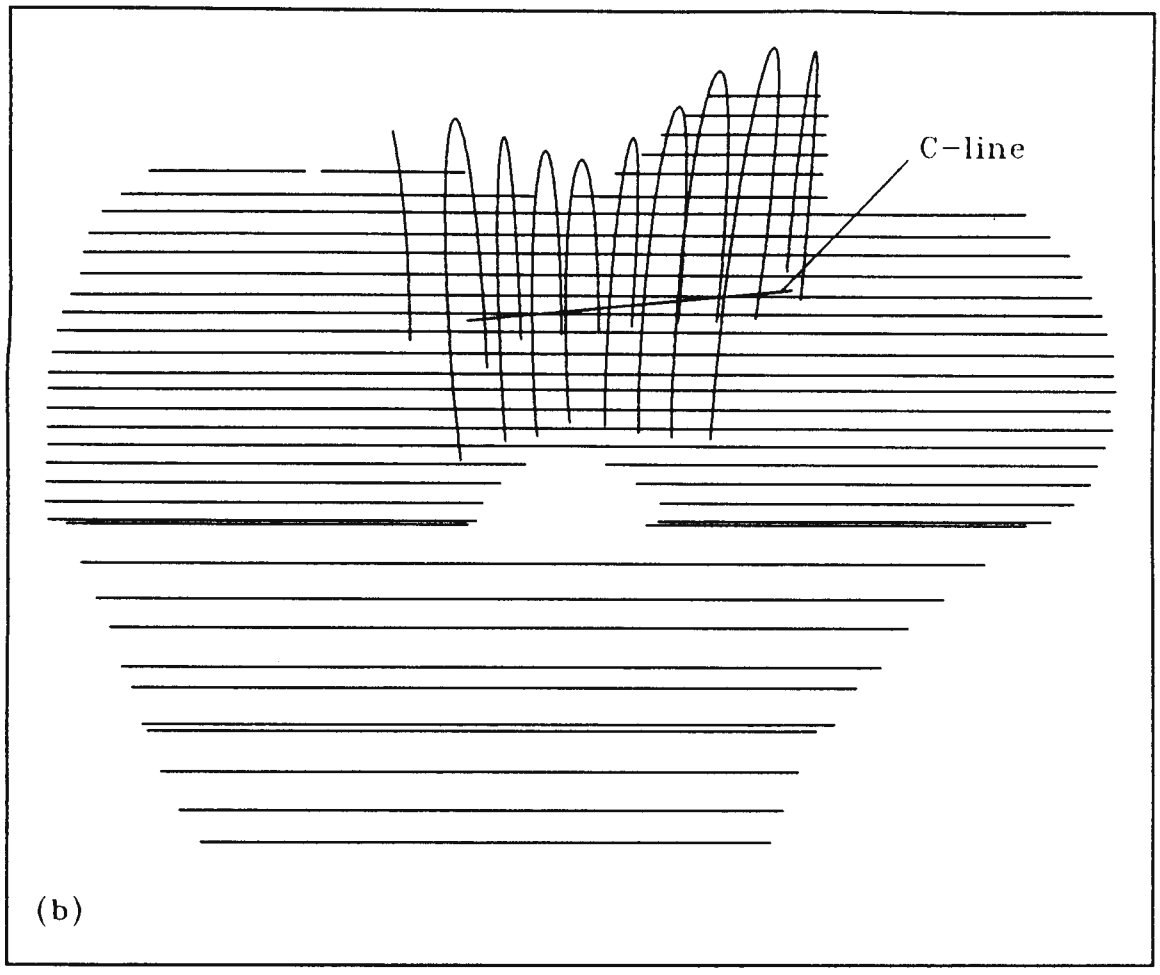

FIGURE 3.33 (b). 3-d reconstruction of the distal humerus: Anterior-posterior view.

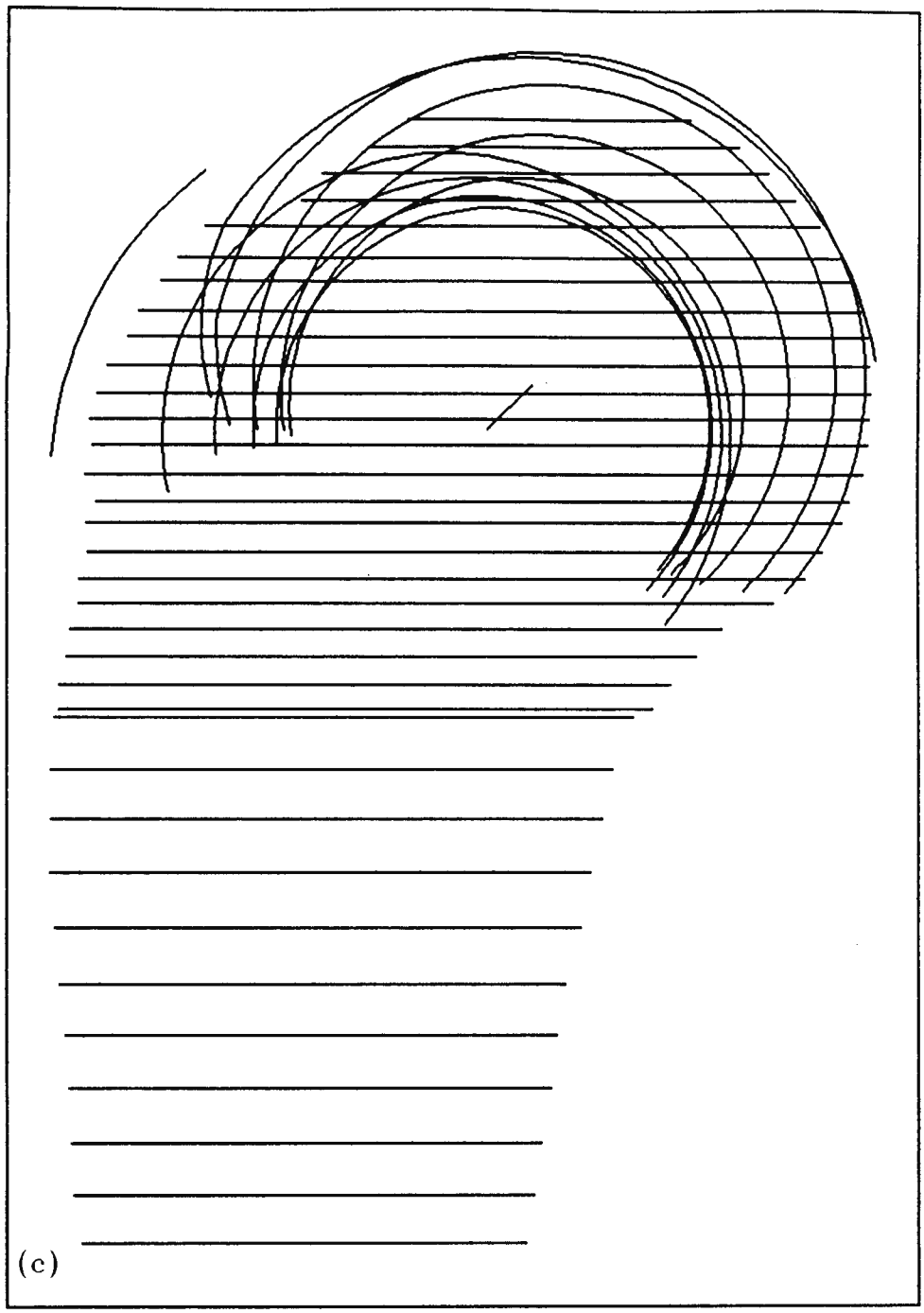

FIGURE 3.33 (c). 3-d reconstruction of the distal humerus: Lateral view.

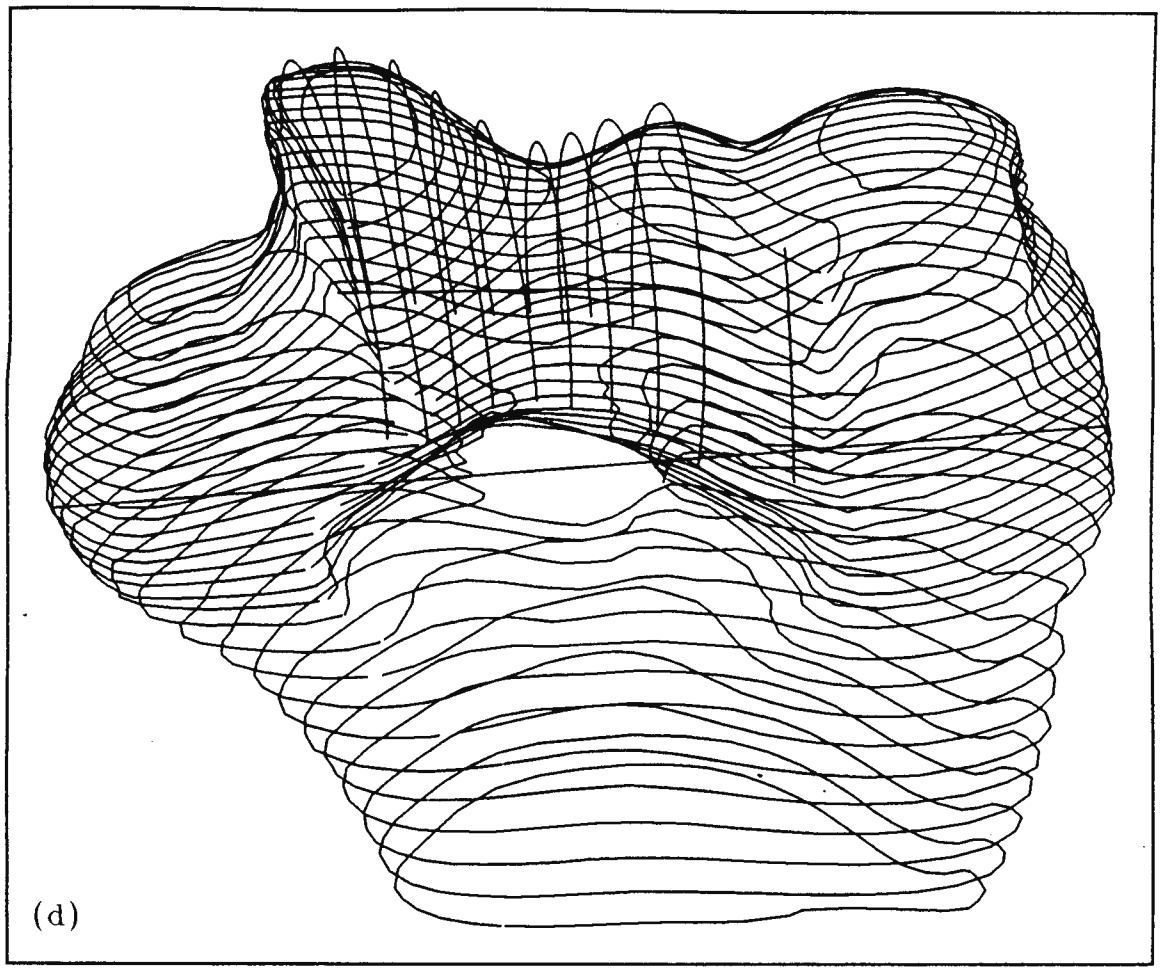

FIGURE 3.33 (d). 3-d reconstruction of the distal humerus: "Plan" view.

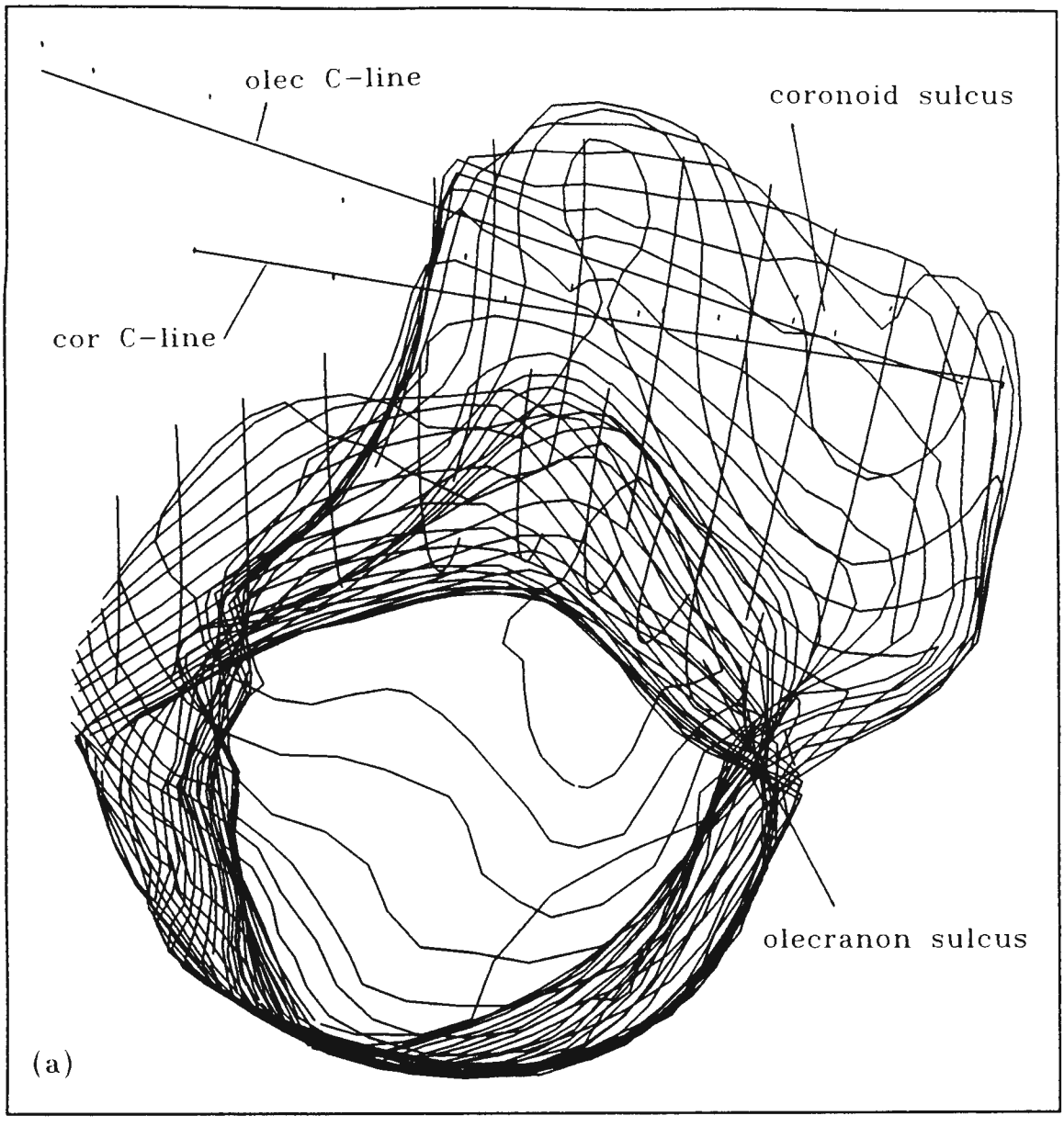

FIGURE 3.34 (a). 3-d reconstruction of the proximal ulna: Distal view.

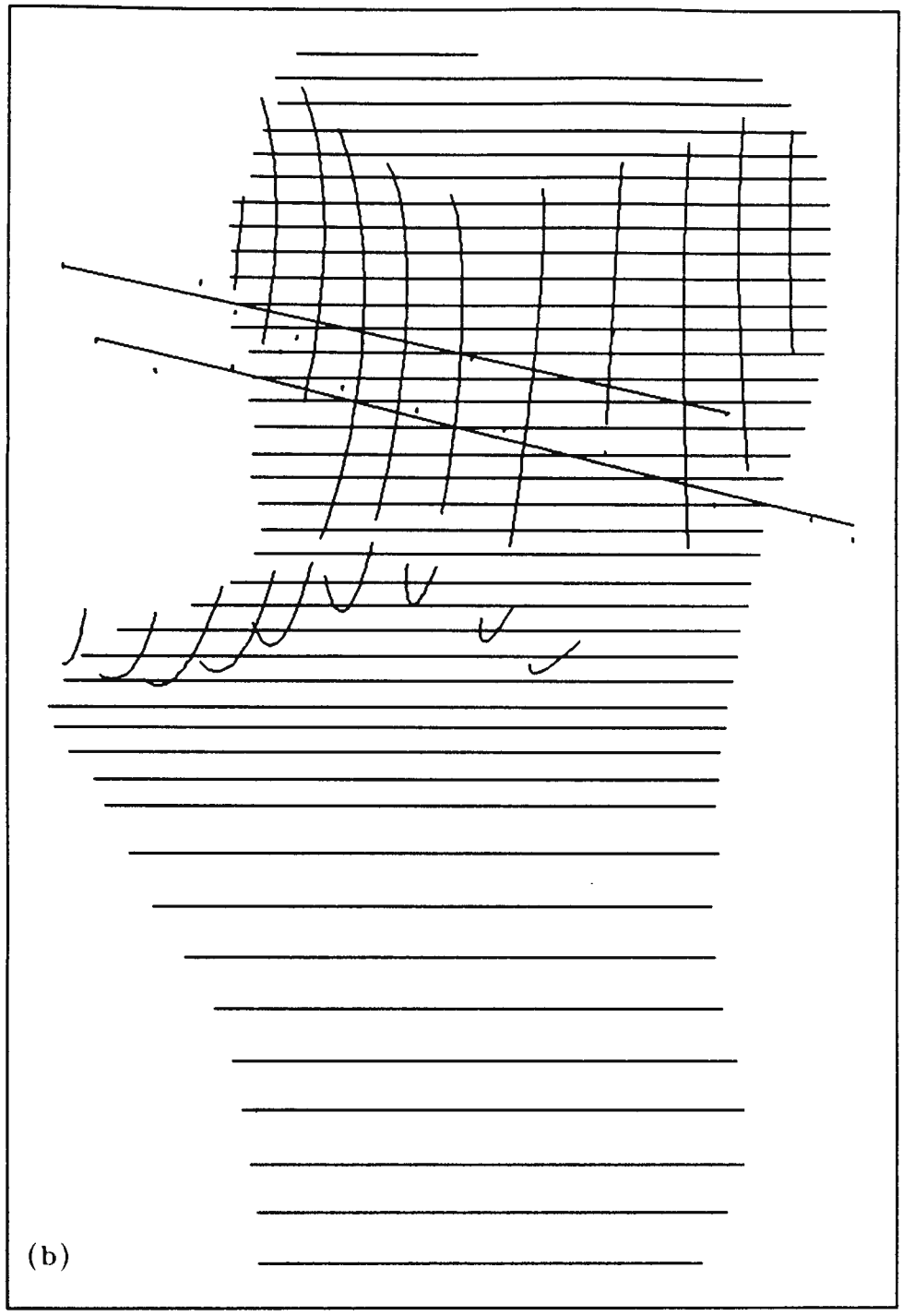

FIGURE 3.34 (b). 3-d reconstruction of the proximal ulna: Anterior-posterior view.

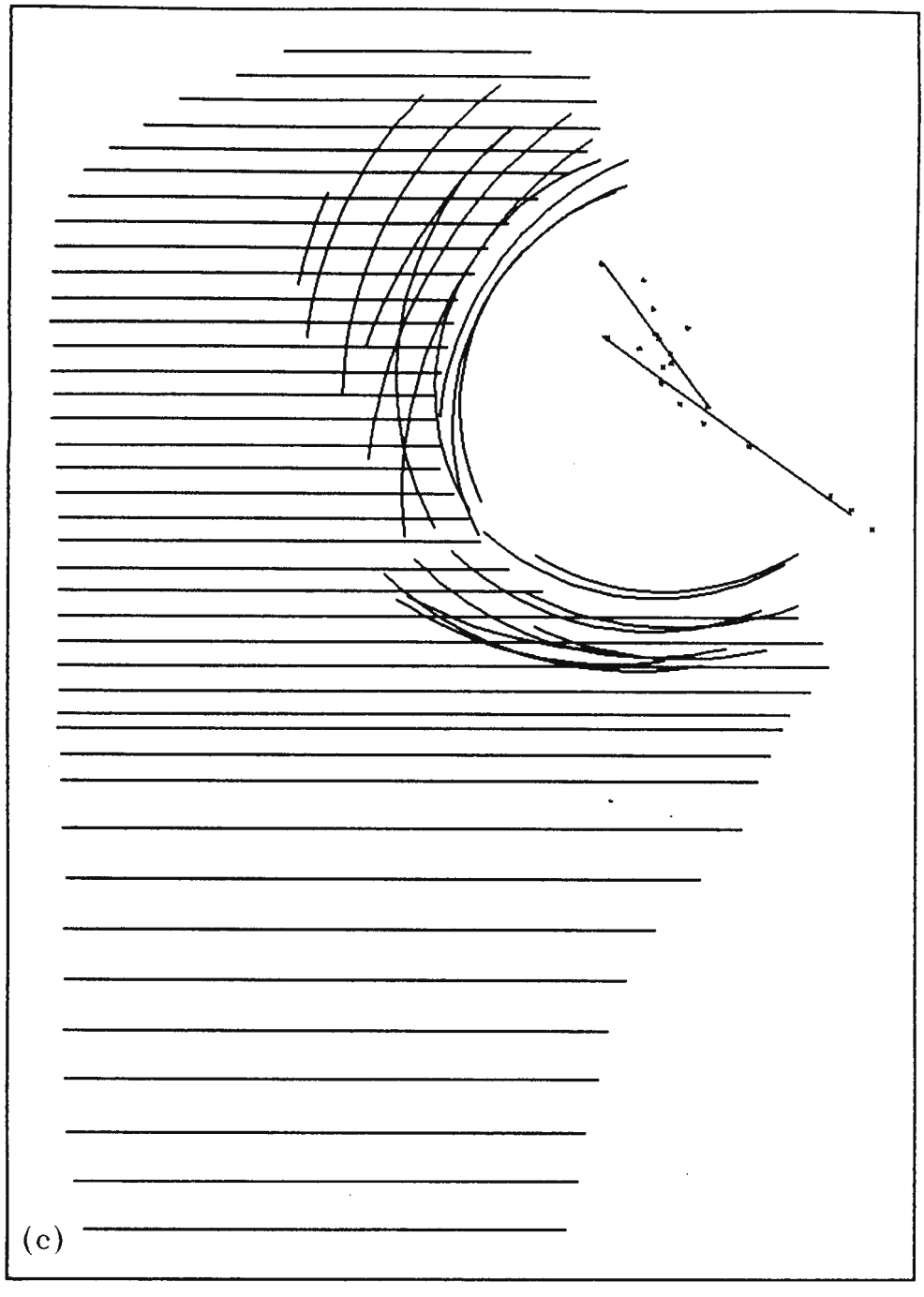

FIGURE 3.34 (c). 3-d reconstruction of the proximal ulna: Lateral view.

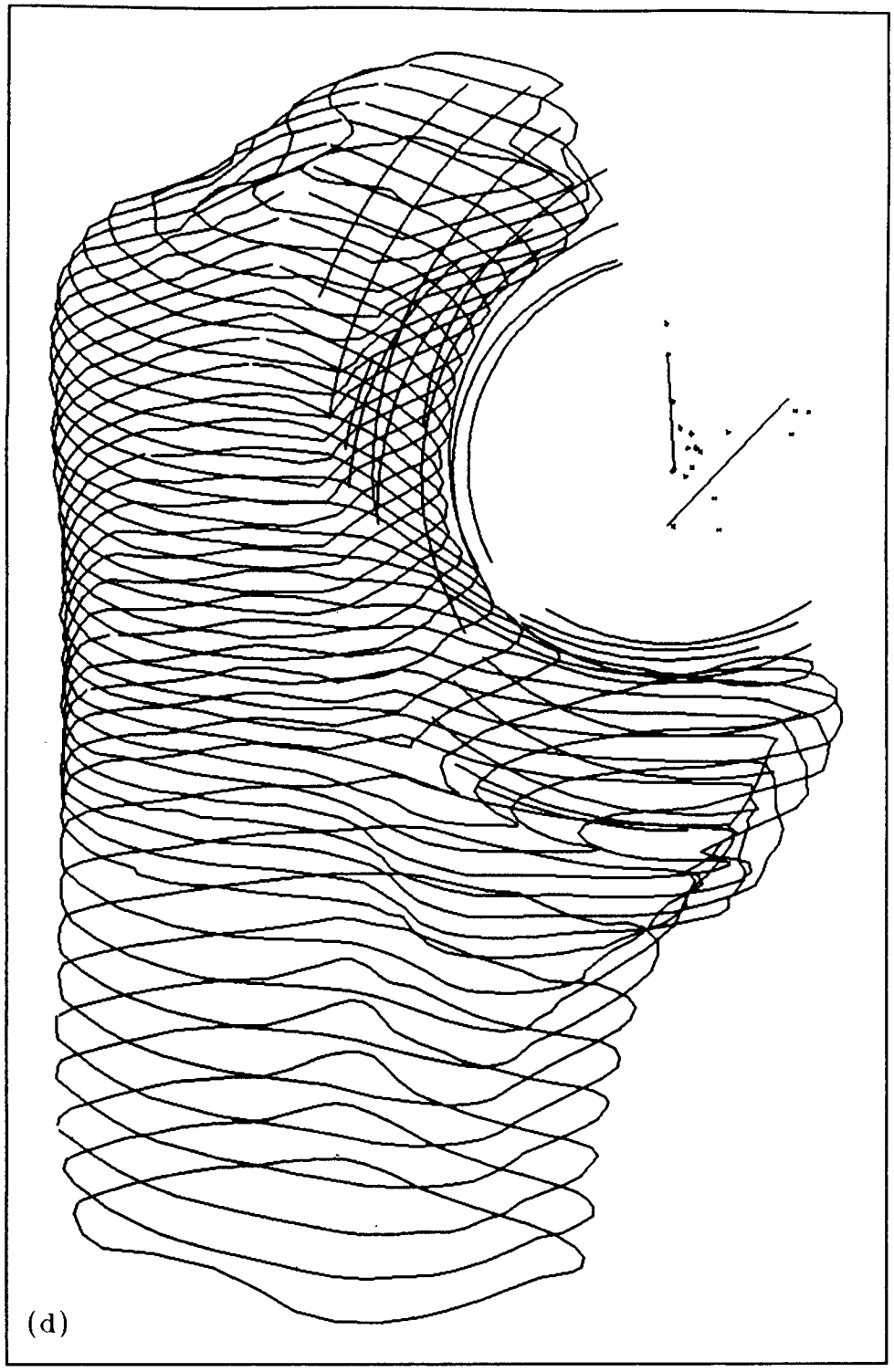

FIGURE 3.34 (d). 3-d reconstruction of the proximal ulna: "Plan" view.

The individual profiles were analyzed to determine suitable sites for the prosthesis fixation flanges and stems. Figure 3.35 is an example of one of the profiles showing the outer and inner cortex and several dimensions.

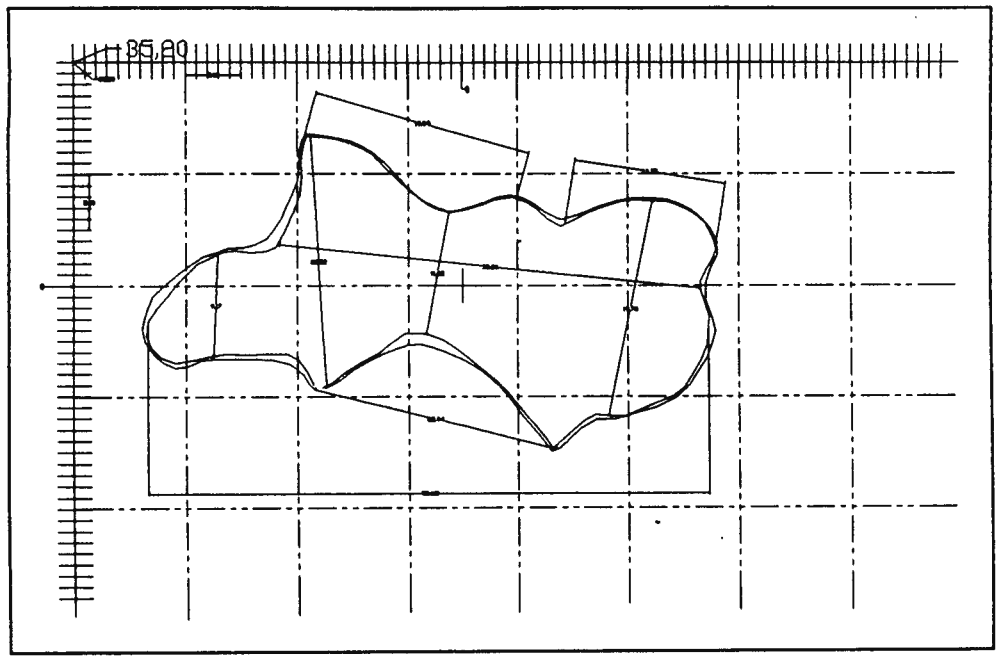

FIGURE 3.35. Individual profile of the humerus indicating the outer and inner cortex.

The geometry of the capitulum and the medial epicondyle were of particular importance in the design of the humeral component, since these are the sites where anatomical flanges will be positioned to resist the large rotational stresses encountered. The geometrical analysis thus supplied suitable sites for the flanges to be situated. The geometry of the individual profiles were all analyzed in the same manner to provide the dimensions for the design of the humeral component fixation devices.

3.8 SOURCES OF ERROR

3.8.1 Precision results

The precision test results of the transformations show that a precision on the order of 0.05 mm is well feasible. Precision values for a data set (trochlea #4, for example) are indicated in Table 3.8.

CONTROL POINT	Dx	Dy	Dz
1	0.031	- 0.015	- 0.071
2	0.046	0.026	0.051
3	- 0.033	- 0.034	- 0.026
4	- 0.045	0.023	0.046

Table 3.8. Precision test results of transformation (precision estimation - see Appendix B).

3.8.2 Repeatability of measurements

The technique employed to determine the cartilage thickness was used in this part of the study to obtain a contour plot quantifying the difference of the repeated measurements of articular surfaces. The difference plot will supply quantitative

data indicating the magnitude of the bias (error) introduced into the measurements by the observer. A difference plot with contour values of zero would indicate no error in the repeated measurement of a surface.

Three bone trochlea articular surfaces were measured (reflex microscope) immediately after the removal of the cartilage, and then for a second time two months later. The exact same procedure was followed as that used in creating cartilage thickness plots.

The resultant contour plots displayed large areas with contour values of zero and a few areas with maximum values of 0.10 mm (eg. Figure 3.36). This indicates an error of less than 0.10 mm over an entire surface, and a possible cause of this error is the dehydration of the bones.

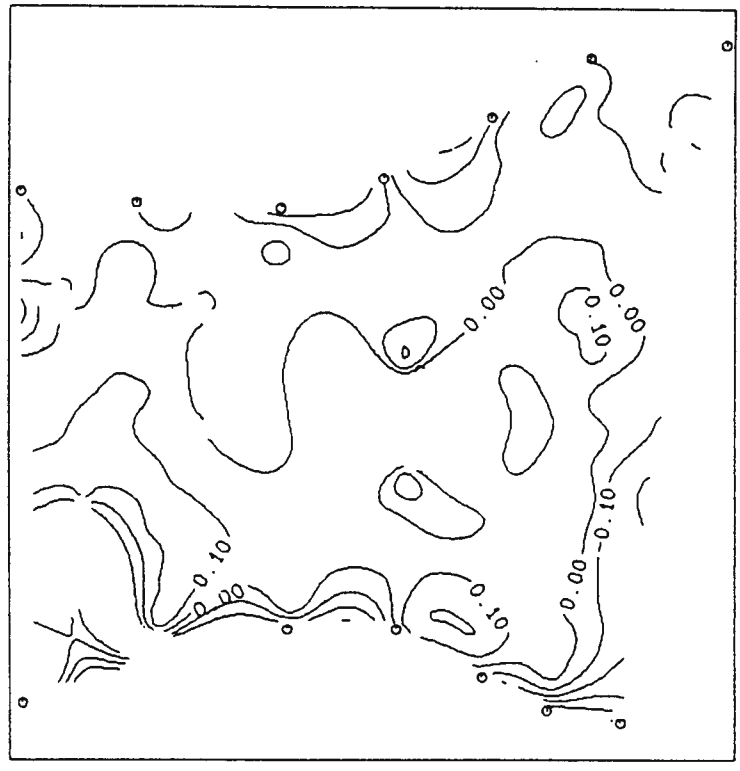

FIGURE 3.36. Repeatability of measurement contour plot.

3.9 PROSTHESIS DESIGN

3.9.1 Articular surface

This study has shown that the trochlea, and the olecranon and coronoid facet articular surfaces are circular in form in the sagittal plane. This has permitted the determination of the exact curvature dimensions for specifications for the design of the articular surfaces of the prosthesis. Following this, curves were fitted to the coronal plane profile of the cartilaginous articular surfaces, defining the surfaces with several radii of curvature. The design of the surfaces could then be represented by the anatomically designed articular surfaces shown in figures 3.37 and 3.38. The plane formed by the trochlear sulcus was inclined at an angle of three degrees and open proximally and medially from the plane containing the line perpendicular to the centre-line (anterior-posterior view). It was decided that this angle of inclination be included in the design of the humeral component. From a distal-proximal aspect, the plane is perpendicular to the centre-line.

The "circle" theory study revealed that the ulna has two distinct axes of rotation, thus the design of the ulnar component will include two distinct articulating facets.

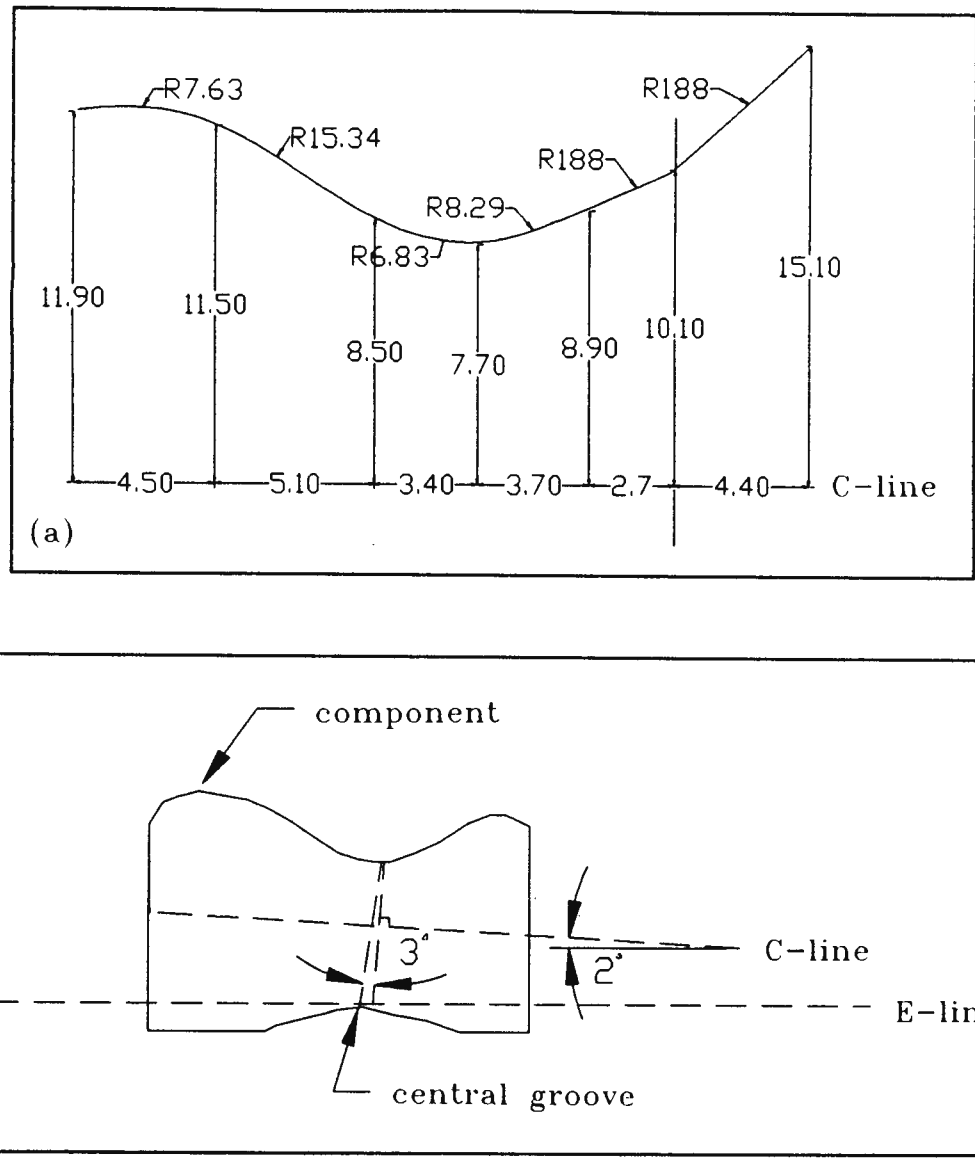

FIGURE 3.37. Articular surface design of the humeral component. (a) curvature dimensions, (b) component geometry.

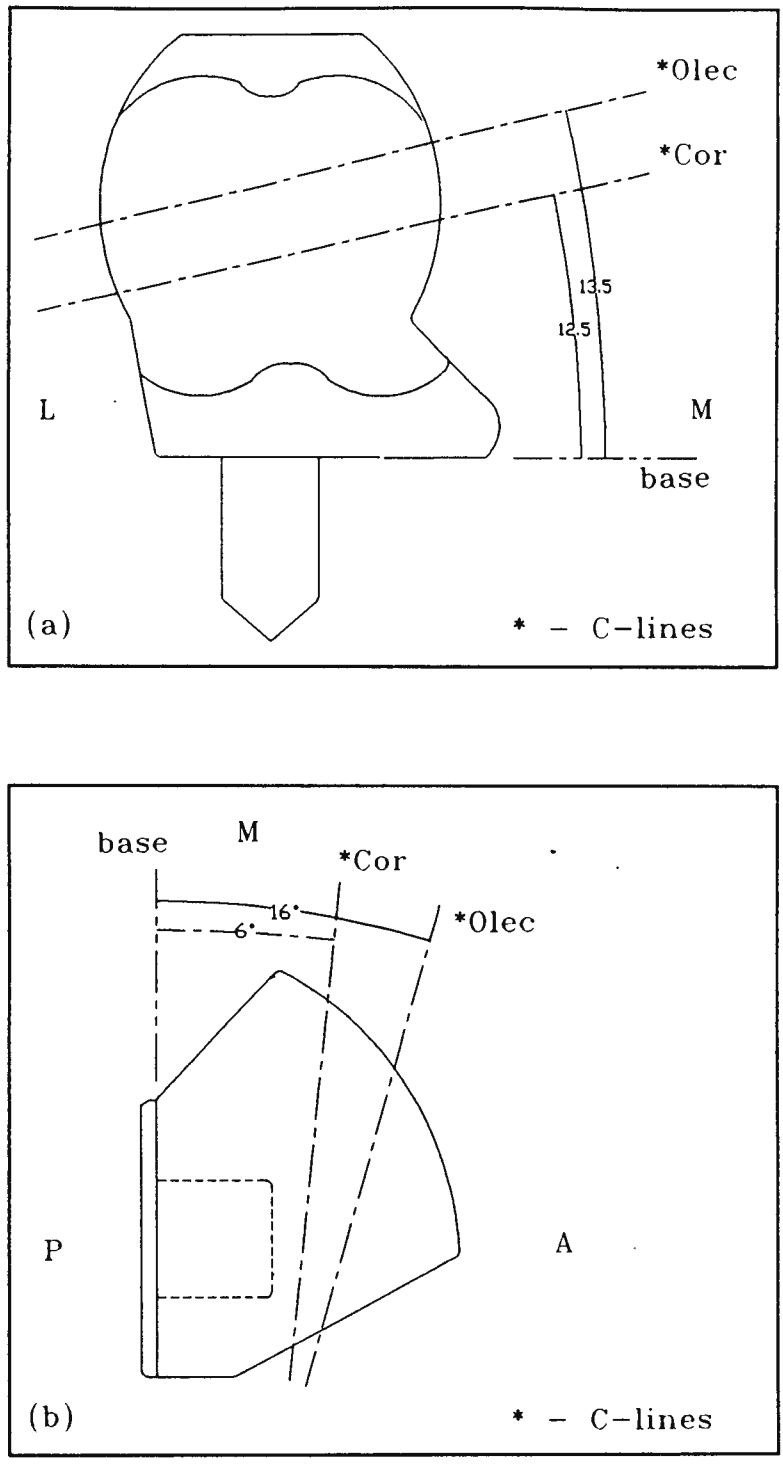

FIGURE 3.38. Articular surface design of the ulnar component: (a) A-P view, (b) proximal-distal (top) view.

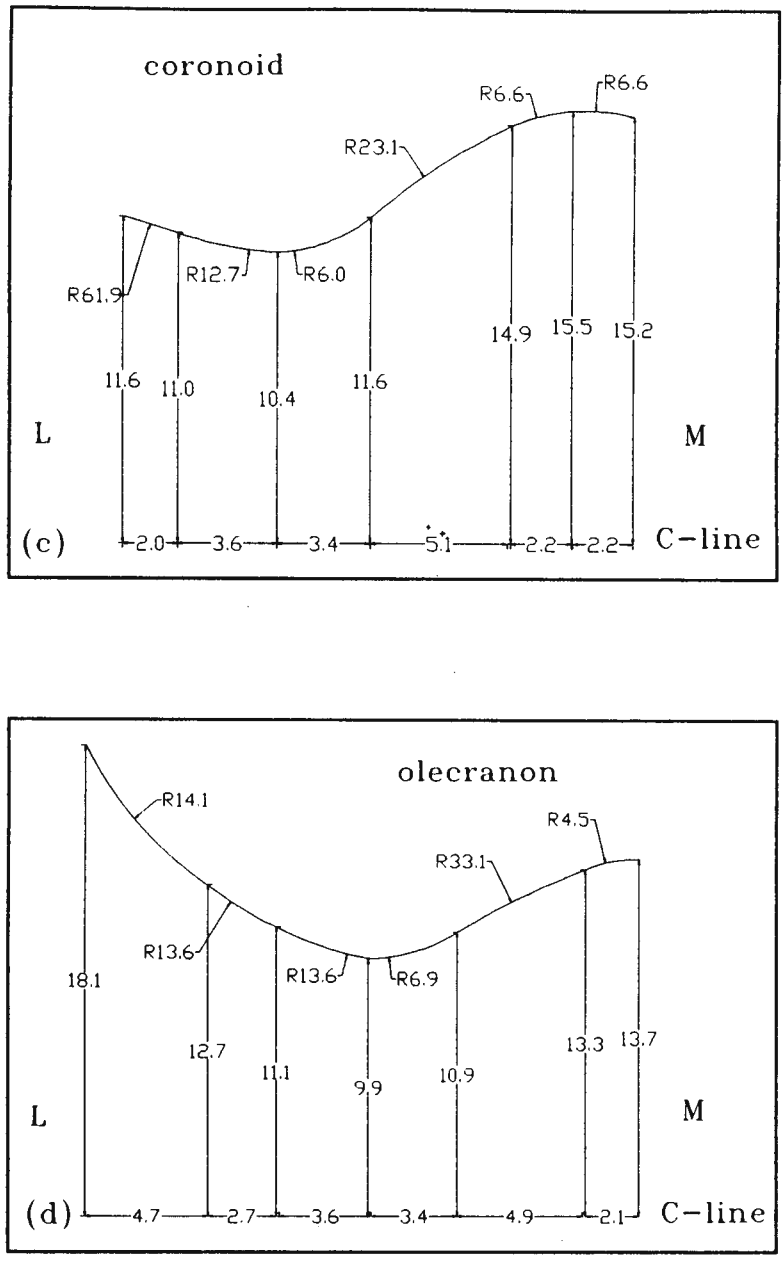

FIGURE 3.38. Articular surface design of the ulnar component: (c) coronoid radii of curvature, (d) olecranon radii of curvature.

3.9.2 Fixation

Clarification of material requirements: The prosthesis will have a cementless humeral component made from a metal alloy, and a cemented ulnar component made out of UHMWPE and not metal backed but with a metal cross.

Humeral component

It has been stated by Souter, 1990, that the primary cause of humeral component failure is the lack of design features to resist the large torsional stresses applied across the elbow joint. Thus, the initial task was to determine optimal sites for the location of a flange on either side (medially and laterally) of the articular surface to resist these stresses. Of equal importance when locating suitable areas for flange and stem placement is that a minimal amount of bone stock should be "invaded".

The 40 geometric profiles were individually analyzed and for each profile a two-dimensional possible site of fixation was determined. The profiles were combined and a three-dimensional drawing of the flanges with their geometrical relationship to the axis of rotation and articular surface was obtained.

Another consideration when designing the medial and lateral flanges was that of "ease of insertion" of the component. Current

elbow prostheses involve a complex surgical technique and this is often the cause of component failure due to incorrect insertion (alignment and placement) of the prosthesis; this may lead to the avoidance of performing total elbow replacements by the surgeon.

This "ease of insertion" concept led to the idea of having simple tap-in components that would require a jig to be aligned with known anatomical landmarks, a simple cut or drill-hole to be made, the removal of the jig, and a simple tap-in of the prosthesis.

This could be achieved by designing the humeral component as having the medial and lateral flanges in the shape of a spike that could be tapped in. Thus, the spiked flanges would have two primary functions: (1) to resist the large torsional forces, and (2) to serve as fixation mechanisms providing an easy insertion.

The flange was designed so that its cross-section is in the shape of a filleted rectangle; its tip was sharpened to a point like a spike so that it could be tapped in (Figure 3.39). The rectangular shape was chosen due to the requirement that the flange should resist torsional forces. Torsional loads could therefore be transmitted to the bone as compressive stresses in the attempt to reduce shear stresses at the interface. The geometry of the fixation sites also favoured the rectangular shape. The medial spiked flange extends out medially from the trochlea by 2.3 mm and is therefore not expected to interfere with the medial collateral ligament, the site of attachment of the flexor pronator muscles, or the sulcus of the ulnar nerve. It also has a smaller cross-sectional area than the lateral spike

because the medial epicondyle is smaller in size in the anterior-posterior aspect than the lateral epicondyle. Furthermore, this feature prevents invasion of the smaller medial supracondylar bony column which may be vulnerable to fracture with the insertion of the humeral component. The length of the medial spiked flange is determined by the geometry of the medial supracondylar ridge, which curves sharply medially, and the olecranon fossa.

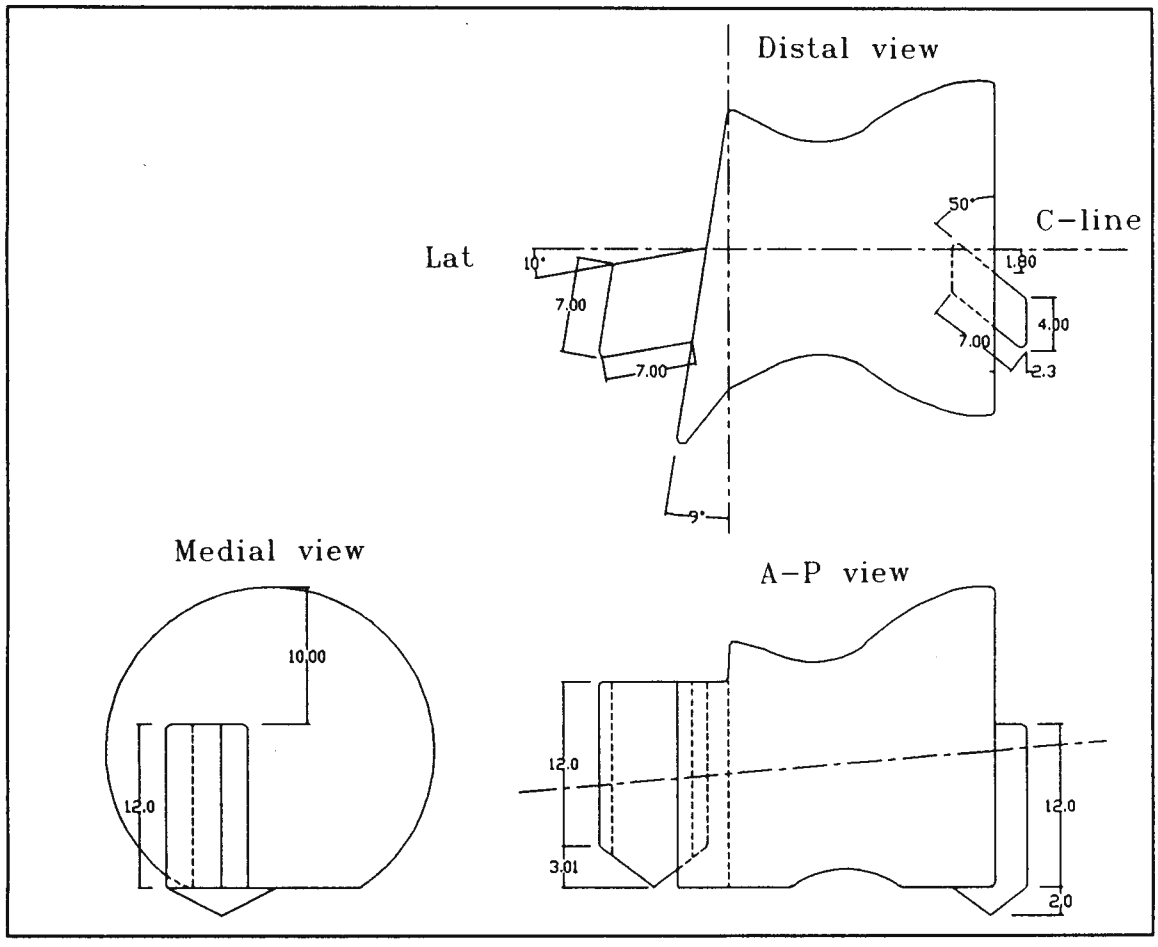

FIGURE 3.39. The geometry of the spiked flanges.

Similar to the medial spiked flange, the lateral flange also has the shape of a filleted rectangle. The lateral flange extends out laterally from the lateral distal trochlea border and inserts into the capitulum towards the strong lateral supracondylar column. The length of the spike is determined by the geometry of the olecranon fossa.

To minimize the invasion of bone stock by the component, an interference fit of the implant will be achieved, and should provide adequate fixation (adequate fixation has been achieved with cementless humeral components such as the Kudo, Sorbie, and Amis-Miller type designs). This type of interface will also provide an accurate insertion and orientation of the component.

The two spiked flanges should provide sufficient fixation in elbows considered for replacement with a late phase 3 or phase 4 rheumatoid disease (as defined by Souter, 1990). In phase 4, there is usually extensive destruction of the humero-ulnar joint; a shell fit trochlea replacement was therefore not considered as a viable design option due to the probability of severe erosion so that the bone available for support and anchorage of an implant is seriously impaired. A solid trochlear design thus evolved with a flat base perpendicular to the shaft of the humerus (Figure 3.40). The base will ensure that the stresses corresponding to the predominantly encountered compressive forces acting on the trochlea (Amis et al, 1980) are reduced by increasing the contact area (bone/prosthesis interface) perpendicular to those forces.

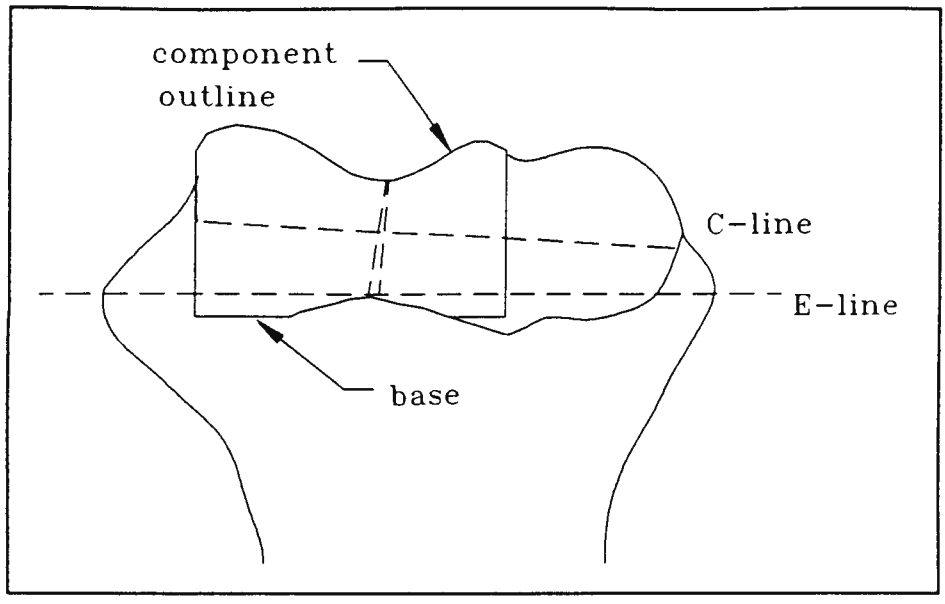

FIGURE 3.40. The solid trochlear design.

Another important factor is the cyclical reversal of the resultant vector of the forces (axial compression during extension and anterior-posterior during flexion) across the elbow during daily activities. In an elbow that has sufficient bone stock to adequately secure the spiked flanges, these design features of the humeral component should provide adequate fixation for the resistance of these cyclical loads.

The retention of the collateral ligaments in the proposed arthroplasty will also reduce the transmission of these forces, and the rotational forces, to the bone/prosthesis interface. It is essential for the unlinked design type prosthesis that the collateral ligaments (especially the MCL) are intact and functional.

The two spiked flanges are situated posterior to the

trochlea centre-line in the coronal plane. The centre-line of the component is at an angle of 5 degrees to the base which is parallel to the epicondylar-line in the transverse plane. This angle is the angle of inclination of the trochlea sulcus added to the angle formed by the centre-line and the epicondylar-line. The geometry of the solid trochlea articular surface and spiked flanges is shown in Figure 3.41.

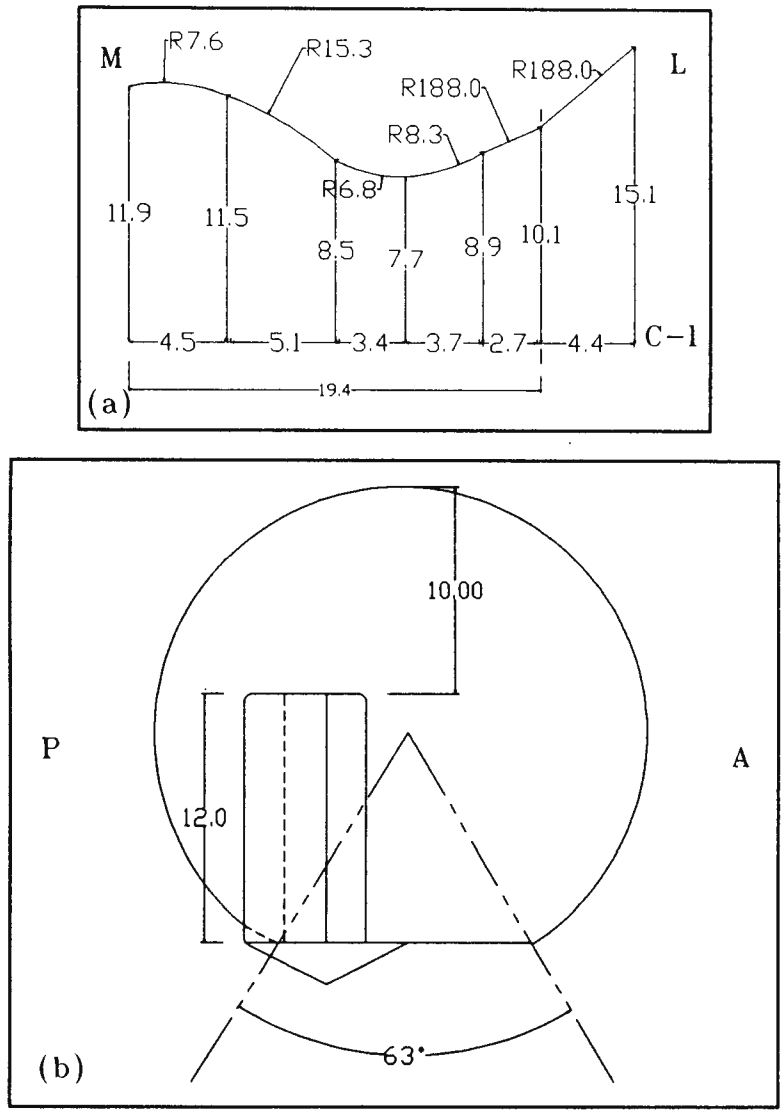

FIGURE 3.41. The geometry of the solid trochlea articular surface and spiked flanges: (a) articular surface, (b) side view.

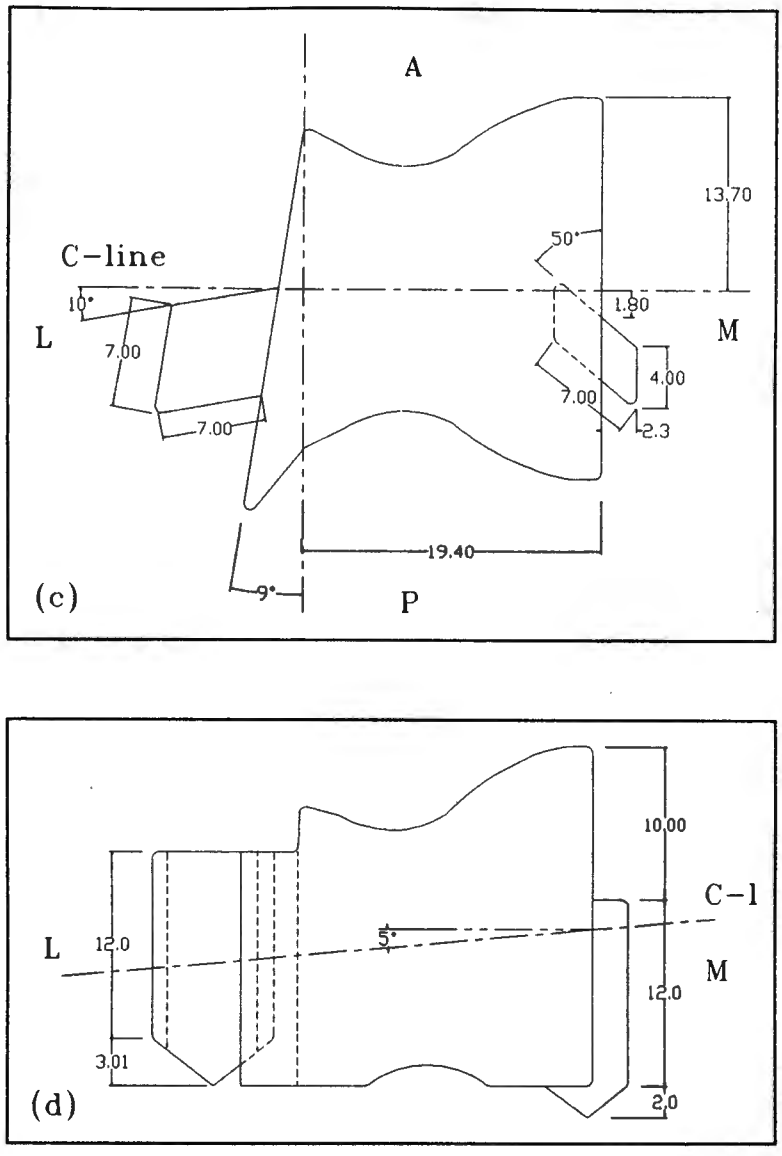

FIGURE 3.41. The geometry of the solid trochlea articular surface and spiked flanges: (c) top view, (d) front view.

Ulnar component

Joint forces on the articular surface of the ulna have been reported by Amis et al, 1980. They have concluded that during activities involving resistance of flexion and extension moments

at various elbow joint positions, the medial-lateral force components, causing varus-valgus stresses, are small compared with those acting in the sagittal plane. Thus, the design of the ulnar component consists of a flat posterior (olecranon) base and a flat coronoid base to ensure that the stresses corresponding to the compressive forces, acting alternately on the olecranon and coronoid surfaces, are reduced by increasing the area of interface perpendicular to those forces. The component will have the simple shape of a 'L' in the sagittal plane to make for a simple cut of the bone for component insertion (Figure 3.41).

The borders were defined following a geometrical analysis of the individual profiles observed in the extra-articular geometry study. Of important consideration during this analysis was that a minimal amount of bone should be resected.

It is noted by Amis et al, 1980, that although the medial-lateral forces encountered are smaller than those in the sagittal plane, there still exists a substantial lateral component of force on the olecranon. This will put a shear force on the component resting on the olecranon. Thus, a "cross" protruding from the olecranon base was designed to convert these forces to compressive ones (Figure 3.41).

The "cross" will require a minimal invasion of the olecranon bone stock (as compared to other design types with large flanges or keels). It will be 1 mm in height and could be made out of a metal alloy. It will be pressed firmly into PMMA until the cross touches the underlying bone. This will also ensure that correct and accurate alignment and positioning of the component will be achieved.

For added fixation and resistance of possible shear stresses on the flat coronoid base, a cross-hatched pattern will be cast into the base (coronoid) surface and this base will be pressed firmly into a PMMA layer. A short stem has been included in the design. The stem will be located at the posterior aspect of the coronoid base and is perpendicular to this base and parallel to the posterior base. The stem will also be cemented into the intramedullary canal.

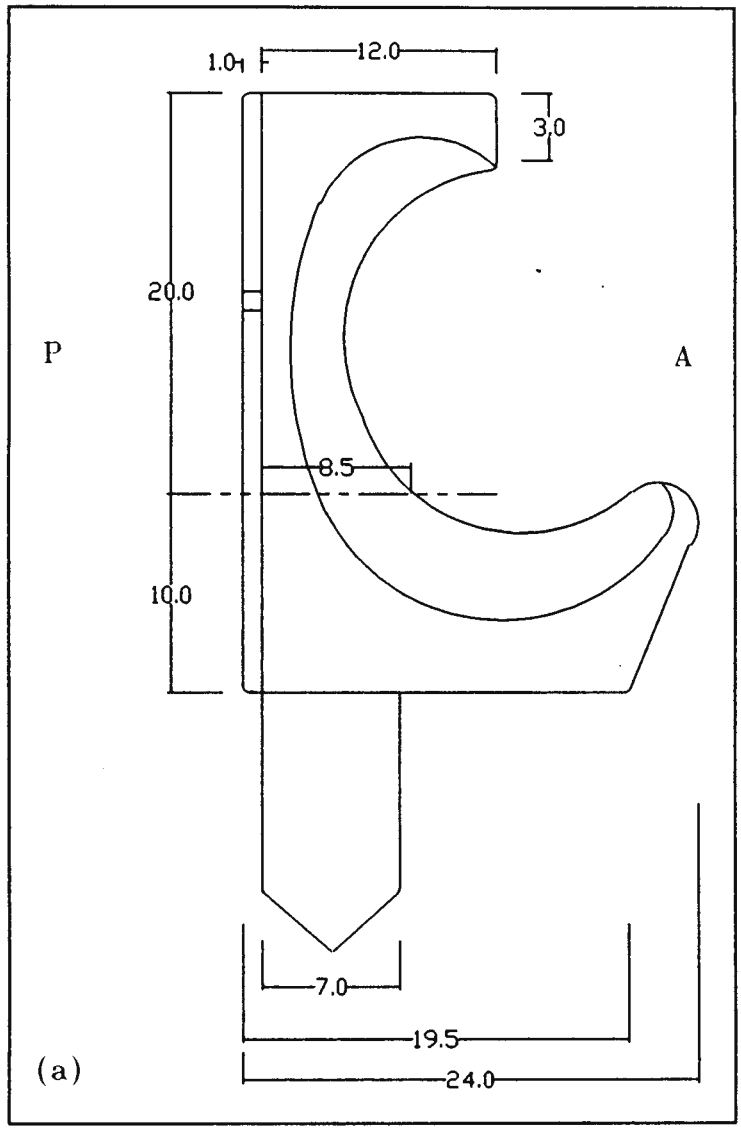

FIGURE 3.42 (a). Ulnar component: Side view.

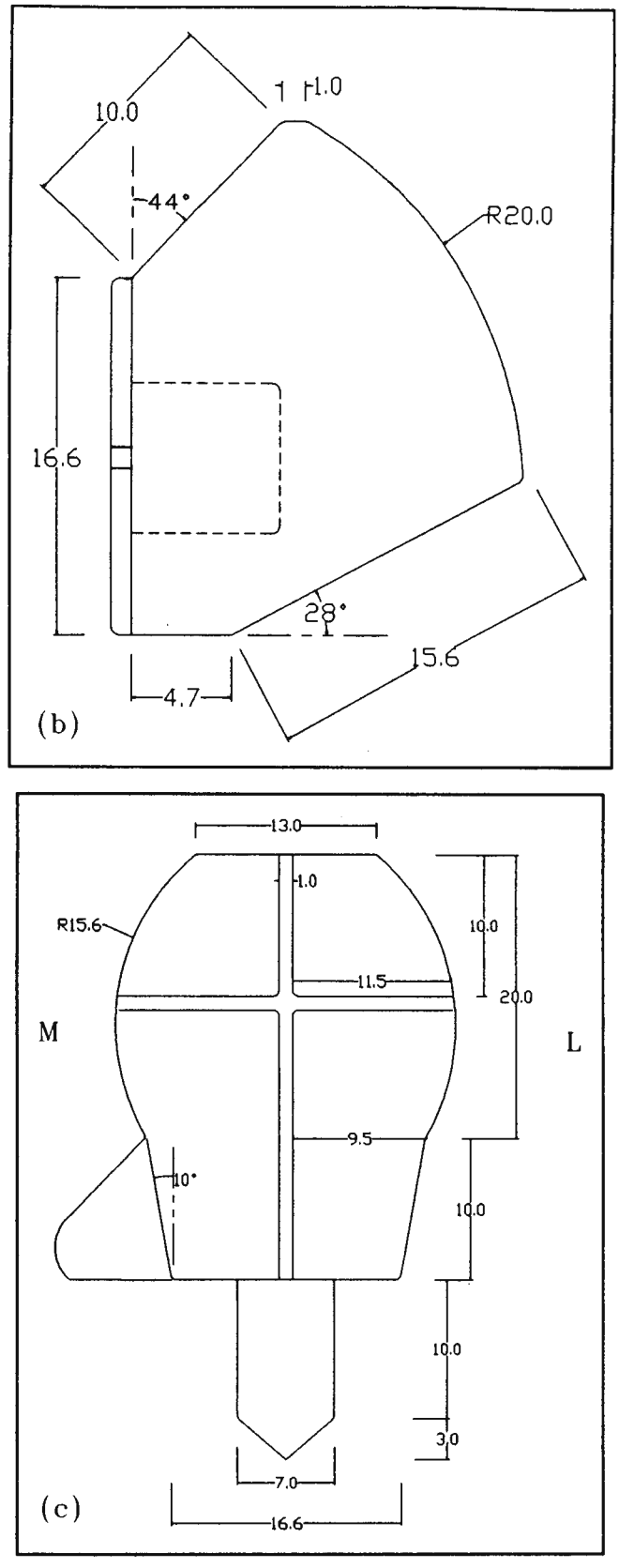

FIGURE 3.42. Ulnar component: (b) top view of coronoid base, (c) back view showing metal alloy "cross".

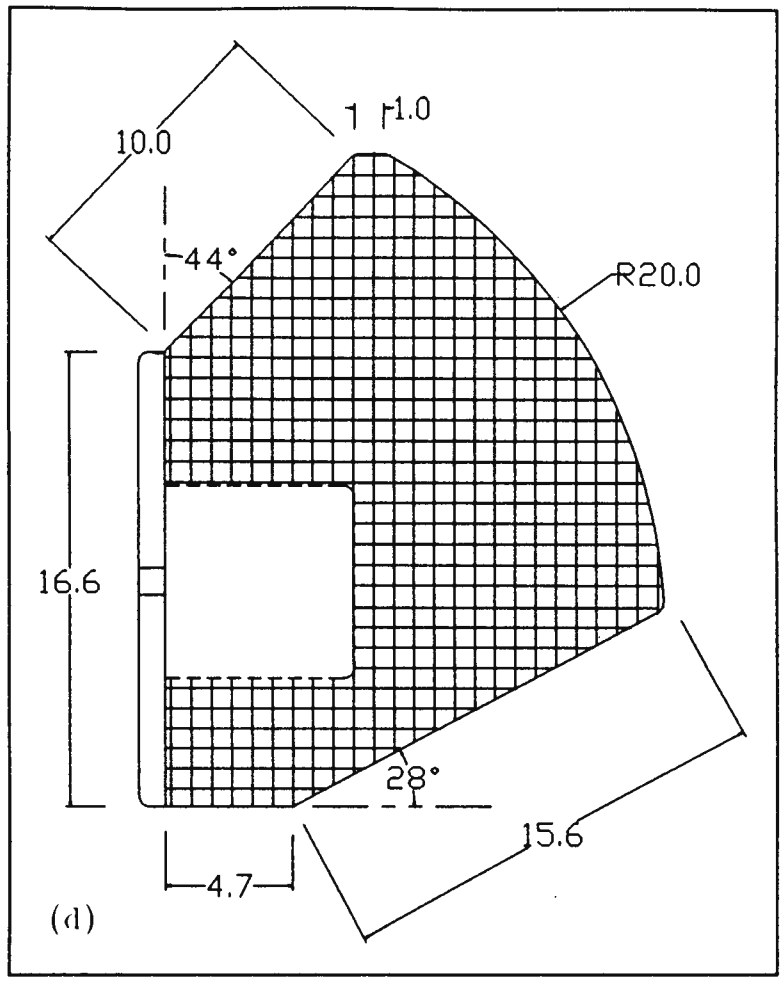

FIGURE 3.42. Ulnar component extra-articular design: (d) bottom view showing "cross-hatched" pattern.

3.10 PROTOTYPE MANUFACTURE

A prototype was manufactured, based on the design drawings (Appendix G), for functional testing of the prosthesis. A detailed knowledge of the processes of prosthesis manufacture and the necessary specialized equipment was not available to accurately duplicate the complex articular surfaces. However, it was felt that for the functional testing to be performed, the standards of dimensional accuracy were not critical. Thus, the humeral and ulnar component prototypes were manufactured using the following casting technique.

(1) The distal humerus and proximal ulna of a fresh specimen were dipped in liquid rubber latex to apply a thin uniform and conforming coat to the bony articular surfaces. Several coats were applied in sufficient number to make the accumulation of latex thick enough to represent the observed cartilage thickness.

(2) A mold was made of Silicone RTV 585 (Duroplastic) having a cavity of the shape of the latexed distal humerus and proximal ulna.

(3) The mold was used to make Plaster of Paris models of the distal humerus and proximal ulna.

(4) Metal templates of the coronal plane curvature of the trochlea, olecranon, and coronoid articular surface design were made from AutoCAD drawings. These templates were guided over the plaster articular surfaces by hand, removing very fine layers, and then measured with a calliper until the curvature dimension

matched the curvature of the designed articular surfaces. The plaster articular surfaces were then measured using the reflex microscope technique and reconstructed on AutoCAD. The curvature dimensions, were compared with the design dimensions to ensure that an accurate representation of the designed articular surfaces was achieved.

(5) The non-bearing surfaces of the components were then cut out of the plaster models.

(6) The plaster models of the humeral and ulnar components were now sprayed with a very thin coat of lacquer paint (Aerolak) to prevent the mold to be made of these components from removing the water from the plaster, which could cause the silicone not to harden about the components and alter their shape. This fine coat will also ensure a smooth articular surface is obtained.

(7) A mold was made having a cavity of the shape of the humeral and ulnar components.

(8) The humeral component mold was used to make a metal model of the component using Steel Putty (Eli-Fil FR/913). The metal has adequate mechanical properties of stainless steel (Hardness, Shore D75-80; Compressive strength, 75-80 MPA) for the functional tests to be performed. The ulnar component mold was used to make a plastic model of the component using Polynate 9400 and 6755. This plastic had a hardness of Shore A95 which is comparable to that of HDPE, and is sufficient for the functional testing to be performed.

(9) The articular surfaces were finished by abrasion using successively finer abrasive paper.

Figures 3.43 and 3.44 show the humeral and ulnar component prototypes.

FIGURE 3.43. Humeral component prototype.

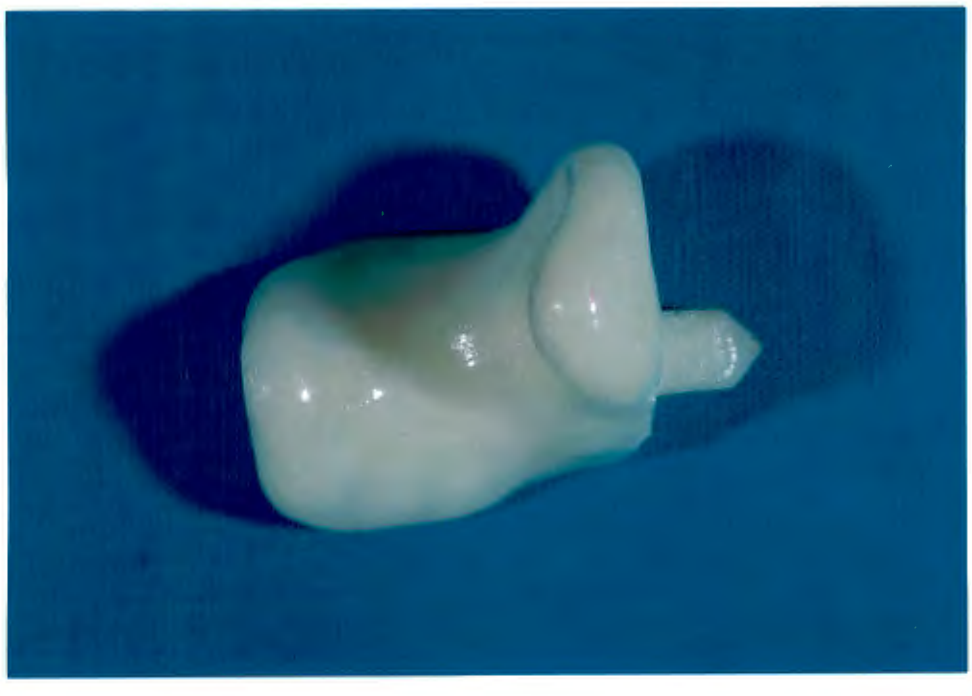

FIGURE 3.44. Ulnar component prototype.

3.11 FUNCTIONAL TESTING

A simple rig was built, simulating normal muscular and ligamentous activity, for initial basic functional tests to be performed. The results required would include: the range of motion, possible component impingement, normal alignment reproduction, possibility of dislocation, articular stability, and contact area observation at flexion and extension extremes for humeral component stem placement.

The components were inserted into resin bone models of the distal humerus and proximal ulna for the functional testing. This allows for several design concepts, such as "ease of insertion" and "minimal bone resection", to be observed, and an initial assessment of the instrument requirements, salvage potential, and the surgical approach. The rig will be evaluated initially using several bone models to determine if the rig is sufficiently capable of simulating normal joint functions. This will be accomplished by comparing the measured data with data found in the literature.

3.11.1 Rig development

The functional anatomy of the elbow joint is complex, and testing of elbow bone models - especially with prostheses

implanted - requires a system of support for the joint. A method of achieving this is to maintain the posture of the joint under load, with the muscles and ligaments represented by mechanical springs.

The muscles which have been modelled are biceps, brachialis, and brachioradialis for elbow flexion, and the triceps and anconeus for elbow extension. These muscles were indicated as the primary flexors and extensors in an electromyographic (EMG) analysis of muscles across the elbow joint by Funk et al, 1987. The muscle paths, and origins and insertions of the chosen muscles were obtained from a musculo-skeletal geometric analysis of the upper limb by Amis et al, 1979a. The relative muscle strengths and contributions at different flexion and extension angles were based upon reported data (An et al, 1989, and Amis et al, 1979a) and represented on the model by mechanical springs having different spring constants. Using the equal-stress concept (see 2.2.3), An et al (1989) determined the distribution of muscle forces across the elbow joint during isometric loading conditions. The individual muscle forces at the various flexion angles were obtained for the condition of a unit of one Newton of force applied perpendicularly at the distal forearm and 32 cm from the elbow joint centre in the sagittal plane. With the magnitudes of the muscle forces and the lengths of the muscles represented known, the mechanical springs' lengths were accordingly adjusted using a standard spring scale so that the tensions in the springs were equal to the relative muscle forces indicated by An et al, 1989.

The capsuloligamentous structures and articular surfaces constitute the primary mechanism to provide valgus-varus support and joint stability (Morrey et al, 1983), and with the radial head resected the lateral collateral ligament will take up loading of the radial collateral ligament, which is resected. Regan et al, 1991, have indicated that both the medial collateral ligament (MCL) and the lateral collateral ligament (LCL) will remain taut through most of flexion. Thus, the MCL and the LCL were included in the model, and the paths, and origins and insertions of the ligaments were obtained from a geometric analysis by Amis et al, 1979a.

The rig consists of a support base with a vertical bar attached to it, and a humeral bone support block screwed onto the bar (Figure 3.45). The ulna bone support block is completely detached from the rest of the rig. The distal humerus and proximal ulna are attached to these blocks by two screws, and the matching cut of the block and bone aided in providing adequate fixation and stability. Screws with holes drilled into the heads, for spring attachment, were inserted into muscle and ligament origin and insertion sites based upon three-dimensional anatomical data provided by Amis et al, 1981.

FIGURE 3.45. The rig developed for initial functional testing.

3.11.2 Rig evaluation

Molds were made having cavities of the shape of matching distal humerus and proximal ulna bones. The molds were then used to make resin models of the bones. The bone models were cut, and muscle and ligament origin and insertion screws inserted. The models were then attached to their respective blocks and the

various springs representing the different muscles and ligaments were attached.

The variation of muscle moment arms at the elbow during flexion was reported by Amis et al, 1979a, and the spring paths were accordingly adjusted with the use of a flexible band about the joint. The weight of the forearm is assumed to be 26 N acting at a point of centre of gravity 0.16 m from the joint axis (Amis et al, 1981).

The first test performed on the models determined the range of motion (ROM) of the joints. At the flexion-extension extremes, the structures limiting these ranges of motion were observed and compared with limitations noted by Morrey, 1985b. Valgus-varus stability was maintained by keeping the MCL and LCL taut throughout flexion as suggested by Regan et al, 1991. The carrying angles were measured and checked against normal values of 10 - 15 degrees (Morrey et al, 1985a). Pronation and supination could not be measured due to the absence of the radius bone.

Three bone models were tested and the results were comparable with data found in the literature. The averaged values for ROM were -5 degrees in the extended position to 150 degrees full flexion, compared to 0 - 145 degrees listed by Morrey, 1985b. The ROM was limited by the impact of the olecranon process on the olecranon fossa and the coronoid process against the coronoid fossa.

The joint was manipulated by hand to subjectively observe the varus/valgus stability of the articulation and the overall joint alignment from an antero-posterior view. The articulation

controlled the movement of the to the extent that no gross varus/valgus instability was observed. The carrying angle was measured and at full extension was recorded to be 10 degrees. At varying angles of flexion the ulna followed a natural course as controlled by the articulation.

The models were each tested twice and the results were consistent. Based on all the results and observations the rig appeared to provide an adequate reproduction of the normal elbow joint for an initial functional analysis of the prosthesis.

3.11.3 Prosthesis evaluation

The molds having the cavities of the shapes of the distal humerus and proximal ulna of a specimen were used to make models of the components implanted into resin bone casts. This method would provide an accurate geometrical fit of the prosthesis and ensure that an accurate alignment of the components is achieved. The resin would be reinforced with glass fibres for added strength, but will still be transparent enough to allow for adequate evaluation of the fixation devices and the amount of bone removed.

The metal humeral component and the plastic ulnar component were inserted into the respective molds and aligned with and pressed into the articular surface cavities. The resin was then poured into the mold to assume the shapes of the 'cut' bones, with the components taking the place of the resected bone.

The components were now implanted in the resin bone models and several design concepts were observed (Figure 3.46). The fixation devices on both components were anatomically accurate with sufficient bone stock surrounding the devices to provide adequate support and to prevent cortical bone impingement. A minimal amount of bone stock is removed from the distal humerus, and compared with most other established elbow prostheses, this design allows a substantial amount more bone stock to be saved.

The bone/prosthesis models were cut, aligned, and attached to the rig blocks. The necessary muscle and ligament origin and insertion screws were inserted and the various springs attached.

FIGURE 3.46. The prototypes implanted in resin bone models.

The range of motion (ROM) was measured and the structures limiting the motion at the extremes were also observed. A value of 0 degrees was recorded in the extension position and 135 degrees in flexion. The extension value is in agreement with normal values reported (Morrey, 1985b), but the flexion value was possibly 5 - 10 degrees below an acceptable value, especially since the structures limiting extreme flexion ROM were the ulnar component's olecranon process and the humeral bone's olecranon sulcus. This component's impingement with the bone can be avoided by removing a certain amount of the olecranon process from the ulnar component. At extreme extension, the ROM was limited by the coronoid process of the component and the coronoid sulcus of the distal humerus.

The anatomy of the elbow joint articulation provides the joint with an inherent stability, with the joint articulation recognized as a primary stabilizer of the elbow (Morrey and An, 1983). Thus, the joint with the prosthesis was expected to be stable as the prosthesis articular surfaces were modelled on normal anatomical surfaces. No gross valgus-varus instability was observed following manipulation of the block by hand.

No possibility of dislocation was apparent, but the load imparted across the joint was extremely small and elbow dislocation is usually a high-energy episode.

This initial functional testing on the simple rig developed has allowed the evaluation of several design criteria. The articulation and stability of the joint appears adequate, but this is expected with accurate reconstruction of the articular

surfaces and the collateral ligaments preserved and assumed to be functionally sound.

An initial assessment of the instrument requirements indicated that special purpose instrumentation would be necessary to provide an accurate alignment of the components and this will also provide convenience for the surgeon. With the anatomical (geometrical) design of the components and the "ease of insertion tap-in" design concept, the alignment and cutting instrumentation could be one instrument allowing for a simple cut of the bone and simple accurate positioning of the components. The geometrical analysis and anatomical design will allow accurate three-dimensional positioning of the axis of rotation with respect to extra-articular landmarks such as the humerus and ulna shafts, trochlea flanges, epicondyles, or other acceptable landmarks.

CHAPTER 4: DISCUSSION

No studies were found in the literature that supplied accurate numerical data on the geometry of the articular surfaces of the elbow joint. Thus, an extensive geometrical analysis of the articular surfaces was undertaken. Several methods were considered in the determination of the three-dimensional geometry of the articular surfaces of the distal humerus and proximal ulna. The methods considered were "close-range" stereophotogrammetry (SPG), a slicing technique (Shiba et al, 1988), and a biostereometric technique (Reflex Microscope).

Accuracies encountered by several authors (Huiskes et al 1985, Ghosh 1983, Ateshian et al 1991, Scott 1981) using the SPG method are in the ranges of .09 - .2 mm, but the Biostereometric measuring instrument which was used in this project (Reflex Microscope) can achieve accuracies of ± 0.02 mm (Scott, 1981) on objects whose largest dimension is 100 mm. This indicates a greater accuracy than the stereophotogrammetric technique. Other authors who have measured joint surfaces do not report on the accuracy or precision obtained. This includes Shiba et al, 1988, whose method included cutting the surface with a bone milling machine, photographing the cuts, and finally digitising the outlines. It is doubtful this method is more precise than the stereophotogrammetric one. The procedure is also a much simpler

one compared to the other methods discussed, requiring no cutting of the bone and no photographic evaluation. The precision obtained in this study was of the order of 0.05 mm, which when compared to other methods (.116 - .27 mm) is far more precise. The reflex microscope thus was used to provide accurate three-dimensional data for the "fitting" of equations, the articular surface curvature determination, and the extra-articular geometric analysis.

Following the accurate observations of the articular surfaces, the various mathematical approximations were made.

The first hypothesis tested was that of the hyperbolic paraboloid. The trochlea articulating surface appeared to resemble the shape of this known quadric form, and Morrey (1985a) also described the surface as being hyperboloid in shape. The estimated errors indicated that the fit of the hyperbolic paraboloid to the trochlear, olecranon, and coronoid articular surfaces was not acceptable, with errors in the order of 1 mm in certain traces.

The assumption of circularity was tested by fitting a circle to profiles measured in the sagittal plane. The results of our study revealed that the curved surface of the trochlea is circular in the sagittal plane and that the centres of these circles lie virtually on a straight line. This agrees with London's (1981) view that a single axis of rotation exists through most of the elbow joints range of motion.

Most current prostheses have an ulnar component that is

totally congruent with the humeral component. Our study however, found that the ulna has two distinct articular facets with noncoincident centres of curvature, which agrees with Shiba et al, 1988. The coronoid facet thus appears to articulate with the trochlea during early flexion and the olecranon facet during terminal flexion.

The deviation from the straight centre line of the trochlea by the posterior lateral flange section could be of importance. During terminal flexion of the elbow this lateral flange section might be the primary stabilizer and bearing surface of a valgus stress (Shiba et al, 1988). This structure, therefore, was included in the design of the articular surface, but is disregarded in prostheses that do not duplicate the normal elbow joint articulation.

It is important to note that although this design allows for a certain amount of incongruency between the humeral and ulnar component, due to the two ulnar component bearing surfaces, it does not imply that incongruent contact occurs. The articular surface of the humeral component articulates mainly with the coronoid facet of the ulnar component during early flexion and with the olecranon facet during late flexion. This provides two articulating surfaces of congruent-type contact. Thus, the concern of highly incongruent contact producing high contact stresses and a high wear rate is avoided. However, an experimental contact stress analysis will need to be performed to ensure that the surface contact is adequate and that the prosthesis is competent to support the expected loads.

Morrey (1985a) described the central groove of the trochlea as being helical in form. Furthermore, one of the prosthesis designs (Helfet, DePuy, USA) allowed for helical motion to take place about the trochlear groove. This study, however, revealed that a poor fit was achieved testing the helical hypothesis, indicating that the trochlea is not a circular helix in form.

The trochlear groove was determined to be at an angle of inclination of about 3 degrees in the antero-posterior aspect. Similarly, Shiba et al 1988, found that from an anterior view the plane formed by the central groove of the trochlea was inclined at an angle (2.5 degrees for male and 6.5 degrees for female specimens) from the plane containing the line perpendicular to the centre line of the trochlea. The angle of inclination of the prosthesis tested (Helfet), calculated at 10.3 degrees, appears too large when compared to the anatomical values determined.

The accurate three-dimensional cartilage thickness data obtained helped to advance our understanding of the complex geometry and biomechanics of the elbow joint and aided in the development of an anatomically accurate artificial joint. In the future developmental phase of the prosthesis, this information will aid in ascertaining variations over the joint surfaces, which are important in determining stresses and strains within the implants during joint function, and the development of accurate finite element models.

With the renewed interest over the last few years in the wear of the UHMWPE components in artificial joints, which may contribute to loosening of prostheses, the use of low elastic

modulus layers, or "cushion form" bearings, is being investigated for the hip (Unsworth et al, 1981) and the knee (Murakami and Ohtsuki, 1989) prostheses. The determination of articular cartilage thickness has provided information required for the future investigation into the possibility of incorporating such a "compliant layer", or the "cushion" bearing concept, into the design of the implant. Materials with an elastic modulus between 3 and 50 MPa are being considered as potential synthetic cartilage equivalents. An artificial joint with this thin compliant layer would then articulate with full fluid film lubrication which could greatly reduce wear and frictional torque, and thus reduce the incidence of loosening. Contact area and wear studies are being performed (O'Carrol et al, 1990) to provide a sound basis for design analysis of "cushion forms" of total replacement joints. With favourable results this concept could be incorporated into the design of this elbow prosthesis.

The extra-articular geometric analysis supplied suitable sites for the bases, trochlear flanges, and ulnar stem and cross to be situated. The study has also provided accurate data for the orientation and placement of the articular surfaces with regards to the extra-articular structures and landmarks.

The geometric analysis ensured that the design of the posterior and inferior bases supporting the articular surfaces of the ulnar component and the medial and lateral spiked flanges of the humeral component allowed minimal resection of bone.

Severe erosion or total destruction of the joint, as

encountered in late phase 4 or early phase 5 rheumatoid arthritis (as defined by Souter, 1990), may require additional fixation. Thus, an anatomical stem could be incorporated into the design of an optional stemmed humeral component. An initial analysis of the geometry of the humero-ulnar joint indicates that a solid stem could originate from the trochlear groove base of the solid trochlear shell and then follow the anatomy of the distal humerus proximally. The stem of the implant should be parallel to the cortex of the medullary canal, otherwise if the component stem is anteriorly orientated atrophy of the metaphyseal bone and hypertrophy of the cortical bone about the tip of the stem could be encouraged.

With the stemmed humeral component, the corresponding ulnar component will have a flatter and not as prominent olecranon process to prevent any process-stem impingement.

The real elbow joint is considerably more complicated in material properties and loading conditions than that represented by the model. Despite these simplifications and idealizations, it is believed that the analysis offered valuable insight into the range of motion (ROM) capabilities, and possible limitations, of the elbow with the prosthesis implanted. Morrey, 1985b, states that limitation of ROM is due to a combination of surface/bone impact, capsules, ligaments and muscles. The springs on the rig however, could not be the primary ROM limiting factor as this restriction would prove to be an artificial constraint imposed by the test apparatus.

The olecranon process of the ulnar component did however

impinge with the olecranon sulcus of the distal humerus during extreme flexion, limiting the ROM to 135 degrees. A visual contact area observation at this stage revealed that removal of a small amount of UHMWPE from the ulnar component would not affect the ROM any further.

To theoretically ascertain the probability of success of the proposed prosthesis, it is important to compare it to other total elbow replacements. The clinical results with the existing prostheses can be examined in order to establish the reasons of failure of these implants. It is sometimes obvious that clinical failures could be attributed to "bad" design features of prostheses and these were carefully assessed. In the same manner, the advantageous design features were analyzed and incorporated into our prosthesis design. One of the problems with this method is the lack of information in the literature critically evaluating the failure mechanisms of failed prostheses. However, based upon the clinical complication and failure rates observed in the literature, it is clear that the unlinked type prosthesis is proving to be more successful than the linked type. It must be made clear though that the semi-constrained type prosthesis still has its place in TEA: to be used in patients with deficient bone stock and who do not have ligamentous and soft tissue competence. Of major importance in the design aspect of this elbow prosthesis was that a minimal amount of bone should be resected for the insertion and placement of the components. A resurfacing procedure (unlinked) would best accomplish this and then would be sufficient bone stock for a revision surgery should

the prosthesis fail. This prosthesis appears to resect less bone than several currently available unlinked type designs (e.g. Souter/Strathclyde, Capitello-Condylar).

Instability is the major complication (Kudo and Iwano 1990, Poll and Rozing 1991, Rosenburg and Turner 1983) encountered with current unlinked type prostheses. Many prostheses have disregarded the normal anatomical articulation of the elbow joint and this could be a primary factor accounting for this specific complication. This prosthesis design accurately models the normal elbow joint articulating surfaces in the attempt to reproduce the natural joint articulation and kinematics, and recreate a normal functional stabilized elbow joint.

The fixation has also been designed to resist the large torsional forces across the elbow noted by Souter (1990), and the cyclical pattern of forces at the joint as indicated by Amis and Miller (1984).

In a final analysis of the design of the prosthesis, it was evaluated based upon the basic requirements and design criteria for total joint replacements as described by Elloy et al, 1976. They have determined that there are several design criteria which need to be employed to ensure the longevity of a joint replacement. The important criteria include: 1) Appropriate articulation, 2) Good stability, 3) Adequate strength, 4) Good fixation, 5) Correct choice of materials, 6) Low friction forces, 7) Acceptable wear rate, 8) Good salvage potential and surgical instrumentation.

The four factors that satisfy the appropriate articulation

criteria of this prosthesis are: a) the axis of rotation of the prosthesis accurately approximates that of the normal joint, b) the degrees of freedom of the prosthesis matches those of the normal joint, c) the range of motion is sufficient to provide adequate function, and d) the components articulate with each other and do not impinge with other parts of the joint.

Elloy et al (1976) also indicate that the stability of the normal joint derives from the proper relationship between the shape of the articular surfaces, the muscles about the joint, and position of the ligaments. The extensive articular surface analysis allowing for an accurate reconstruction of the shape of the normal joint surfaces, and the preservation of the collateral ligaments should ensure that good stability is achieved.

The components have been designed to support the loads to which the elbow is subjected as indicated in force analyses by several authors.

The fixation devices were designed to make use of the natural load bearing structures. A minimal amount of cement is required for fixation of the ulnar component, and the humeral component achieves fixation by an interference fit, thus requiring no cementing. This should reduce the possible damage to the adjacent bone either by avascular necrosis or thermal damage. Good surface contact between the prosthesis and the bone should be achieved with the interference fit aided by precision instrumentation.

The choice of the now standard implant materials should satisfy the correct choice of materials requirement. The metal alloy against UHMWPE combination is chosen because of the low

friction of the materials. This material selection and the attempt to reproduce the normal surface contact areas should provide an acceptable wear rate. The choice of the metal alloy (Stainless steel 316L medical grade or Cobalt-Chrome-Molybdenum alloy) will only be determined after consultation with the possible manufacturer of the prosthesis. Titanium alloy is contra-indicated as the material to be used for articular surfaces.

An important part of the design phase of this implant was ensuring that it was possible to carry out a salvage procedure should the prosthesis fail. This was achieved by the "minimal bone resection" concept, and the fixation design to allow for "ease of removal" of the failed implant. The salvage potential was assessed and due to the design allowing a minimal amount of bone to be resected, the surgeon is left with a greater choice of procedures for revision surgery. The prosthesis has not been designed to resist large tensile forces and the direct straight-line orientation and "ease of insertion tap-in" of the components should not make them particularly difficult to remove.

The simple "tap-in" concept, and the accurate geometrical analysis performed, allowing availability of special instrumentation, will ensure that the surgical procedure is relatively simple; thus, reducing the risk of surgical error and minimizing operative time and trauma.

Ideally a single implant suitable for bilateral use is desirable. However, this study has revealed the complex nature of the anatomy of the elbow joint, and a right and left prosthesis is indicated to achieve an accurate reconstruction of

the normal joint. This could be acceptable from a technical standpoint.

CHAPTER 5: CONCLUSIONS AND RECOMMENDATIONS

Conclusions:

• The "fit" of the known quadric form, hyperbolic paraboloid, to the articular surface data was not acceptable.

• The curved surface of the trochlea is circular in the sagittal plane and the centres of these circles lie virtually on a straight line. The posterior lateral flange section of the trochlea however, deviates from the centre line of the trochlea. The ulna surface has two distinct articular facets (olecranon and coronoid) with noncoincident centres of curvature.

• The trochlea is not a circular helix in shape. The trochlear groove however, is inclined at an angle, ± 3 degrees in the anterior-posterior aspect, to the plane containing the line perpendicular to the centre line of the trochlea. From the distal view, there is no inclination angle.

• An exact description of the curvature, extra-articular geometry, and cartilage thickness was established and is essential for prosthesis design considerations.

• Good fixation, minimal invasion of the surrounding bone, an

"ease of insertion" technique, and the reproduction of the natural joint articulation and kinematics are objectives that were achieved with the development of this elbow prosthesis.

At this stage of the design phase, the prosthesis has satisfied the numerous design criteria, and the various design concept requirements have also been achieved, all of which provide a good basic design upon which to build. It is clear that the prosthesis must now undergo further experimental testing before a final design can be introduced to clinical trials.

Follow-up testing would involve the insertion of the prototype into cadavers. The functional tests performed on the rig could be repeated on the cadaver and the results compared. Further testing would include:

- checking for possible component interference (bone, nerve, and vessels),
- surgeon developing his surgical approach,
- accurate assessment of instrument requirements,
- surgeon assessing possible salvage procedure(s).

Additional testing would include:

- contact area determination for evaluation of contact stresses,
- an experimental stress analysis.

In the end, it is hoped that the results achieved with this

study will help to provide a satisfactory prosthesis that will reduce the high complication frequency, of loosening and instability, currently encountered with Total Elbow Replacement Arthroplasty.

APPENDICES

APPENDIX A

Digitisation flowchart (as determined by the Biostereometrics Laboratory).

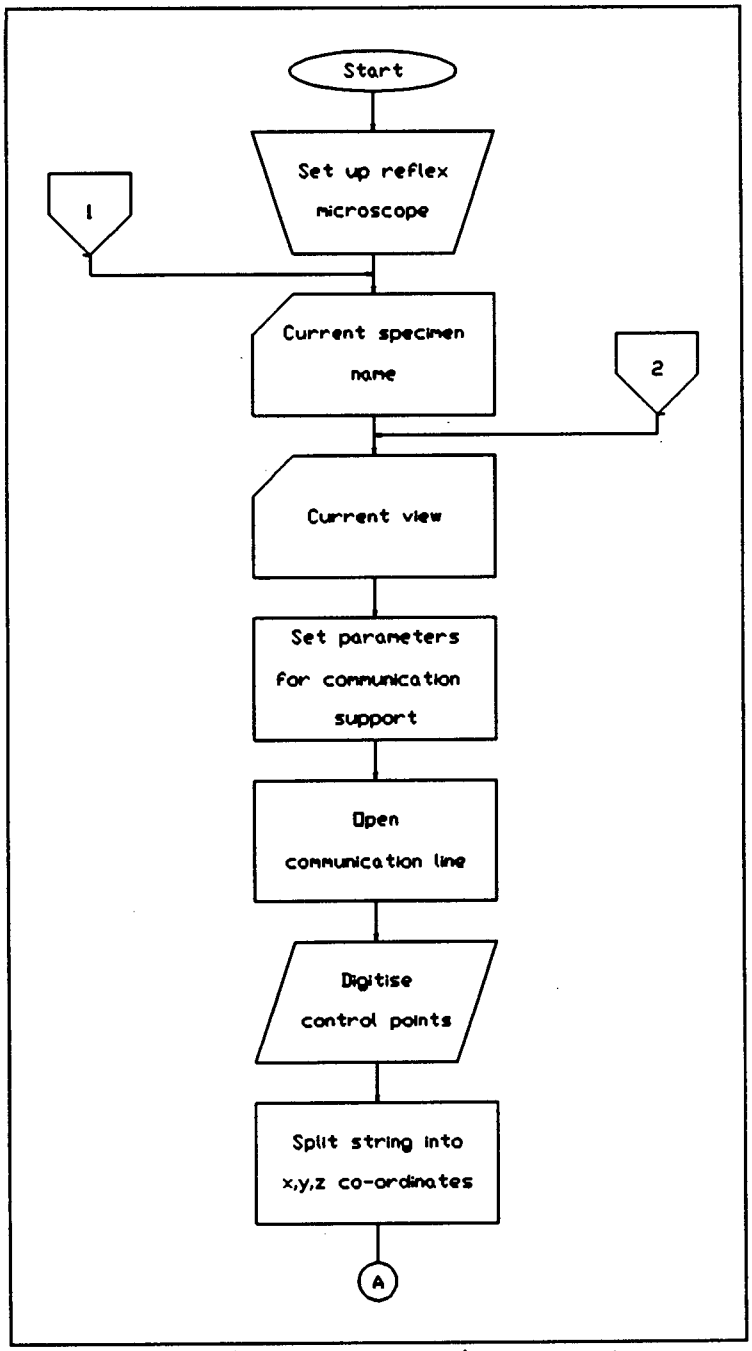

(continued following page)

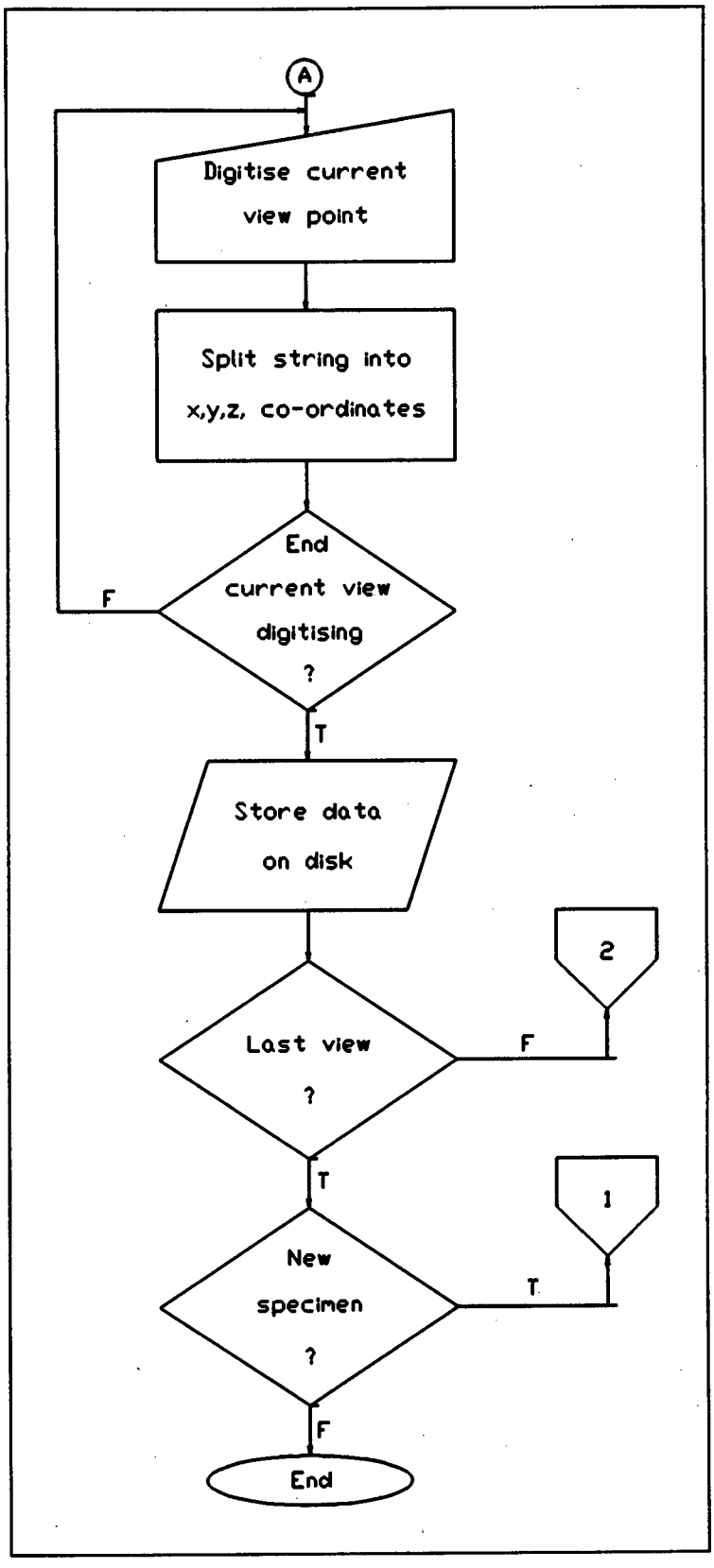
A
Digitise current view point
Split string into x,y,z, co-ordinates
End current view digitising ?
F
T
Store data on disk
2
Last view ?
F
T
1
New specimen ?
T
F
End

APPENDIX B

Transformation algorithm

Principles of the mathematical procedure of the transformation method

Three-dimensional Photogrammetric case.

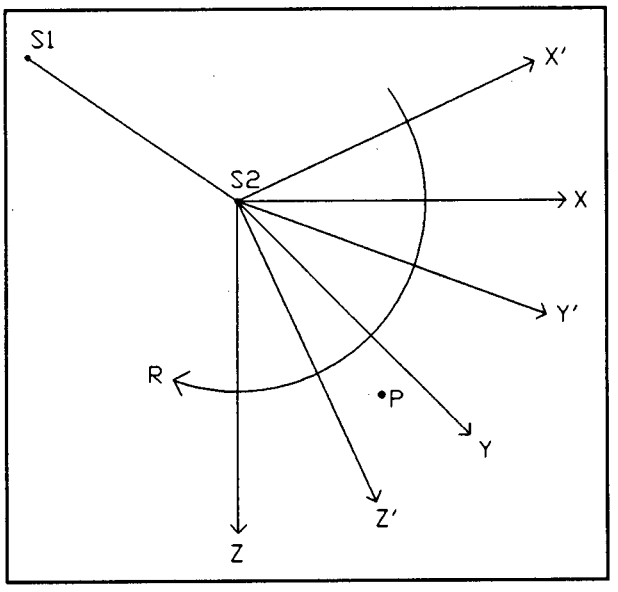

FIGURE A.1. Rotation of axes.

The xyz co-ordinates of the points in the first view (eg. anterior view of the trochlea articular surface) were measured in the co-ordinate system S1 having axes x,y,z. The co-ordinates of the points in the second view (eg. posterior view of the trochlea articular surface) were measured in the co-ordinate system x′,y′,z′ (S2). To create a single image of the two views (i.e. entire trochlea), it is required to have the co-ordinates

of each point (P) in the second co-ordinate system in terms of the first system. Thus, P remains fixed and the second views axes are rotated into the system of the first views axes by a rotation matrix R (Figure A.1).

$$\begin{bmatrix} x_p \\ y_p \\ z_p \end{bmatrix} = R \begin{bmatrix} x_p' \\ y_p' \\ z_p' \end{bmatrix}$$

If **R** is orthogonal

$$R^{-1} = R^T$$

$$\therefore \quad \begin{bmatrix} x_p' \\ y_p' \\ z_p' \end{bmatrix} = R^T \begin{bmatrix} x_p \\ y_p \\ z_p \end{bmatrix} \qquad \ldots (a)$$

and **R** is given by

$$R = (I-S)\ (I+S)^{-1} \qquad \textit{(Caley's formula)}$$

The method is described below and the computational algorithm is also included after this description.

R is a rotation matrix and is given by

$$\mathbf{R = (I - S)\ (I + S)^{-1}}$$

which is Caley's formula. **S** is a skew symmetric matrix expressed in terms of three independent parameters (the Rodrigues'

parameters: lambda, mu, and nu). Following substitution into equation (a) and multiplying out, three linear equations can now be formed for every common point. It is now possible to solve for lambda, mu, and nu using "least squares" methodology. Following this, the rotation matrix **R** is formed which allows for the transformation of any point in the second co-ordinate system into the first system.

Computing algorithm for solving the Rodrigues parameters and forming the orthogonal matrix **R**.

Caley's formula states that, if **S** is a real skew-symmetric matrix, then

$$R = (I-S)\,(I+S)^{-1}$$

is orthogonal.

If **S** is of order 3 × 3 we may put

$$S = \frac{1}{2}\begin{vmatrix} 0 & \nu & -\mu \\ -\nu & 0 & \lambda \\ \mu & -\lambda & 0 \end{vmatrix}$$

where lambda, mu, and nu are known as the Rodrigues parameters.

If **S** is substituted into Caley's formula the following relation is obtained:

$$R = \frac{1}{\Delta}\begin{pmatrix} 1+\frac{1}{4}(\lambda^2-\mu^2-\nu^2) & -\nu+\frac{1}{2}\lambda\mu & \mu+\frac{1}{2}\lambda\nu \\ \nu+\frac{1}{2}\mu\lambda & 1+\frac{1}{4}(-\lambda^2+\mu^2-\nu^2) & -\lambda+\frac{1}{2}\mu\nu \\ -\mu+\frac{1}{2}\nu\lambda & \lambda+\frac{1}{2}\nu\mu & 1+\frac{1}{4}(-\lambda^2-\mu^2+\nu^2) \end{pmatrix} \quad \cdots\cdots(1)$$

where

$$\Delta = |I+S| = 1+\tfrac{1}{4}(\lambda^2+\mu^2+\nu^2)$$

This result is very useful because it expresses a general orthogonal matrix of order 3 × 3 in terms of three independent parameters (the Rodrigues parameters) and without trigonometrical functions.

<u>To solve for lambda, mu, and nu.</u>

$$R = (I-S)\,(I+S)^{-1}$$

is orthogonal, and **S** is skew symmetric

$$\therefore \quad S^T = -S$$

$$R^T = \left[(I-S)\ (I+S)^{-1}\right]^T$$

$$\therefore \quad R^T = (I-S)^{-1}\ (I+S)$$

But

$$\begin{bmatrix} x' \\ y' \\ z' \end{bmatrix} = R^T \begin{bmatrix} x \\ y \\ z \end{bmatrix}$$

$$\therefore \quad (I-S) \begin{bmatrix} x' \\ y' \\ z' \end{bmatrix} = (I+S) \begin{bmatrix} x \\ y \\ z \end{bmatrix}$$

In terms of λ, μ, and ν

$$\begin{bmatrix} 1 & -\nu/2 & \mu/2 \\ \nu/2 & 1 & -\lambda/2 \\ -\mu/2 & \lambda/2 & 1 \end{bmatrix} \begin{bmatrix} x' \\ y' \\ z' \end{bmatrix} = \begin{bmatrix} 1 & \nu/2 & -\mu/2 \\ -\nu/2 & 1 & \lambda/2 \\ \mu/2 & -\lambda/2 & 1 \end{bmatrix} \begin{bmatrix} x \\ y \\ z \end{bmatrix}$$

Multiplying out and gathering terms gives:

$$\begin{bmatrix} 0 & -(z+z') & (y+y') \\ (z+z') & 0 & -(x+x') \\ -(y+y') & (x+x') & 0 \end{bmatrix} \begin{bmatrix} \lambda \\ \mu \\ \nu \end{bmatrix} = 2 \begin{bmatrix} (x'-x) \\ (y'-y) \\ (z'-z) \end{bmatrix} \quad \cdots\cdots (2)$$

For every common point we can form 3 linear equations. A single common point will of course not allow us to solve for λ, μ, and ν since the left handed matrix is skew symmetric and hence singular, but if we have a number of common points referred to a single origin (the centre of gravity of the points) we can set up solution equations in the form of

$$\begin{bmatrix} \lambda \\ \mu \\ \nu \end{bmatrix} = (\boldsymbol{A}^T \boldsymbol{A})^{-1} \boldsymbol{A}^T \boldsymbol{L} \quad \cdots\cdots(3)$$

which will give the 'least squares' solution for λ, μ, and ν.

The transformation method adopted assumes that there is no scale change between the two systems which is sensible since the common transformation points are measured in the same instrument and to the same precision.

λ, μ, and ν are now substituted in equation (1) and the rotation matrix **R** is formed which allows for the transformation of any point of the common origin second point observations set into the first set of co-ordinates from the relationship:

$$\begin{bmatrix} x_p \\ y_p \\ z_p \end{bmatrix} = \boldsymbol{R} \begin{bmatrix} x'_p \\ y'_p \\ z'_p \end{bmatrix}$$

Precision test of the transformation.

The precision is estimated by comparing the co-ordinates obtained in repeated measurements of the transformation (control) points from:

$$Dx = x_k^1 - x_k^2$$

$$Dy = y_k^1 - y_k^2$$

$$Dz = z_k^1 - z_k^2$$

where x_k^1 is the first x co-ordinate the control point 'k', and x_k^2 the second x co-ordinate of this same control point 'k' (y and z co-ordinates accordingly).

APPENDIX C

The hyperbolic paraboloid hypothesis

The best fit process, as an optimization problem is formulated in the following manner.

Following the observation of the surface, find the best fit hyperbolic paraboloid, minimizing the sum of squares of the observation errors. For any **c**, corresponding values for **a** and **b** exist. Thus, choosing a value for **c**, best estimates of **a**, **b**, and x_0, y_0, z_0 parameters can be computed without affecting the shape and size of the hyperbolic paraboloid. The estimated shift parameters and the adjusted observations are invariant quantities meaning that the best fitted hyperbolic paraboloid is the same for any value of **c**.

Computing algorithm

The original non-linear equation of the hyperbolic paraboloid,

$$\left(\frac{x-x_0}{a}\right)^2 - \left(\frac{y-y_0}{b}\right)^2 - \frac{z-z_0}{c} = 0$$

has the form:

$$\boldsymbol{u}(\boldsymbol{x}^a, \boldsymbol{y}^a) = \mathbf{0}$$

where

$\boldsymbol{x}^a$ = m×1 *vector of unknown parameters*

$\boldsymbol{y}^a$ = n×1 *vector of observed quantities*

The corresponding linear equations have the form;

$$\boldsymbol{w} + \boldsymbol{A}\boldsymbol{x} = \boldsymbol{B}\boldsymbol{v}$$

where

- $\boldsymbol{w}$ = s×1 *vector of observed points*

$$\boldsymbol{w} = \boldsymbol{u}(\boldsymbol{x}^0, \boldsymbol{y}^b)$$

with

$\boldsymbol{x}^0$ = *vector of approximate values of parameters*

$\boldsymbol{y}^b$ = *vector of observations*

- $\boldsymbol{v}$ = *error vector of observations*:

$$\boldsymbol{v} = \boldsymbol{y}^b - \boldsymbol{y}^a$$

- $\boldsymbol{A}$ = *the design matrix* s×m:

$$\boldsymbol{A} = \left.\frac{\partial \boldsymbol{u}}{\partial \boldsymbol{x}^a}\right|_{0,b}$$

- $\boldsymbol{B}$ = *a matrix s×n*:

$$\boldsymbol{B} = \left.\frac{\partial \boldsymbol{u}}{\partial \boldsymbol{y}^{a}}\right|_{0,b}$$

- $\boldsymbol{x}$ = *a vector m×1*:

$$\boldsymbol{x} = \boldsymbol{x}^{a} - \boldsymbol{x}^{0}$$

The least square algorithm is applied and the best estimates are computed:

$$\hat{\boldsymbol{x}} = -(\boldsymbol{A}^{T}\boldsymbol{M}^{-1}\boldsymbol{A})^{-1}(\boldsymbol{A}^{T}\boldsymbol{M}^{-1}\boldsymbol{w})$$

Where

$$\boldsymbol{M} = \boldsymbol{B}\boldsymbol{P}^{-1}\boldsymbol{B}^{T}$$

$$\boldsymbol{P}^{-1} = \textit{unit matrix}$$

$$\hat{\boldsymbol{x}}^{a} = \boldsymbol{x}^{0} + \hat{\boldsymbol{x}}$$

$$\hat{\boldsymbol{v}} = \boldsymbol{P}^{-1}\boldsymbol{B}^{T}\boldsymbol{M}^{-1}(\boldsymbol{w} + \boldsymbol{A}\hat{\boldsymbol{x}})$$

$$\hat{\boldsymbol{y}}^{a} = \boldsymbol{y}^{b} - \hat{\boldsymbol{v}}$$

APPENDIX D

Circle theory

Adams (1976) elegantly describes the theoretical determination of the co-ordinates of the centre and the radius of a circle in his paper. The testing of the "circularity" hypothesis used Adams's methodology and it is included in detail in the following section (Adapted from Adams, 1976).

The equation of a circle of radius R, centre at x_0, y_0 is:

$$(x-x_0)^2+(y-y_0)^2 = R^2$$

From 3 suitably sited points on the circumference of the circle, the approximate centre co-ordinates and the approximate radius are calculated:

let

x_a, y_a = *approximate centre co-ordinates*

R_a = *approximate radius*

Now let:

$$x_0 = x_a+\Delta x$$

$$y_0 = y_a+\Delta y$$

$$R = R_a + \Delta R$$

Then substituting and expanding:

$$x^2 - 2x_a x - 2x\Delta x + x_a^2 + 2x_a\Delta x + (\Delta x)^2 + y^2 - 2y_a y$$

$$-2y\Delta y + y_a^2 + 2y_a\Delta y + (\Delta y)^2 = R_a^2 + 2R_a\Delta R + (\Delta R)^2 \qquad \ldots (1)$$

A line between the approximate values of the circle centre and any point on the circumference of the circle gives:-

$$(x_a - x)^2 + (y_a - y)^2 = D^2 \qquad \ldots (2)$$

Expanding, then subtracting equation (2) from equation (1), eliminating squared terms $(\Delta x)^2$, $(\Delta y)^2$, and $(\Delta R)^2$, (Δx, Δy, and ΔR are small, therefore $(\Delta x)^2$ etc. are of second order of smallness), and simplifying yields:

$$(x_a - x)\Delta x + (y_a - y)\Delta y - R_a\Delta R = \frac{R_a^2 - D^2}{2}$$

For simplification,

$$Let \quad \frac{R_a^2 - D^2}{2} = d$$

For 'n' observations, NORMAL EQUATIONS can then be formed as follows:-

Δx	Δy	ΔR	$= L$
$[(x_a - x)^2]$	$[(x_a - x)(y_a - y)]$	$-[(x_a - x)(R_a)]$	$[(x_a - x)(d)]$
	$[(y_a - y)^2]$	$-[(y_a - y)(R_a)]$	$[(y_a - y)(d)]$
		$[(R_a)^2]$	$-[(R_a)(d)]$

A single iteration is sufficient, and following the determination of Δx, Δy, and ΔR, the values are applied to x_a, y_a, R_a to obtain x_0, y_0, and R_0.

APPENDIX E

The Grid Interpolation algorithm - SACLANT

The method of two-dimensional interpolation consists of an initial assignment of values to the grid points followed by a process whereby the grid values are iteratively improved until the surface through the original data points has attained a satisfactory state of "smoothness" (Saclant Graphics Package, User Support Services, University of Cape Town, 1989).

- The grid points initially receive the values of the data points nearest them.
- The grid points "near" to original data points are called "DATAPOINTS" and the other grid points remain as "NON-DATAPOINTS".
- The "DATAPOINTS" are assigned the values of the nearest original data points and the "NON-DATAPOINTS" receive the values of their "DATAPOINT" neighbours.

- The grid values are now improved by an iterative process:-
(a) The "NON-DATAPOINTS" are adjusted by a combination of linear and third degree polynomial interpolations through their immediate neighbours indicated in Figure D.1.

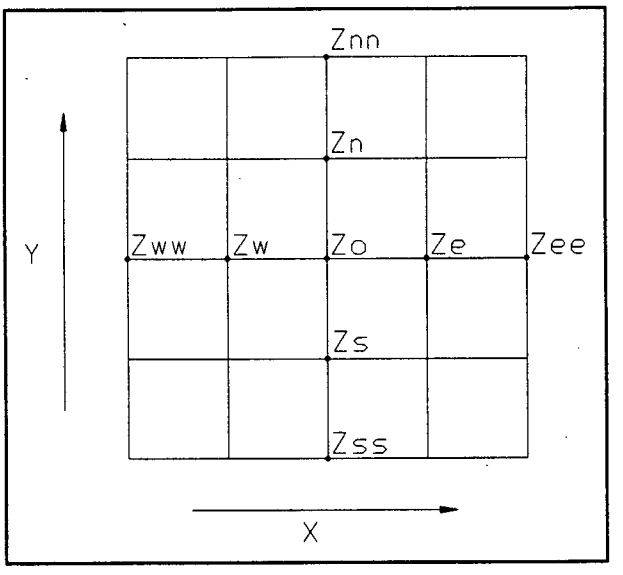

FIGURE D.1. "NON-DATAPOINT" grid.

The "ideal" z value is a weighted average of four different interpolated values and is determined as follows:

$$z\text{-}ideal = (2(z_0 \textit{ linearly interpolated between } z_w \textit{ and } z_e)$$

$$+ 6 \times CAY \times (z_0 \textit{ polynomially interpolated between } z_{ww}, z_w, z_e, \textit{and } z_{ee})$$

$$+ \textit{similar in the y-direction}) \; / G$$

where

$$G = 2(2+6(CAY))$$

and CAY determines the type of interpolation used; as CAY is increased the polynomial interpolation predominates over the linear.

z_0 is adjusted by the amount Dz × R, where Dz = (z-ideal) - z_0 and 1 < R < 2. R initially has the value 1, and is enlarged if necessary after 20, 40, and 60 iterations.

(b) The "DATAPOINTS" are improved by shifting them closer to their original positions (Figure D.2).

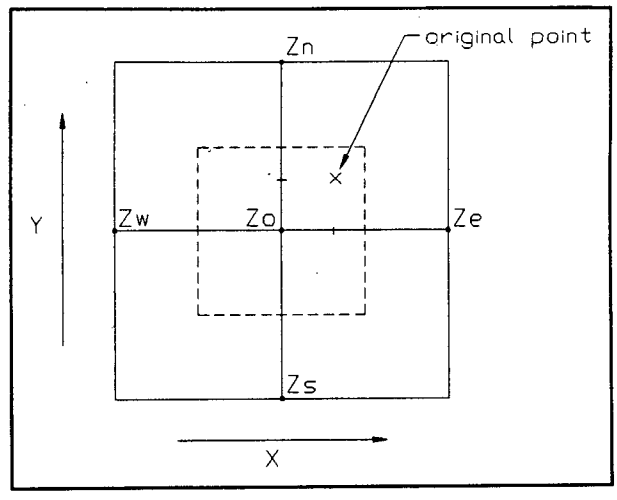

FIGURE D.2. "DATAPOINT" grid.

Parabolas are fitted through z_w-z_0-z_e (x-direction) and z_s-z_0-z_n (y-direction). Values at x and y are calculated and the grid value, z_0, is then adjusted by using:

Dz = (value at x - z_0) + (value at y - z_0).

- Four Laplacian smoothings of the final grid values are then performed.

APPENDIX F

Conversion of data files into AutoCAD drawing files

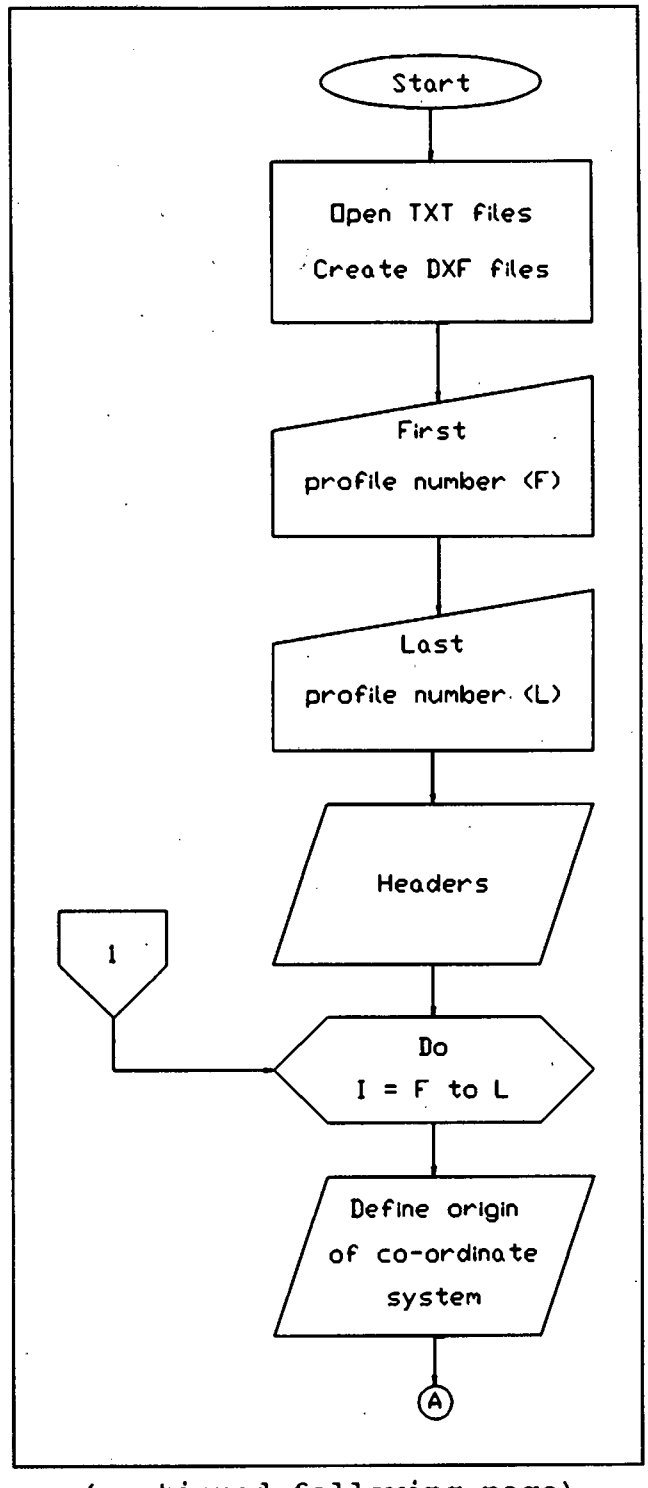

(continued following page)

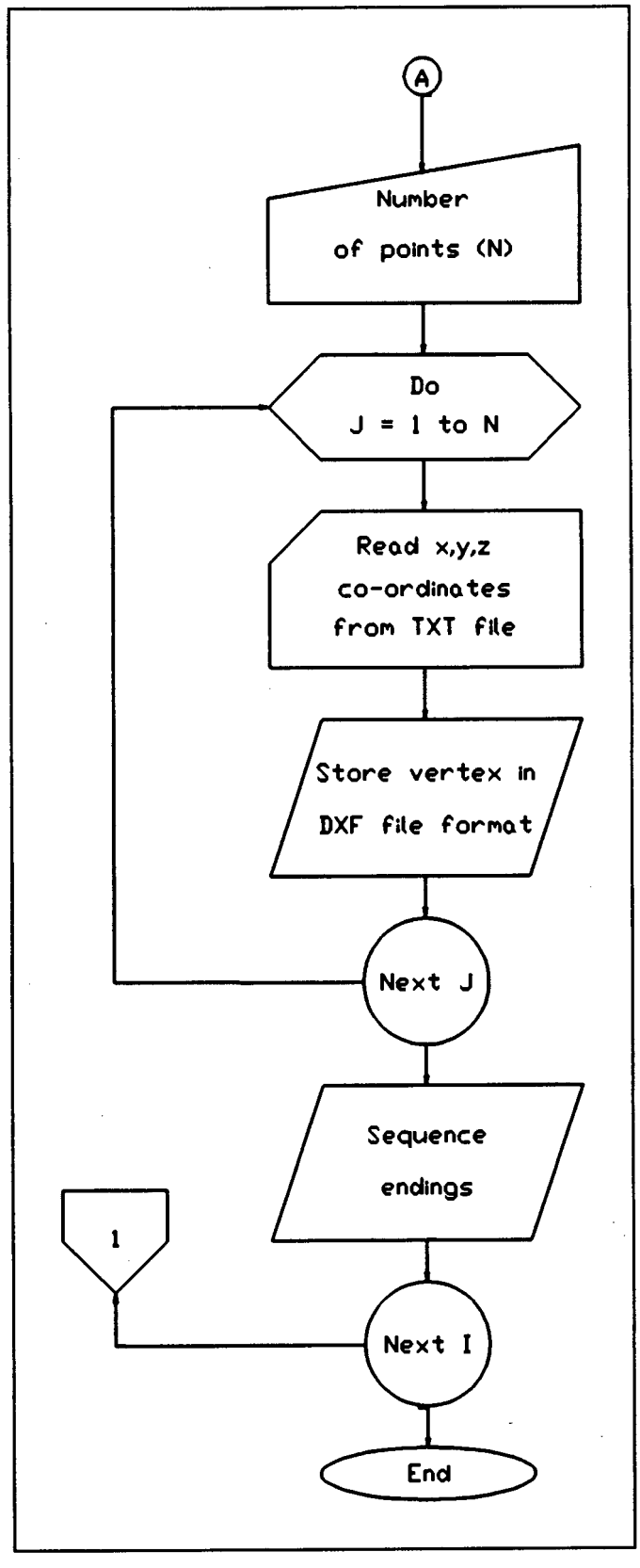
A
Number
of points (N)
Do
J = 1 to N
Read x,y,z
co-ordinates
from TXT file
Store vertex in
DXF file format
Next J
Sequence
endings
1
Next I
End

APPENDIX G

Final drawings of component prototypes

Prototype drawings of the humeral and ulnar components

Figures G1 - G12 present the drawing of the final prototype. Humeral component: G1) articular surface, G2) side view, G3) top view, G4) front view.

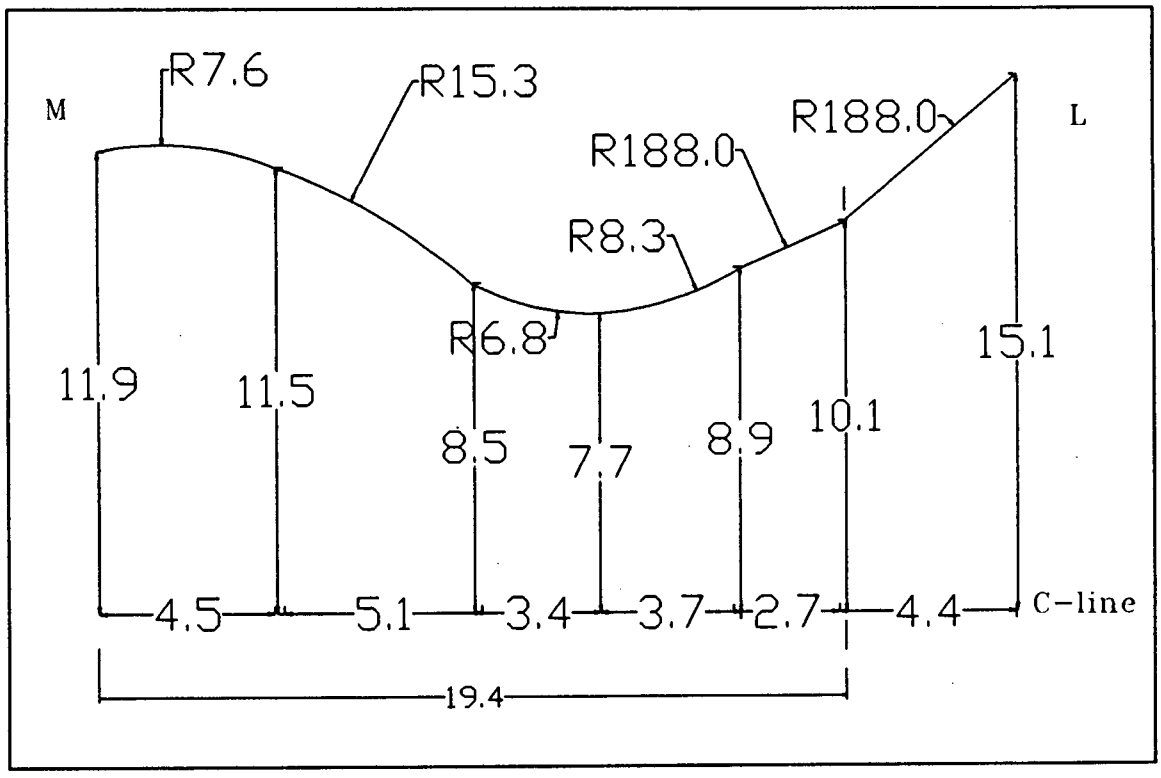

FIGURE G1. Articular surface of humeral component.

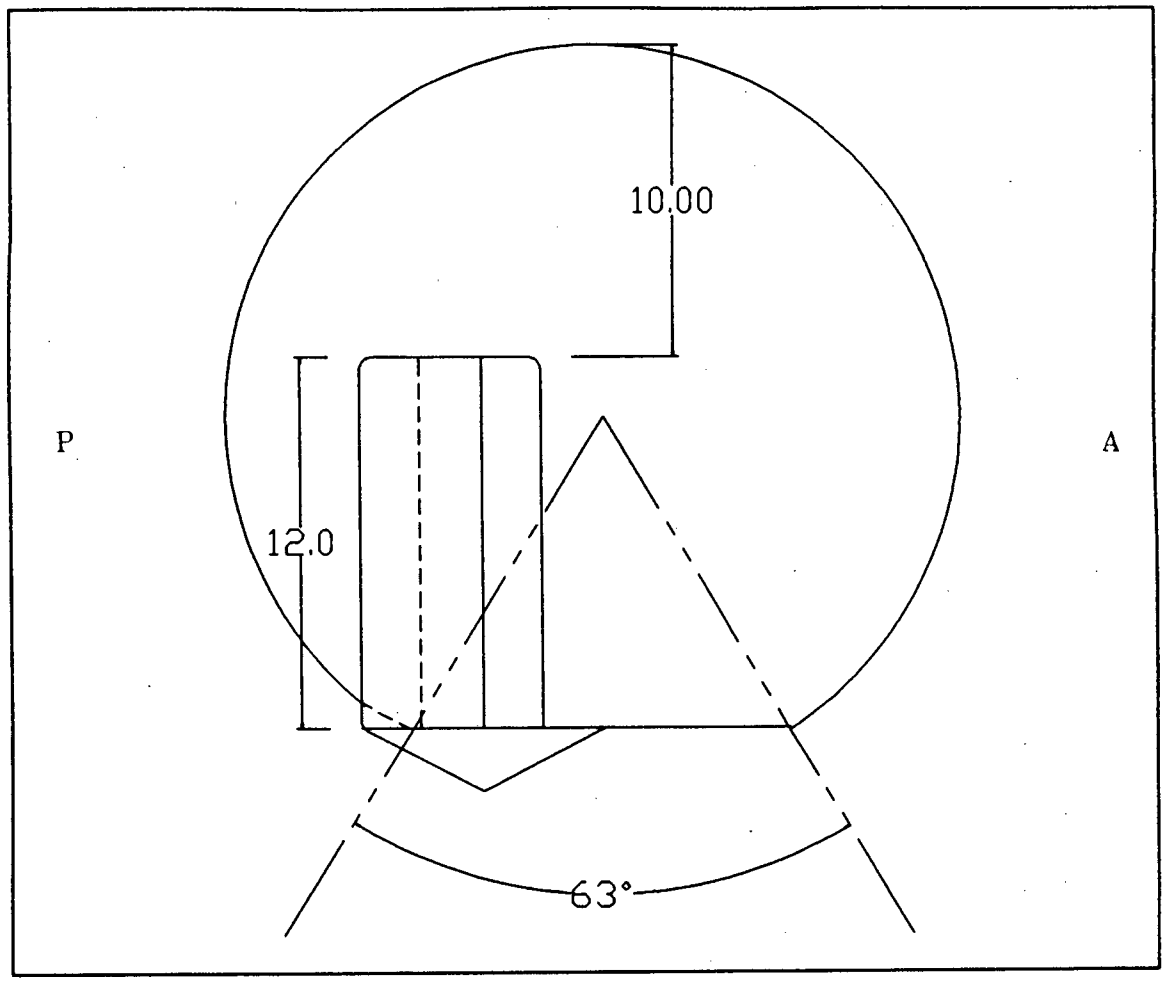

FIGURE G2. Side view of the humeral component.

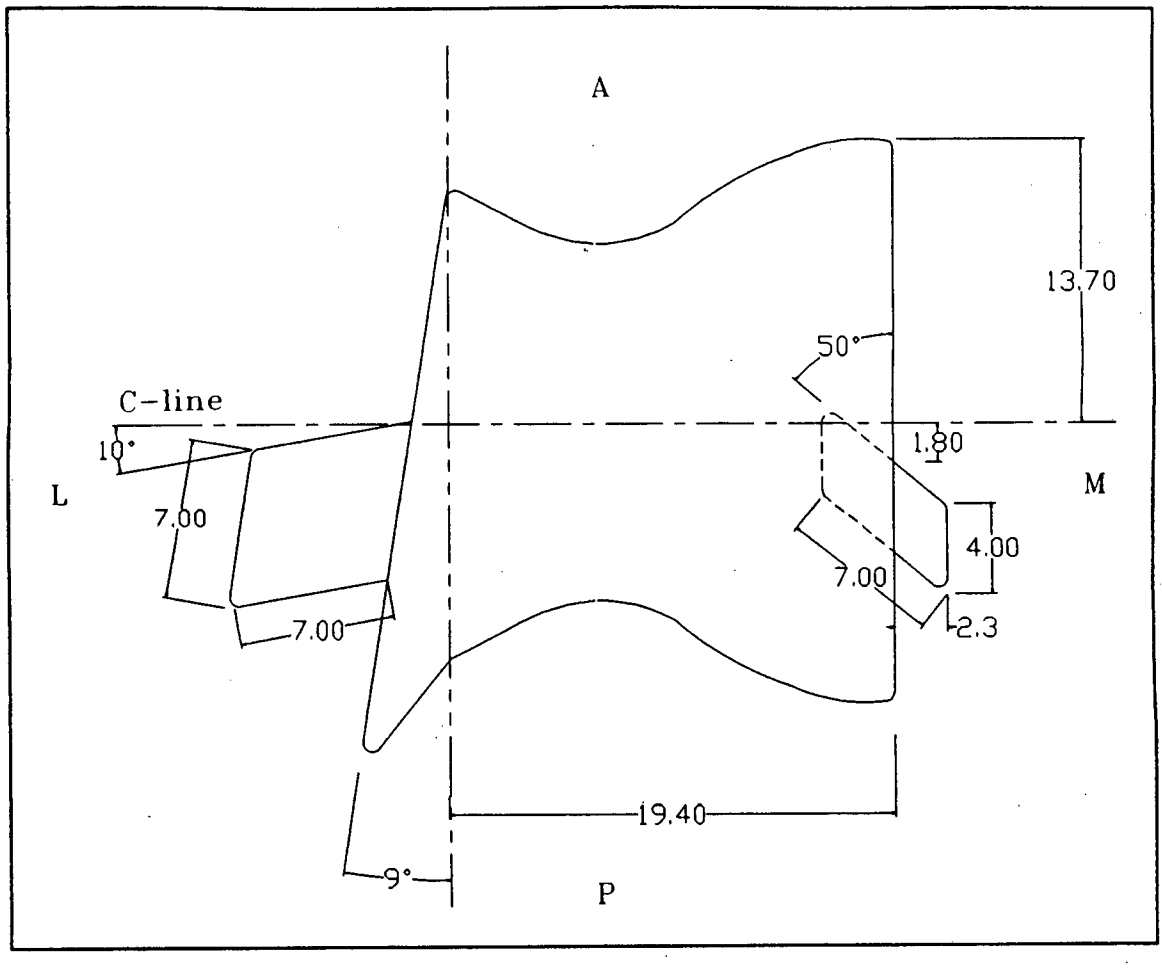

FIGURE G3. Top view of the humeral component.

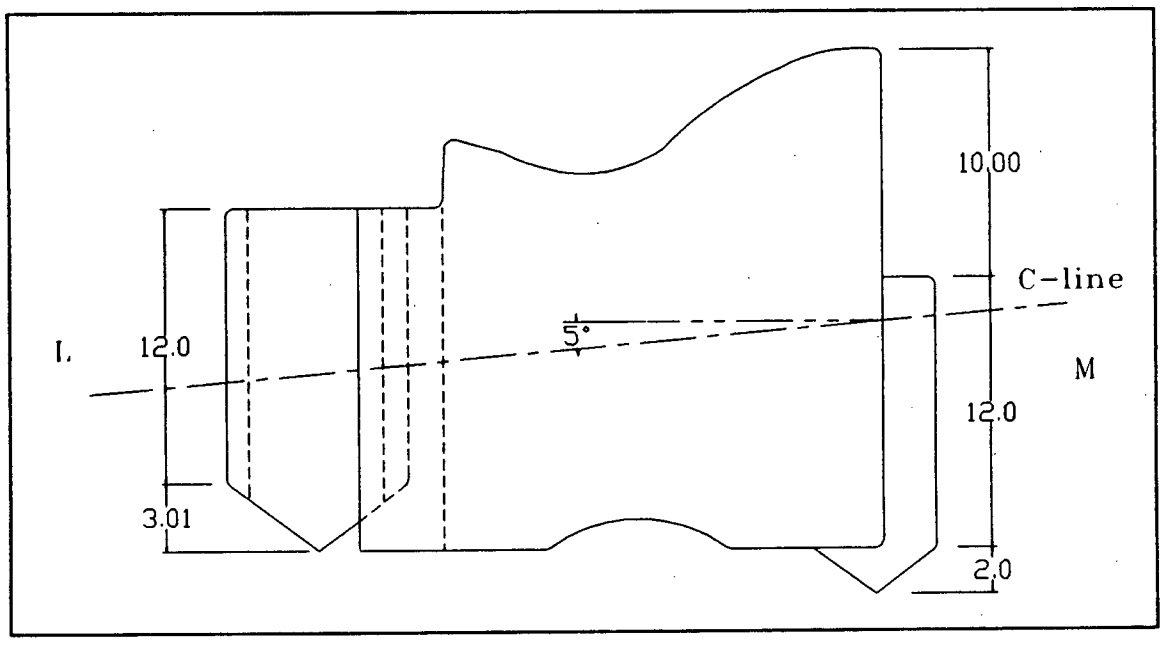

FIGURE G4. Front view of the humeral component.

Ulnar component: (G5) side view, (G6) top view, (G7) back view.

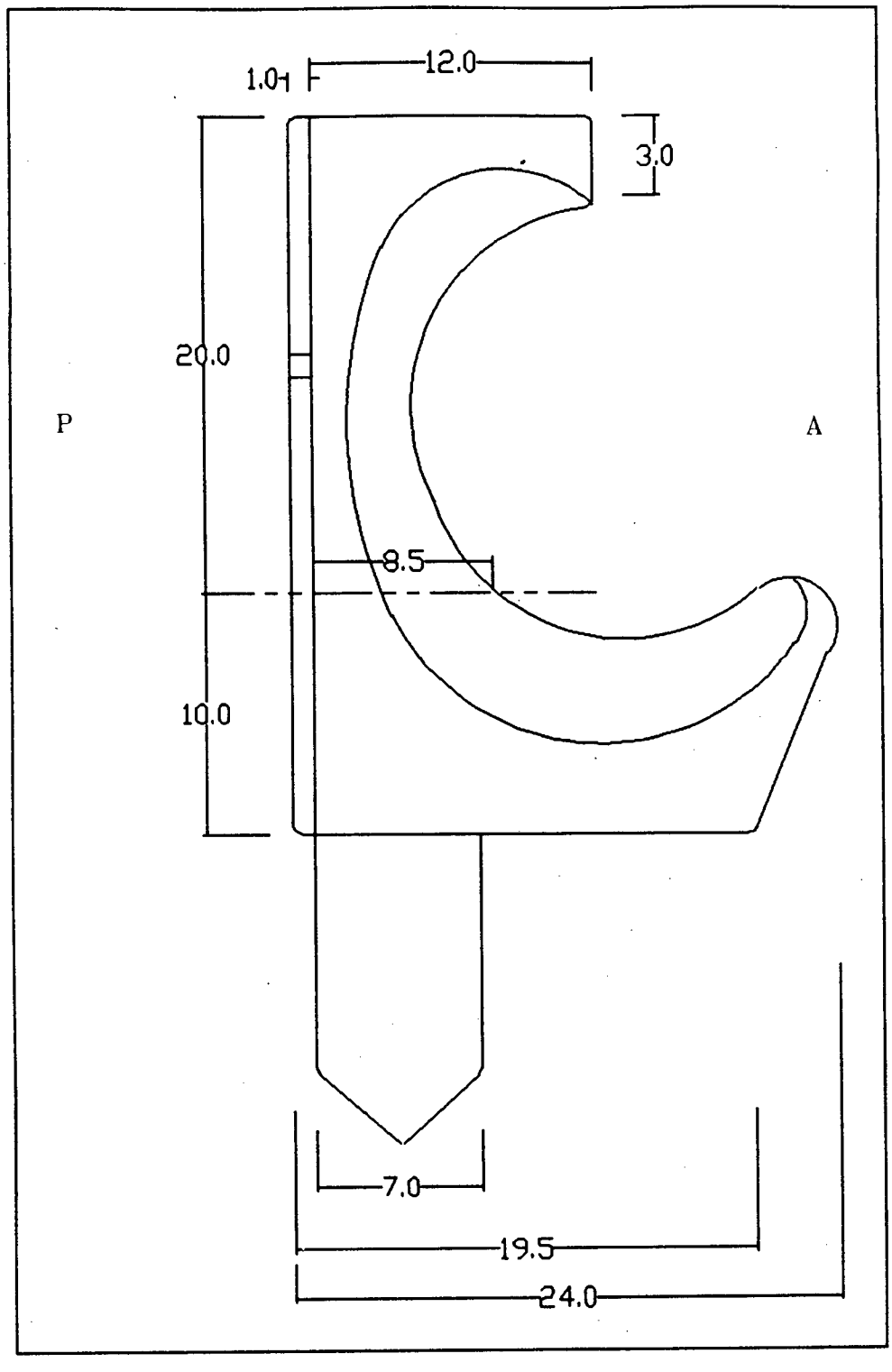

FIGURE G5. Side view of the ulnar component.

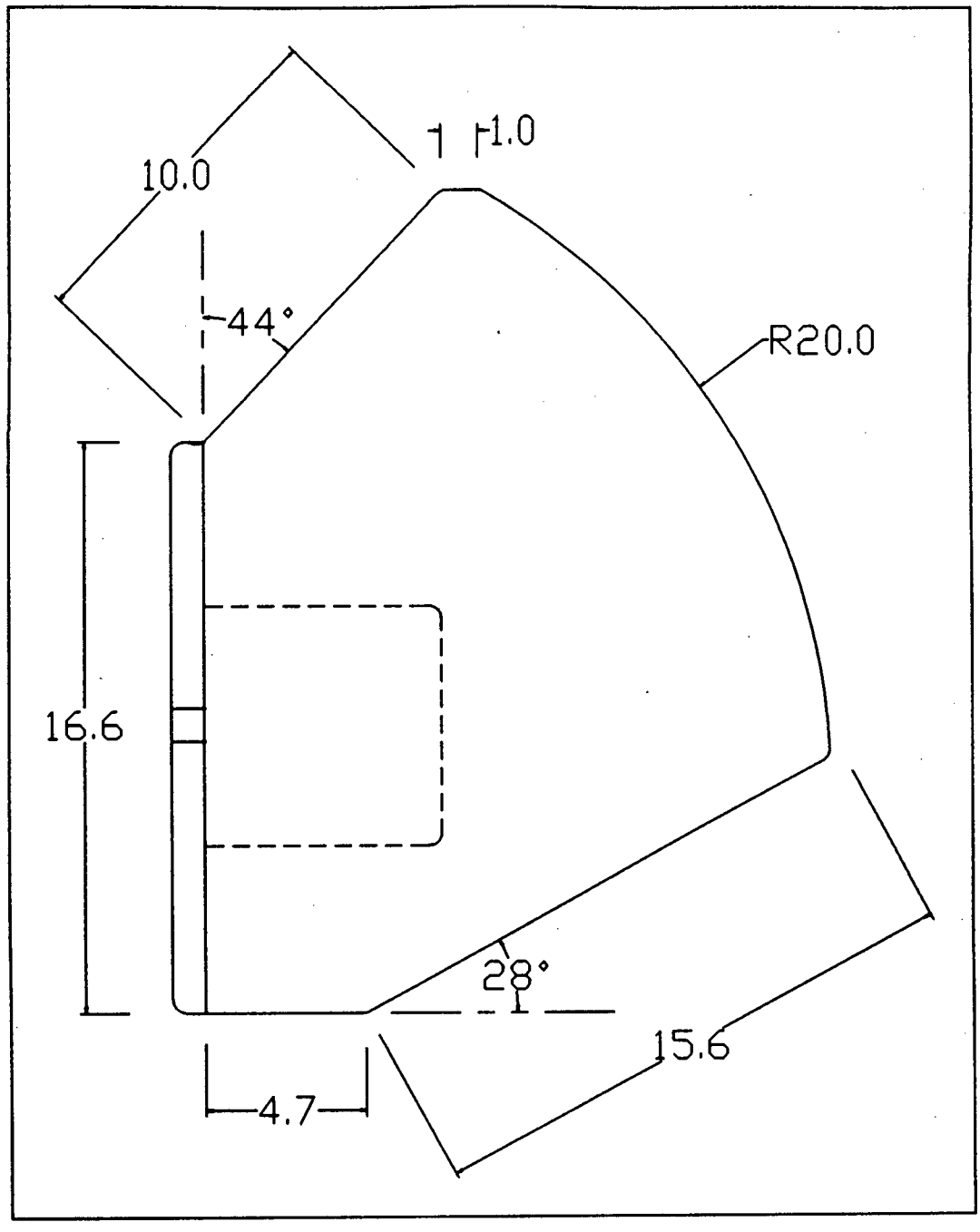

FIGURE G6. Top view of the ulnar component.

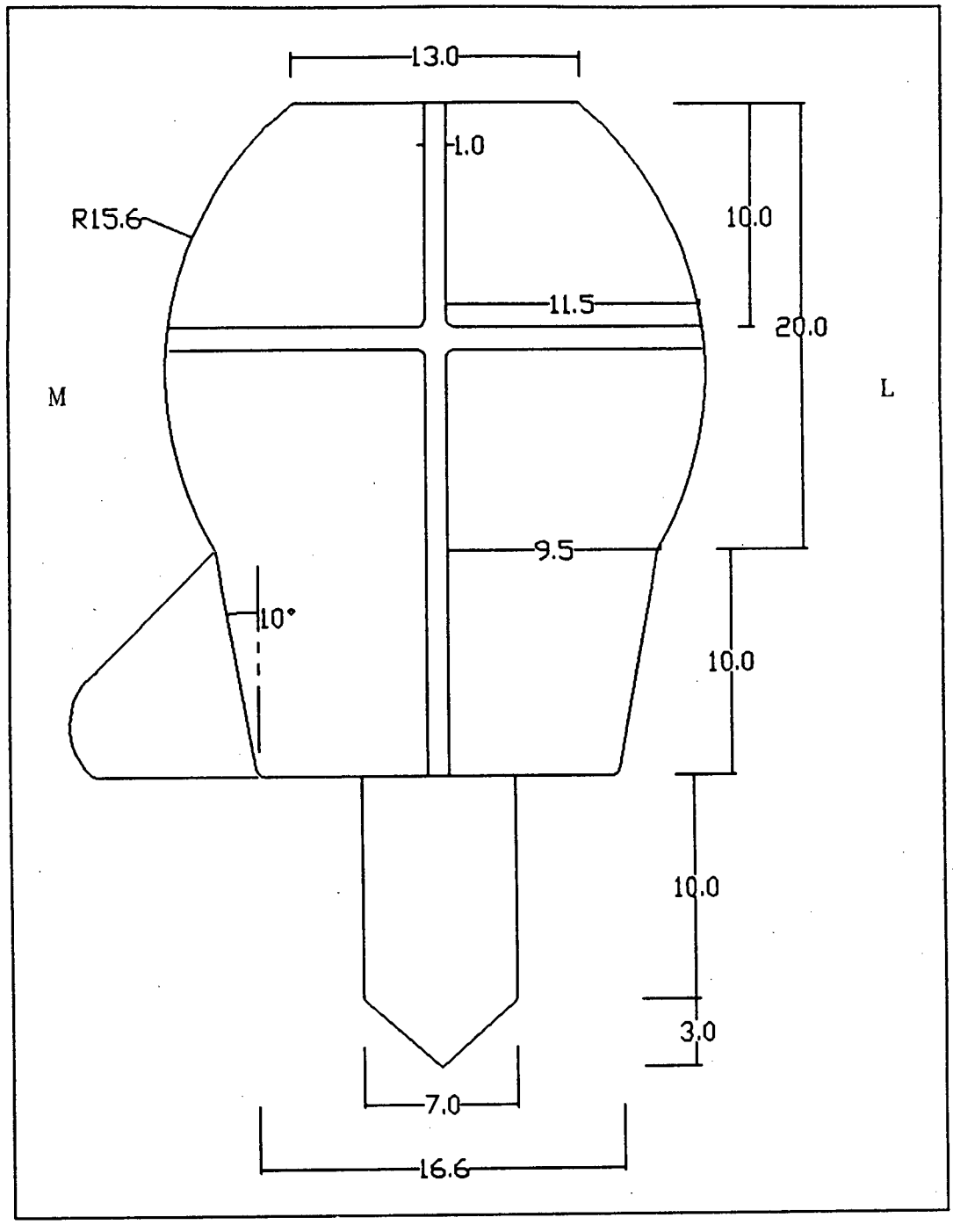

FIGURE G7. Back view of the ulnar component.

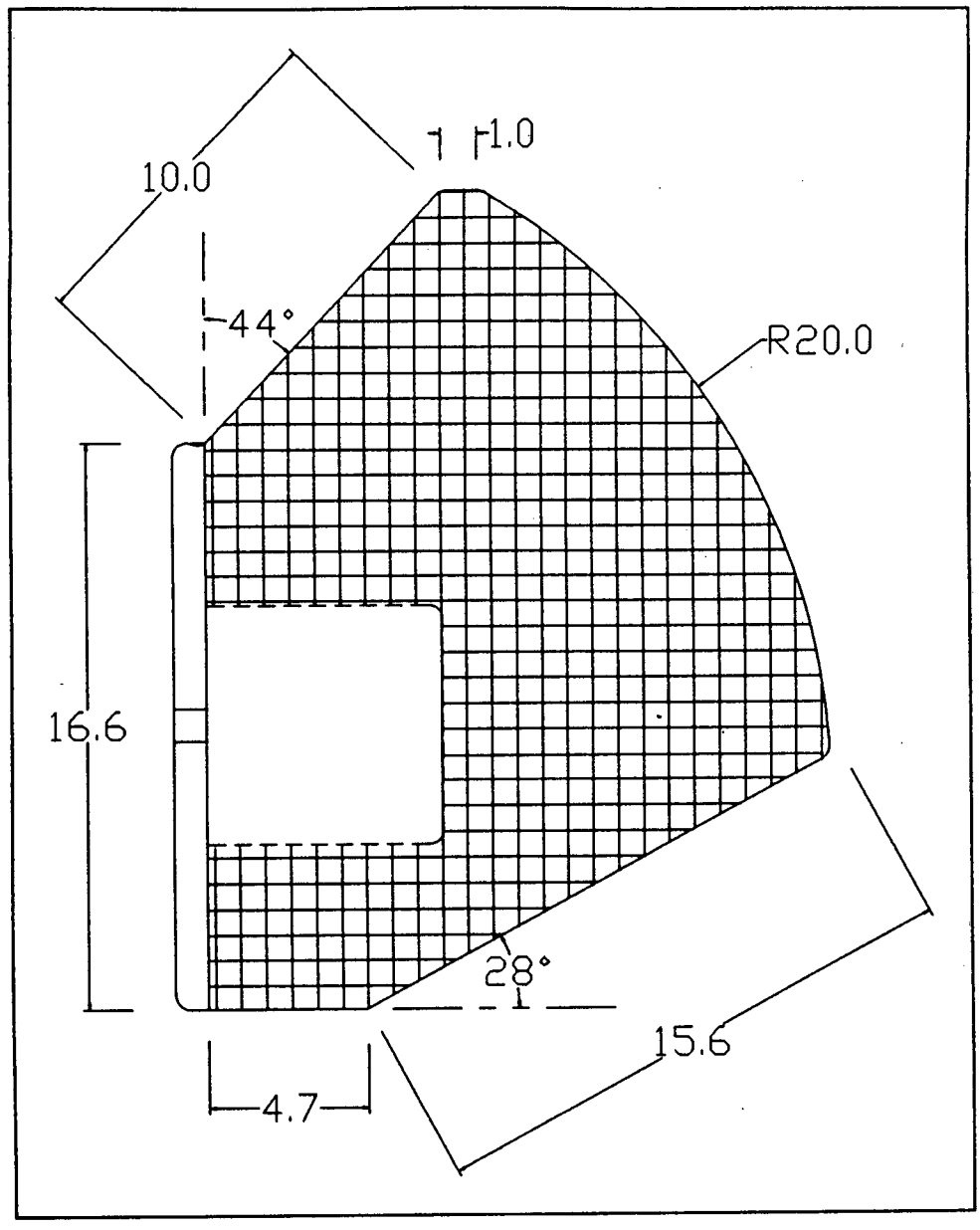

FIGURE G8. Bottom view of the ulnar component indicating the cross-hatching.

Ulnar component articular surface: (G9) front view, (G10) top view, (G11) coronoid surface, (G12) olecranon surface.

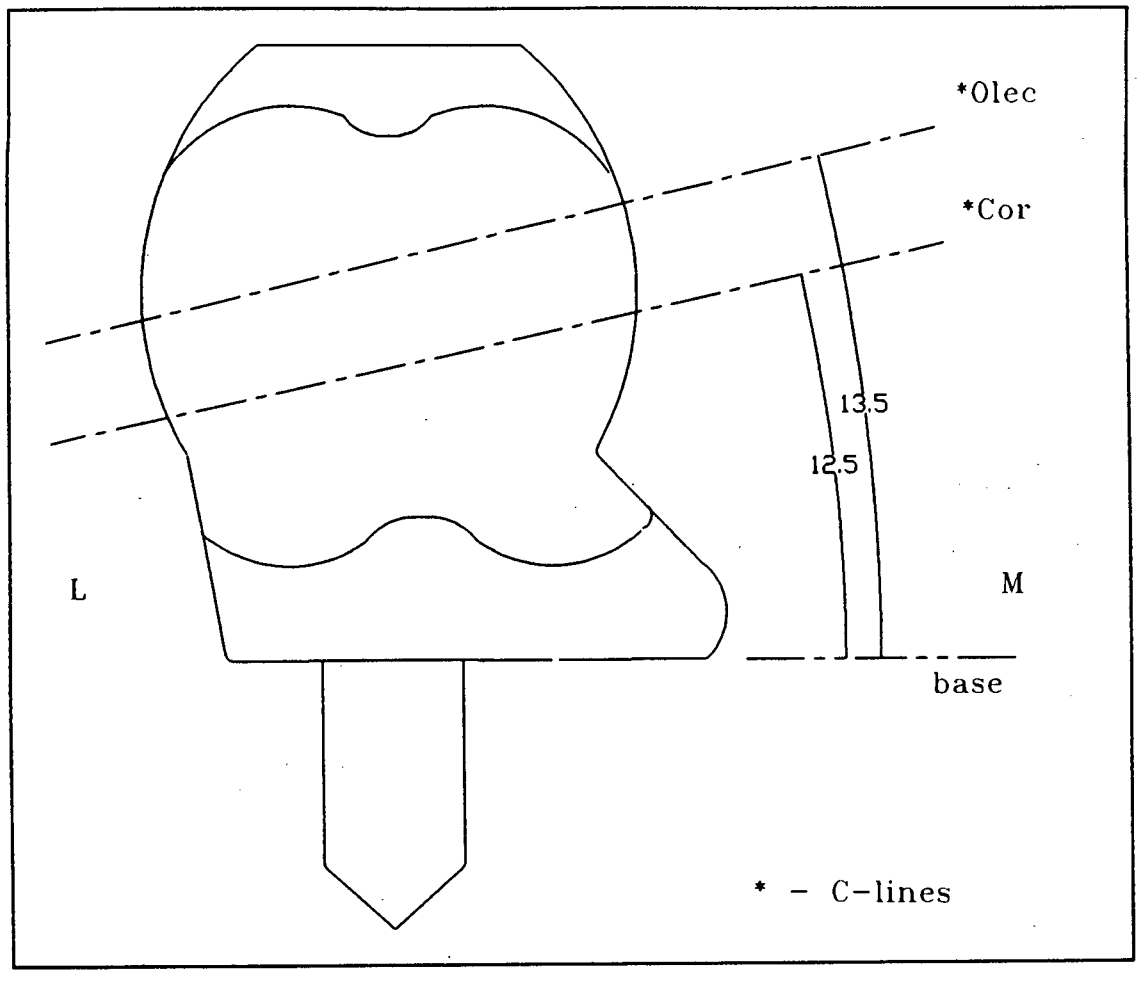

FIGURE G9. Front View of ulnar component indicating orientation of the articular surface.

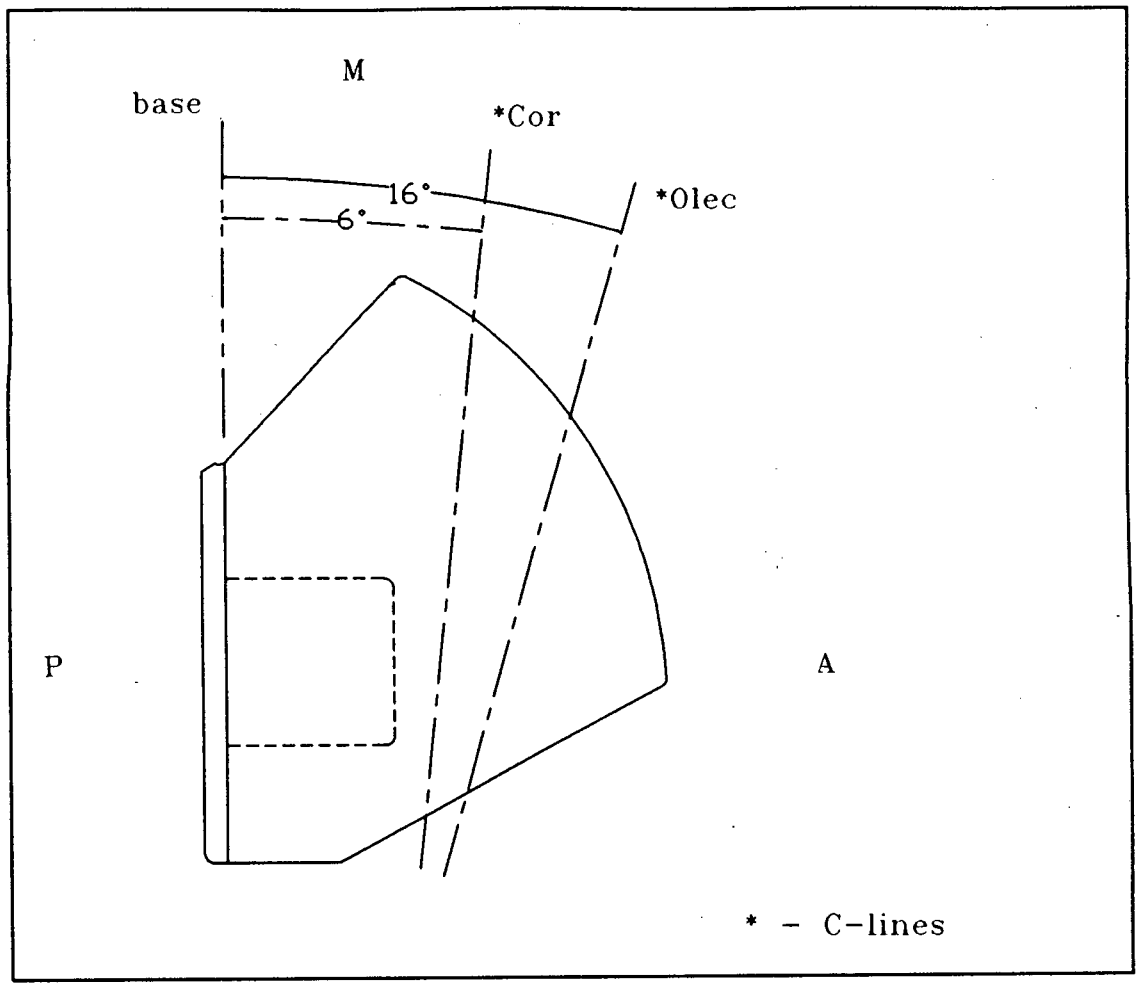

FIGURE G10. Top view of the ulnar component indicating the orientation of the articular surface.

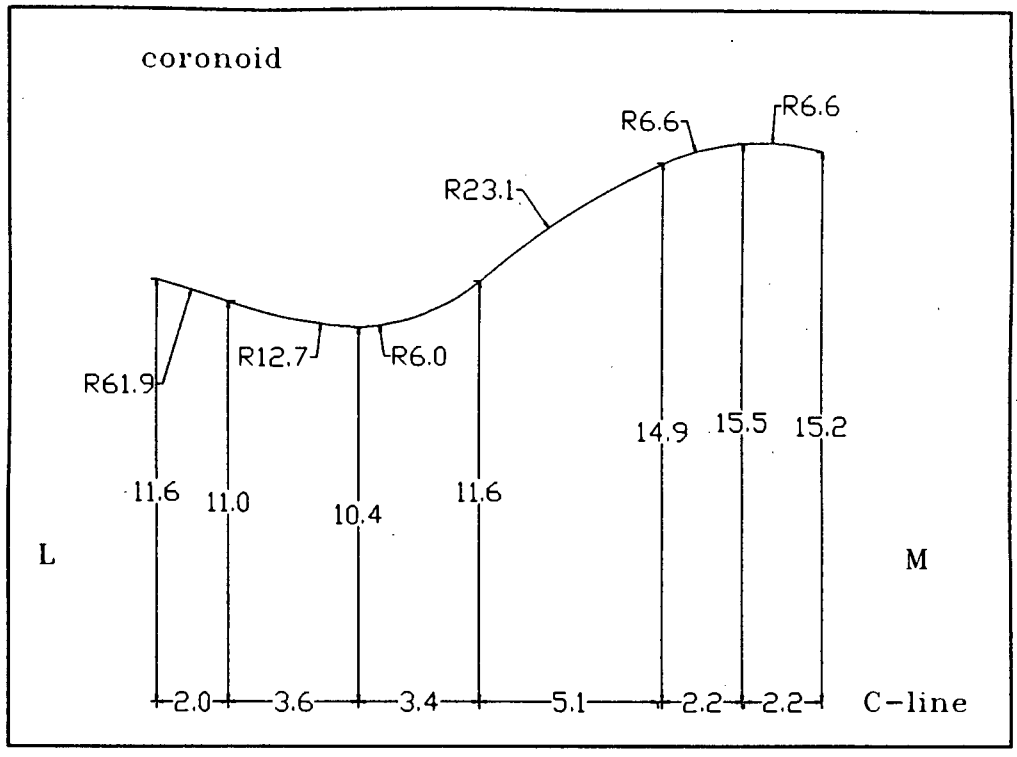

FIGURE G11. Coronoid articular surface of the ulnar component.

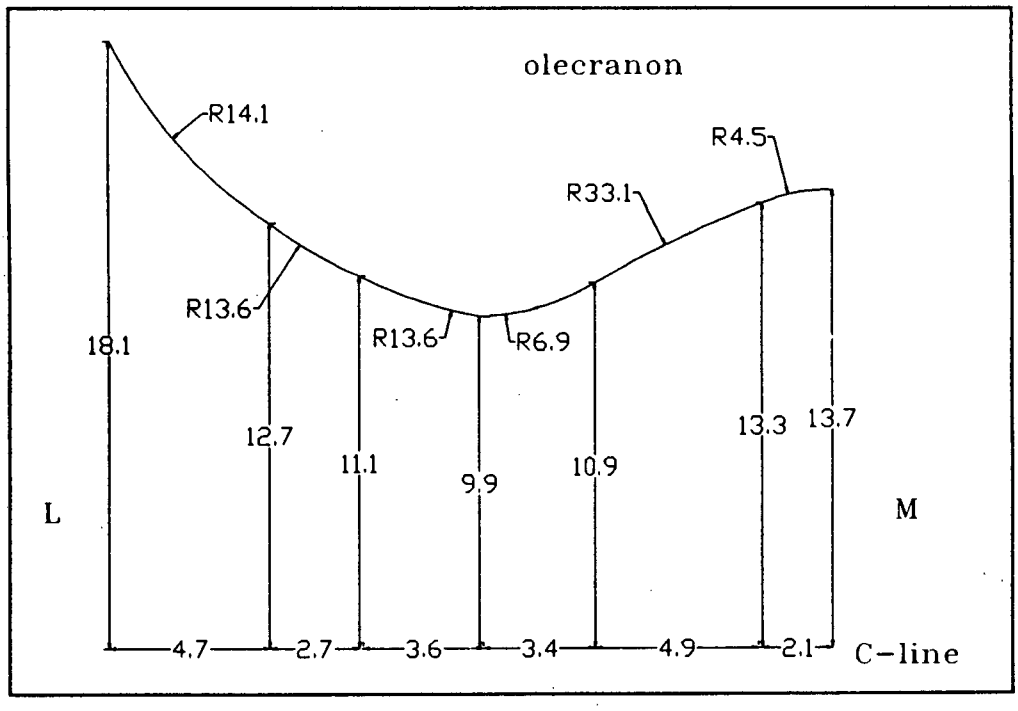

FIGURE G12. Olecranon articular surface of the ulnar component.

REFERENCES

ADAMS LP.
1976.
Palatal analysis by a stereo photogrammetric method.
The South African Survey Journal, 93:35-49.

AMIS AA, DOWSON D, UNSWORTH A, MILLER JH, WRIGHT V.
1977.
An examination of the elbow articulation with particular reference to variation of the carrying angle.
Engineering in Medicine, 6:76-80.

AMIS AA, DOWSON D, WRIGHT V.
1979a.
Muscle strength and musculo-skeletal geometry of the upper limb.
Engineering in Medicine, 8:41-48.

AMIS AA, HUGHES S, MILLER JH, WRIGHT V, DOWSON D.
1979b.
Elbow joint forces in patients with rheumatoid arthritis.
Rheumatology and Rehabilitation, 18:230-234.

AMIS AA, DOWSON D, WRIGHT V.
1980.
Elbow joint force predictions for some strenuous isometric actions.
Journal of Biomechanics, 13:765-775.

AMIS AA, MILLER JH, DAWSON D, WRIGHT V.
1981.
Biomechanical aspects of the elbow: Joint forces related to prosthesis design.
Engineering in Medicine, 10:65-68.

AMIS AA, MILLER JH.
1982.
The elbow.
Clinics in Rheumatic Diseases, 8:571-593.

AMIS AA, MILLER JH.
1984.
Design, development, and clinical trial of a modular elbow replacement incorporating cement-free fixation.
Engineering in Medicine, 13:175-179.

AN KN, HUI FC, MORREY BF, LINSCHEID RL, CHAO EY.
1981.
Muscles across the elbow joint: A biomechanical analysis.
Journal of Biomechanics, 14:659-669.

AN KN, KAUFMANN KR, CHAO EYS.
1989.
Physiological considerations of muscle force through the elbow joint.
Journal of Biomechanics, 22:1249-1256.

ANTON H.
1984.
Three Dimensional Space.
pp.819-857 In: Anton H ed. Calculus with analytical geometry.
J. Wiley and Sons, USA.

ATESHIAN GA, SOSLOWSKY LJ, MOW VC.
1991.
Quantitation of articular surface topography and cartilage thickness in knee joints using stereophotogrammetry.
Journal of Biomechanics, 24:761-776.

BASMAJIAN JV.
1982.
Muscular system.
pp.151-152 In: Basmajian JV, ed. Primary Anatomy.
Williams and Wilkins.

BEALS RK.
1976.
The normal carrying angle of the elbow.
Clinical Orthopaedics and Related Research, 119:194-196.

BRUMFIELD RH, KUSCHNER SH, GELLMAN H, REDIX L, STEVENSON DV.
1990.
Total elbow arthroplasty.
Journal of Arthroplasty, 5:359-363.

CHAO EY, MORREY BF.
1978.
Three-dimensional rotation of the elbow.
Journal of Biomechanics, 11:57-73.

CHAO EY, AN KN, ASKEW LJ, MORREY BF.
1980.
Electrogoniometer for the measurement of human elbow joint rotation.
Journal of Biomechanical Engineering, 102:301-310.

CNOCKAERT JC, LENSEL G, PERTUZON E.
1975.
Relative contribution of individual muscles to the isometric contraction of a muscular group.
Journal of Biomechanics, 13:765-775.

DAVIS RF, WEILAND AJ, HUNGERFORD DS, MOORE JR, VOLENEC-DOWLING S.
1982.
Nonconstrained total elbow arthroplasty.
Clinical Orthopaedics and Related Research, 171:157-160.

ELLOY MA, WRIGHT JTM, CAVENDISH ME.
1976.
The basic requirements and design criteria for total joint prostheses.
Acta Orthopaedica Scandinavica, 47:193-202.

ENGELBRECHT E, BUCHOLZ HW, ROTTGER J, SIEGEL A.
1977.
Total elbow replacement with a hinge and a non-blocked system.
pp.83-88 In: Institute of Mechanical Engineers Conference Publications 1977-5 ed. Joint Replacement in the Upper Limb.
Berlington Press, Foxton, Royston, Hertfordshire.

EWALD FC, THOMAS WH, SLEDGE CB, SCOTT RD, POSS R.
1977.
Non-constrained metal to plastic total elbow arthroplasty in rheumatoid arthritis.
pp.77-81 In: Institute of Mechanical Engineers Conference Publications 1977-5 ed. Joint Replacement in the Upper Limb.
Berlington Press, Foxton, Royston, Hertfordshire.

EWALD FC, SCHEINBERG RD, POSS R, THOMAS WH, SCOTT RD, SLEDGE CB.
1980.
Capitellocondylar total elbow arthroplasty. Two to five year follow-up in rheumatoid arthritis.
The Journal of Bone and Joint Surgery, 62-A:1259-1262.

EWALD FC, JACOBS MA.
1984.
Total elbow arthroplasty.
Clinical Orthopaedics and Related Research, 182:137-142.

FIGGIE HE, INGLIS AE, MOW C.
1986.
A critical analysis of biomechanical parameters affecting functional outcome in Total Elbow Arthroplasty.
Journal of Arthroplasty, 1:19-26.

FOTIOU A, LIVIERATOS E, LOMBARDINI G, PARASCHAKIS I.
1991.
Dome representation using photogrammetrically derived data and best fitting techniques.
ISPRS Journal of Photogrammetry and Remote Sensing, 46:231-246.

FREYBURG RH.
1968.
A study of the time of onset of structural joint damage in rheumatoid arthritis (Abstract).
Arthritis and Rheumatism, 11:481.

FUNK DA, AN KN, MORREY BF, DAUBE JR.
1987.
Electromyographic analysis of muscles across the elbow joint.
Journal of Orthopaedic Research, 5:529-538.

GHOSH SK.
1983.
A close-range photogrammetric system for 3-D measurements and perspective diagramming in biomechanics.
Journal of Biomechanics, 16:667-674.

GOEL VK, SINGH D, BIJLANI V.
1982.
Contact areas in human elbow joints.
Journal of Biomechanical Engineering, 104:169-175.

GOEL VK, BLAIR WF.
1985.
Biomechanics of the elbow joint.
Automedica, 6:119-139.

GOLDBERG VM, FIGGIE HE, INGLIS AE, FIGGIE MP.
1988.
Current concepts review. Total elbow Arthroplasty.
The Journal of Bone and Joint Surgery, 70-A:778-781.

GOODFELLOW JW, BULLOUGH PG.
1967.
The pattern of ageing of the articular cartilage of the elbow joint.
The Journal of Bone and Joint Surgery, 49-B:175-181.

GSCHWEND N, LOEHR J, IVOSEVIC-RADOVANOVIC D, SCHEIER H, MUNZINGER U.
1988.
Semi-constrained elbow prosthesis with special reference to the GSB 3 prosthesis.
Clinical Orthopaedics and Related Research, 232:104-111.

HUISKES R, KREMERS J, DE LANGE A, WOLTRING HJ, SELVIK G, VAN RENS TGJ.
1985.
Analytic stereophotogrammetric determination of three-dimensional knee-joint geometry.
Journal of Biomechanics, 18:559-570.

INGLIS AE, PELLICCI PM.
1980.
Total elbow replacement.
The Journal of Bone and Joint Surgery, 62-A:1253-1258.

JOBBINS B.
1981.
General considerations in joint replacements.
pp.159-161 In: Dowson D, Wright V, eds. Introduction to the biomechanics of joints and joint replacements.
William Clowes (Beccles) Ltd.

JOHNSON JR, GETTY CJM, LETTIN AWF, GLASGOW MMS.
1984.
The Stanmore total elbow replacement for rheumatoid arthritis.
The Journal of Bone and Joint Surgery, 66-B:732-736.

JONSSON B, LARSSON S-E.
1990.
Elbow arthroplasty in rheumatoid arthritis. Function after 1-2 years in 20 cases.
Acta Orthopaedica Scandinavica, 61:344-337.

KAPANDJI IA.
1970.
The elbow.
pp.79-121 In: Kapandji IA, ed. The Physiology of the joints.
Baltimore, The Williams and Wilkins Comp.

KARANJIA ND, STILES PJ.
1990.
The Guildford elbow.
International Orthopaedics, 14:315-319.

KING GJW, GLAUSER SJ, WESTREICH A, MORREY BF, AN KN.
1993.
In vitro stability of an uncostrained total elbow prosthesis. Influence of axial loading and joint flexion angle.
Journal of Arthroplasty, 8:291-298.

KUDO H, IWANO K.
1990.
Total elbow arthroplasty with a non-constrained surface-replacement prosthesis in patients who have rheumatoid arthritis. A long-term follow-up study.
The Journal of Bone and Joint Surgery, 72-A:355-363.

LAINE V, VAINIO K.
1969.
pp.117-118 In: Hijmans W, Paul WD, Herschel H, eds. Early synovectomy in rheumatoid arthritis.
Amsterdam, Excerpta Medica.

LANGRANA NA.
1981.
Spatial kinematic analysis of the upper extremity using a biplanar videotaping method.
Journal of Biomechanical Engineering, 103:11-17.

LEBER C, MELONE CP.
1988.
Total elbow replacement.
Orthopaedic Review, 27:857-863.

LONDON JT.
1981.
Kinematics of the elbow.
The Journal of Bone and Joint Surgery, 63-A;529-535.

LOWE LW, MILLER AJ, ALLUM RL, HIGGINSON DW.
1984.
The development of an unconstrained elbow arthroplasty.
The Journal of Bone and Joint Surgery, 66-B:243-247.

MADSEN F, GUDMUNDSON GH, SOJBJERG JO, SNEPPEN O.
1989.
The Pritchard Mark 2 elbow prosthesis in rheumatoid arthritis.
Acta Orthopaedica Scandinavica, 60:249-253.

MORREY BF, CHAO EYS.
1976.
Passive motion of the elbow joint: a biomechanical analysis.
The Journal of Bone and Joint Surgery, 58-A:501-508.

MORREY BF, CHAO EY, HUI FC.
1979.
Biomechanical study of the elbow following excission of the radial head.
The Journal of Bone and Joint Surgery, 61-A:63-67.

MORREY BF, BRYAN RS, DOBYNS JS, LINSCHEID RL.
1981.
Total elbow arthroplasty. A five-year experience at the Mayo Clinic.
The Journal of Bone and Joint Surgery, 63-A:1050-1063.

MORREY BF, AN KN.
1983.
Articular and ligamentous contributions to the stability of the elbow joint.
American Journal of Sports Medicine, 11:315-319.

MORREY BF.
1985a.
Anatomy of the elbow.
pp.1-42 In: Morrey BF, ed. The elbow and its disorders.
Philadelphia: WB Saunders.

MORREY BF, AN KN.
1985b.
Biomechanics of the elbow.
pp.43-61 In: Morrey BF, ed. The elbow and its disorders.
Philadelphia: WB Saunders.

MORREY BF, BRYAN RS.
1985c.
Total joint replacement.
pp.546-569 In: Morrey BF, ed. The elbow and its disorders.
Philadelphia: WB Saunders.

MORREY BF, TANAKA S, AN KN.
1991.
Valgus stability of the elbow: A definition of primary and secondary constraints.
Clinical Orthopaedics and Related Research, 265:187-195.

MURAKAMI T, OHTSUKI N.
1989.
Effect of lubricants on improvement of fluid film formation in knee prostheses under walking conditions.
pp.403-410 In: Fung YC, Hayashi H, Seguchi H, eds. Progress and new directions of biomechanics.
Mita Press, Japan.

O'CARROLL S, JIN ZM, DOWSON D, FISHER J, JOBBINS B.
1990.
Determination of contact area in "cushion form" bearings for artificial hip joints.
Engineering in Medicine, 204:217-223.

POLL RG, ROZING PM.
1991.
Use of the Souter-Strathclyde Total Elbow Prosthesis in patients who have rheumatoid arthritis.
The Journal of Bone and Joint Surgery, 73-A:1227-1233.

PORTER BB, RICHARDSON C, VAINIO K.
1974.
Rheumatoid arthritis of the elbow: the results of synovectomy.
The Journal of Bone and Joint Surgery, 56-B:427-437.

REGAN WD, KORINER SL, MORREY BF, AN KN.
1991.
Biomechanical study of ligaments around the elbow joint.
Clinical Orthopaedics and Related Research, 271:170-179.

ROPER BA, TUKE M, O'RIORDAN SM, BULSTRODE CJ.
1986.
A new unconstrained elbow: a prospective review of 60 replacements.
The Journal of Bone and Joint Surgery, 68-B:566-569

ROSENBURG GM, TURNER RH.
1983.
Nonconstrained total elbow arthroplasty.
Clinical Orthopaedics and Related Research, 187:154-162.

RUTH AT, WILDE AH.
1992.
Capitellocondylar total elbow replacement.
The Journal of Bone and Joint Surgery, 74-A:95-100.

RYDHOLM U, TJORNSTRAND B, PETTERSSON H, LIDGREN L.
1984.
Surface replacement of the elbow in rheumatoid arthritis. Early results with the Wadsworth prosthesis.
The Journal of Bone and Joint Surgery, 66-B:737-741.

SCOTT PJ.
1981.
The reflex plotters: Measurement without photographs.
Photogrammetric Record, 10(58):447-456.

SHIBA R, SORBIE C, SIU D, BRYANT JT, COOKE TDV, WEVERS HW.
1988.
Geometry of the humeroulnar joint.
Journal of Orthopaedic Research, 6:897-906.

SONI RK, CAVENDISH ME.
1984.
A review of the Liverpool elbow prosthesis from 1974 to 1982.
The Journal of Bone and Joint Surgery, 66-B:248-253.

SOURMELIS SG, BURKE FD, VARIAN JPW.
1986.
A review of total elbow arthroplasty and an early assessment of the Liverpool elbow prosthesis.
The Journal of Bone and Joint Surgery, 68-B:407-413.

SOUTER WA.
1977.
Total replacement arthroplasty of the elbow.
pp.99-106 In: Institute of Mechanical Engineers Conference Publications 1977-5 ed. Joint Replacement in the Upper Limb.
Berlington Press, Foxton, Royston, Hertfordshire.

SOUTER WA.
1981.
A new approach to elbow arthroplasty.
Engineering in Medicine, 10:59-64.

SOUTER WA.
1990.
Surgery of the rheumatoid elbow.
Annals of the Rheumatic Diseases, 49:871-882.

STOCKWELL RA.
1987.
Structure and function of the chondrocyte under mechanical stress.
pp.126-148 In: Helminen HJ, Kiviranta I, Tamm M, Saamenen AM, Paukonen K, Jurvelin J, eds. Joint Loading.
Wright, Bristol.

STORMONT TJ, AN KN, MORREY BF, CHAO EY.
1985.
Elbow joint contact study: comparison of techniques.
Journal of Biomechanics, 18:329-336.

TOBIAS PV, ARNOLD M, ALLAN JC.
1988.
The elbow joint.
p.131 In: Man's anatomy.
Witwatersrand University Press, Johannesburg.

TORTORA JT.
1989.
The cardiovascular system and the nervous system.
pp. 382-474 In: Tortora JT, ed. Principles of Human Anatomy.
Harper and Row, Publishers NY, USA.

UNSWORTH A, ROBERTS B, THOMPSON JC.
1981.
The application of soft layer lubrication in hip prostheses (Abstract).
The Journal of Bone and Joint Surgery, 63-B:297

WEILAND AJ, WEISS A-PC, WILLS RP, MOORE JR.
1989.
Capitellocondylar total elbow replacement. A long-term follow-up study.
The Journal of Bone and Joint Surgery, 71-A:217-223.

YOUM Y, DRYER RF, THAMBYRAJAH K, FLATT AE, SPRAGUE BL.
1979.
Biomechanical analysis of forearm pronation and supination and elbow flexion-extension.
Journal of Biomechanics, 12:245-255.